



# Tensile Properties of GRCop-84

*David L. Ellis*  
*Glenn Research Center, Cleveland, Ohio*

*William S. Loewenthal*  
*Ohio Aerospace Institute, Brook Park, Ohio*

*Hee Man Yun*  
*Cleveland State University, Cleveland, Ohio*

## NASA STI Program . . . in Profile

Since its founding, NASA has been dedicated to the advancement of aeronautics and space science. The NASA Scientific and Technical Information (STI) program plays a key part in helping NASA maintain this important role.

The NASA STI Program operates under the auspices of the Agency Chief Information Officer. It collects, organizes, provides for archiving, and disseminates NASA's STI. The NASA STI program provides access to the NASA Aeronautics and Space Database and its public interface, the NASA Technical Reports Server, thus providing one of the largest collections of aeronautical and space science STI in the world. Results are published in both non-NASA channels and by NASA in the NASA STI Report Series, which includes the following report types:

- **TECHNICAL PUBLICATION.** Reports of completed research or a major significant phase of research that present the results of NASA programs and include extensive data or theoretical analysis. Includes compilations of significant scientific and technical data and information deemed to be of continuing reference value. NASA counterpart of peer-reviewed formal professional papers but has less stringent limitations on manuscript length and extent of graphic presentations.
- **TECHNICAL MEMORANDUM.** Scientific and technical findings that are preliminary or of specialized interest, e.g., quick release reports, working papers, and bibliographies that contain minimal annotation. Does not contain extensive analysis.
- **CONTRACTOR REPORT.** Scientific and technical findings by NASA-sponsored contractors and grantees.

- **CONFERENCE PUBLICATION.** Collected papers from scientific and technical conferences, symposia, seminars, or other meetings sponsored or cosponsored by NASA.
- **SPECIAL PUBLICATION.** Scientific, technical, or historical information from NASA programs, projects, and missions, often concerned with subjects having substantial public interest.
- **TECHNICAL TRANSLATION.** English-language translations of foreign scientific and technical material pertinent to NASA's mission.

Specialized services also include creating custom thesauri, building customized databases, organizing and publishing research results.

For more information about the NASA STI program, see the following:

- Access the NASA STI program home page at <http://www.sti.nasa.gov>
- E-mail your question via the Internet to [help@sti.nasa.gov](mailto:help@sti.nasa.gov)
- Fax your question to the NASA STI Help Desk at 443-757-5803
- Telephone the NASA STI Help Desk at 443-757-5802
- Write to:  
NASA Center for AeroSpace Information (CASI)  
7115 Standard Drive  
Hanover, MD 21076-1320

NASA/TM—2012-217108



# Tensile Properties of GRCop-84

*David L. Ellis*  
*Glenn Research Center, Cleveland, Ohio*

*William S. Loewenthal*  
*Ohio Aerospace Institute, Brook Park, Ohio*

*Hee Man Yun*  
*Cleveland State University, Cleveland, Ohio*

National Aeronautics and  
Space Administration

Glenn Research Center  
Cleveland, Ohio 44135

---

April 2012

Trade names and trademarks are used in this report for identification only. Their usage does not constitute an official endorsement, either expressed or implied, by the National Aeronautics and Space Administration.

*Level of Review:* This material has been technically reviewed by technical management.

Available from

NASA Center for Aerospace Information  
7115 Standard Drive  
Hanover, MD 21076-1320

National Technical Information Service  
5301 Shawnee Road  
Alexandria, VA 22312

Available electronically at <http://www.sti.nasa.gov>

# **Tensile Properties of GRCop-84**

David L. Ellis  
National Aeronautics and Space Administration  
Glenn Research Center  
Cleveland, Ohio 44135

William S. Loewenthal  
Ohio Aerospace Institute  
Brook Park, Ohio 44142

Hee Man Yun  
Cleveland State University  
Cleveland, Ohio 44115

## **Summary**

This is a chapter in the final report on GRCop-84 for the Reusable Launch Vehicle (RLV) Second Generation/Project Constellation Program. It contains information on the tensile properties of GRCop-84. GRCop-84 (Cu-8 at.% Cr-4 at.% Nb) was produced by extrusion and Hot Isostatic Pressing (HIPing). Some of the extrusions were rolled to plate and sheet while other extrusions were drawn into tubing. The material was further subjected to various heat treatments corresponding to annealing, anticipated typical brazing conditions, an end-of-life condition and various elevated temperature exposures to attempt to improve creep resistance. As anticipated, cold work increased strength while decreasing ductility. Annealing at 600 °C (1112 °F) and higher temperatures was effective. An exposure for 100 h at 500 °C (932 °F) resulted in an increase in strength rather than the anticipated decrease. High temperature simulated-braze cycles and thermal exposures lowered the strength of GRCop-84, but the decreases were small compared to precipitation strengthened copper alloys. It was observed that the excess Cr could form large precipitates that lower the reduction in area though it appears a minimum amount is required. Overall, GRCop-84 exhibits good stability of its tensile properties, which makes it an excellent candidate for rocket engine liners and many other high temperature applications.

## **Introduction**

Future reusable and expendable spacecraft will require high conductivity main combustion chamber (MCC) liners that are capable of operating in a high stress, high temperature environment. Indications are that both operating temperature and pressures will increase as higher performance is sought. While elevated temperature tensile strength is generally not the primary criteria for selecting the liner material, high elevated temperature strength is generally an indication of a high creep stress capability, is required to prevent gross deformation due to thermally-induced stresses and is needed to prevent failure due to the pressure differential between the chamber and the cooling channel. The tensile strength is also a good macroscopic indicator of the thermal stability of a metal exposed to a variety of thermal cycles. This study was conducted to establish the tensile properties of GRCop-84 over a wide range of temperatures in the as-produced conditions and after a variety of thermal exposures.

For the RLV Second Generation program, three general types of regeneratively-cooled main combustion chamber liners were under consideration. In the first case, the liner would be machined from a suitable shape. For engines such as the RS-83 and RS-84 engines, the liner would be made by metal spinning a cylinder into an hourglass shape, machining to final dimensions and brazing the liner into a steel support jacket. The milled liner would be comparable to the liner used in the Space Shuttle Main Engine (SSME) (Refs. 1 and 2) and would require plate between 1.3 and 1.9 cm (0.5 and 0.75 in.) thick.

The plate would be annealed after production but then undergo additional forming, machining and annealing to make the liner. The final heat treatment would be a high temperature braze cycle to join the fully formed and machined liner into the support jacket.

An alternative to producing plate and forming it into an hourglass shaped preform for the milled liner would be to Hot Isostatic Press (HIP) into a cylinder or hourglass shape directly. Considerable material and processing could be saved since HIPing would produce near-net shape parts. After HIPing the liner would be machined and brazed into a support jacket just like the metal spun liner made from plate. Metal spinning would be optional, but the worked structure after metal spinning likely would have better, more uniform properties.

In the second case, which may have been used in the Co-optimized Booster for Reusable Applications (COBRA) engine, the liner would be made using platelet technology (Ref. 3) to create the cooling passages, formed, welded and brazed into a steel support jacket. Thin sheet (0.5 mm or less) is required for platelet liners. For lay-up and working with the etched panels, a stiff sheet is desired, so the sheet would be in a cold-worked condition with maximum cold work being preferred. The platelets would be joined using diffusion bonding to make the liner. After forming and welding to complete the liner, the liner would be brazed into a steel support jacket. It is anticipated that a high temperature braze comparable to the milled liner would be used for this step.

In the third liner option contemplated, a liner would be made from tubing as has been done in the past (Refs. 4 to 6). This technique is generally more suitable for upper stage engines such as the RL-10, but proposed large expansion cycle engines such as the RL-60 have similar designs. GRCop-84 tubing was demonstrated to be feasible by LeFiell Corporation (Ref. 7). The tubing could be formed into the proper profile and assembled into a liner on a mandrel. Following brazing, vacuum plasma spraying or other method to secure the tubing as a liner, a stainless steel support jacket would be brazed or otherwise attached to the outside of the liner for support.

Tensile test results for GRCop-84 have been reported in the past (Refs. 8 and 9). Because of a change in powder supplier and compositional differences, earlier tensile test results are not included in this report to provide consistency in the analyses and comparisons. The earlier results are generally consistent with results for comparable material forms, processing and heat treatments presented in this report.

## **Experimental Procedure**

GRCop-84 tensile testing was conducted in the as-extruded, as-HIPed, and as-rolled conditions. In addition, samples were given a variety of heat treatments to evaluate annealing temperatures, replicate potential brazing or diffusion bonding processes, evaluate potential creep improvements for sheet material, and simulate end-of-life conditions. Drawn and annealed GRCop-84 tubing was also evaluated.

## **Chemistry**

Chemical analyses were conducted at Crucible Research in Pittsburgh, Pennsylvania for all powder lots and at NASA GRC for all consolidated material. Chemical analysis of the major elements and Fe was done at NASA GRC using a Varian Vista Pro Inductively Coupled Plasma (ICP) Atomic Emission Spectrometer (AES). The unit was also used to search for trace contaminants. Oxygen was analyzed using a Leco TC-436 Nitrogen-Oxygen Analyzer. Crucible Research conducted analyses of the HIPed billet using ICP AES and a Leco Nitrogen-Oxygen Analyzer. Both units were comparable to NASA GRC equipment.

One sample was analyzed to determine the composition of the matrix and precipitates. A 1 g ammonium sulfate-1 g citric acid-100 ml H<sub>2</sub>O electrolyte solution was used to electrolytically dissolve away the Cu matrix. The precipitates were collected from the solution using a 0.1 μm filter paper. The precipitates and dissolved Cu matrix were chemically analyzed using ICP AES.

## Powder Particle Size Analysis

Since powder size generally correlates inversely with cooling rate (finer particles cool faster) and directly with precipitate size (quicker cooling inhibits precipitate growth), the average powder size and, as importantly, the powder size distribution may be key factors in determining the tensile properties of GRCop-84. To determine if the average powder size or the powder size distribution affected mechanical properties, four of the five powder lots used for the baseline small extrusions (designated 3B through 3E) were analyzed in more detail. A sample of the powder from the fifth powder lot (designated 3A) was not preserved by Crucible Research, so that lot could not be analyzed.

The powder was first sieved to –150 mesh under an argon atmosphere to produce standard starting powder used in most extruded and HIPed material. To determine the approximate powder size distribution, Crucible Research sieved a sample of each powder lot using 350, 300, 240, and 200 mesh sieves that correspond to openings of 45, 53, 63, and 75  $\mu\text{m}$ , respectively.

A more detailed powder size distribution analysis was conducted at Ricerca LLC in Painesville, Ohio. Powder samples from lots 3B through 3E were examined. Ricerca utilized a Horiba<sup>1</sup> LS-900 unit to determine the average powder size and the powder size distribution for each lot. Powder size distributions were done with and without ultrasonic agitation. Analysis of the results indicated that 2 min of agitation was required to overcome the tendency of the fine particles to stick to each other. Therefore, only results from ultrasonic agitation will be presented.

## Processing of GRCop-84 Specimens

GRCop-84 can be processed in many ways to produce fully-consolidated material suitable for use in main combustion chambers, injector face sheets and a variety of other components. This paper will concentrate on GRCop-84 specimens produced by Hot Isostatic Pressing (HIPing), extrusion, and extrusion plus rolling. Tensile properties of GRCop-84 produced by Vacuum Plasma Spraying (VPS) at NASA Marshall Space Flight Center have been reported by Holmes, Elam and others (Refs. 10 and 11). Limited results from tube drawing will also be included for completeness and to show the consistency of the GRCop-84 tensile properties.

The production details are given elsewhere (Refs. 7 and 12). Only an overview will be presented here. The GRCop-84 baselines for tensile properties are a series of small extrusions and a series of HIPed samples, both taken from the same five powder lots. The extrusions produced fifteen 2.8 cm (1.1 in.) bars. It was felt that these extruded bars represented the best consolidated microstructure that could be obtained because of their high reduction in area to ensure complete consolidation and their relatively fast cooling rate, which minimized grain growth and coarsening of the Cr<sub>2</sub>Nb precipitates. The HIPed specimens provide detailed information on the tensile properties of HIPed GRCop-84 including the variability that can be expected.

### Hot Isostatic Pressing (HIPing)

Five unique sixty-pound lots of GRCop-84 powder were produced independently to give five true repeats for determining the mechanical properties of the baseline HIPed and extruded GRCop-84. This allowed for considerable statistical analysis of the results. All of the GRCop-84 powder was sieved to –150 mesh (<106  $\mu\text{m}$ ). All production and handling was conducted either in vacuum or under high purity Ar gas to minimize the oxygen content of the powder.

For HIPing, the powder was placed in a 1020 carbon steel can nominally 8.4 cm diameter by 8.4 cm tall (3.3 in. diameter by 3.3 in. tall). The cans were filled with powder, evacuated, sealed and leak-checked to ensure a vacuum tight container. Each powder lot had three cans for a total of fifteen HIP cans.

---

<sup>1</sup>HORIBA Instruments, Inc. Headquarters, 17671 Armstrong Avenue, Irvine, California 92614, U.S.A.

The cans were HIPed at 954 °C (1750 °F) for 4 hr using a pressure of 207 MPa (30 ksi). The heating rate was 17 °C (30 °F) per minute. After the HIP cycle was completed the furnace was turned off, and the sample was allowed to free cool without the cooling rate being controlled.

## **Extrusion**

GRCop-84 can be directly consolidated from powder by hot extrusion. Full density is achieved during the extrusion process. Most of the extrusions used –150 mesh (<106 µm) powder. A limited number of specimens made from –270 mesh (<53 µm) powder normally used for VPS were also produced and tested for comparison with the VPS results.

Small extrusion cans (up to 20.3 cm diameter) were typically made from 1018 mild carbon steel to minimize the cost. For the large extrusions (38.4 cm diameter), the force required to extrude the cans would have exceeded the capacity of the extrusion press had steel been used. Instead, copper was substituted for steel to reduce the extrusion force required. All extrusion cans were filled with powder, evacuated, sealed and leak checked prior to extrusion. As with the HIPed material, all handling was conducted in vacuum or under high purity Ar gas to minimize oxidation.

Extrusion was conducted at 857 to 885 °C (1575 to 1625 °F) using a commercial extrusion press at HC Starck in Coldwater, Michigan. The extrusions' reductions in areas ranged from 29:1 for 15.2 cm (6 in.) diameter extrusion cans to 6.2:1 for the 38.4 cm (15.1 in.) diameter extrusion cans. No annealing or other heat treatments were conducted on the material after extrusion to remove any residual stresses.

The baseline small extrusions consisted of five unique –150 mesh powder lots that were the same as those used for the HIPed material. The powder lots were subdivided into thirds and placed into three separate 20.3 cm (6 in.) extrusion cans. These cans were extruded into 2.8 cm (1.1 in.) diameter bars. The –270 mesh powder was also extruded from a 20.3 cm can into a 2.8 cm bar using the same extrusion conditions.

The large extrusions were made from multiple powder lots loaded sequentially into the extrusion cans. Each powder lot was required to meet all chemistry specifications on its own, so the variability in the powder throughout the extrusion can was minimal. Depending upon the size of the extrusion can, up to twenty-four or more powder production runs could be required. The cans were extruded to bars with a 7.4 by 25.1 cm (2.9 by 9.9 in.) cross-section. These extrusions were subsequently rolled into plate and sheet except for samples taken to monitor the mechanical properties of the large extrusions and ensure good quality was achieved.

## **Commercial Rolling**

GRCop-84 is easily cold and warm worked. Traditional hot working is generally not suitable since NASA internal rolling development work showed that rolling GRCop-84 in the 857 to 885 °C (1575 to 1625 °F) temperature range significantly reduced the strength and creep resistance of GRCop-84.

Commercial warm rolling is done between 200 and 400 °C (392 to 752 °F). The pieces are reheated when its temperature drops below 200 °C as measured by a Cole-Parmer handheld IR pyrometer with laser sighting system. The emissivity of the samples was assumed to match that of copper oxide, and the internal values in the pyrometer for copper oxide were used.

Breakdown of the large extrusions was done using a 2-High mill at HC Starck in Euclid, Ohio. The mill was capable of producing finished plate between 0.3 and 2.5 cm (0.120 and 1 in.) thick. Thick sheet, typically 0.1 cm (0.04 in.) thick or thicker, was warm rolled on a 4-High mill using plate as the starting stock. Following warm rolling the plate and sheet were annealed to relieve any residual stresses. Initial results using 400 °C (792 °F) for 15 min. were not suitable, so an annealing study detailed later in this report was conducted, and a new annealing condition of 600 °C (1112 °F) for 30 min was established.

Besides the commercially warm-rolled material, small samples were rolled using a variety of processing parameters to determine the processing window and effects of processing parameters for warm rolling GRCop-84. The results of those tests are detailed elsewhere (Ref. 13) and are not repeated in this report.

Cold rolling of sheet was conducted at HC Starck using a 4-High Tension-Tension mill. The ends of the strip are grabbed and the entire strip pulled during rolling. The tension-tension mill produces thin sheet that is more consistent in thickness and requires less rolling force due to the introduction of a tensile stress in the rolling direction. The final thickness of the cold rolled sheet varied from 0.25 to 0.58 mm (0.010 to 0.023 in.). The thicknesses were selected based upon varying production needs for platelet liners that were supplied by Aerojet.

In addition, one trial specimen was rolled on a Sendzimir mill from 0.51 to 0.05 mm (0.020 to 0.002 in.) for a total cold reduction of 90 percent.

### **Tube Drawing**

Tube drawing was conducted by LeFiell Manufacturing of Sante Fe Springs, California to produce tubes nominally 9.5 mm o.d. by 1.0 mm wall (0.375 in. o.d. by 0.040 in. wall) up to 2.5 m (96 in.) long. Following a Design of Experiments and testing to establish the processing parameters to be used, a production run using the selected parameters was conducted that produced approximately 335 m (1100 ft) of high quality GRCo-84 tubing (Ref. 7).

### **Thermal Exposures**

During production and manufacturing, GRCo-84 may be subjected to several thermal cycles. The most likely ones are annealing between 400 and 600 °C and brazing or diffusion bonding between 935 and 1000 °C (1715 and 1832 °F). In addition, an observation was made by the University of California at Davis that a 600 °C thermal exposure for 24 hr improved the 500 °C (932 °F) creep properties of GRCo-84 sheet. GRCo-84 plate and sheet specimens were subjected to several long-term, high temperature thermal cycles to determine the effects of these heat treatments upon the alloy.

### **Annealing**

The annealing study was broken into two stages as is reported elsewhere (Ref. 14). In the first stage, 23 percent cold worked sheet scrap nominally 0.5 mm (0.023 in.) thick was subjected to thermal exposures at 250, 300, 350, 400, 425, 450, 475, 500, 550, 600, 650, 700, 750, 800, and 900 °C (482, 572, 662, 752, 797, 842, 887, 932, 1022, 1112, 1202, 1292, 1382, 1472, and 1652 °F) for 15, 30, 45, and 60 min to determine the hardness response curve of 23 percent cold worked GRCo-84 to various annealing conditions.

The hardness was measured with a New Age Digital ME-2 Rockwell hardness tester using the Rockwell B scale. The 0.5 mm thick sheet was sufficiently thick to prevent interaction between the ball and anvil during testing.

Once the results of the first stage were analyzed, 30 min was selected as the baseline annealing time. Tensile specimens were exposed at 200, 300, 400, 500, 600, 700, 800, 900, and 1000 °C (392, 572, 752, 932, 1112, 1292, 1472, 1652, and 1832 °F) and tested at room temperature to determine the changes in yield strength, ultimate tensile strength and tensile elongation.

### **Simulated Braze Cycles**

For a rocket engine application, one or more high temperature braze steps will be necessary to join the liner to the structural support jacket and attach manifolds and other hardware. The specifics of the processing vary by rocket engine and will be dependent upon many factors, but the engine companies have indicated that the brazes they favor for these applications are generally used between 935 and 1000 °C (1715 and 1832 °F). This is also a reasonable temperature range for diffusion bonding. Much higher brazing temperatures are unlikely due to the solidus of GRCo-84 being near 1080 °C (1976 °F).

TABLE 1.—LOW TEMPERATURE SIMULATED BRAZE THERMAL CYCLE

Step	Centigrade	Fahrenheit
1	RT to 538 °C at 5.6 °C/min	RT to 1000 °F at 10 °F/min
2	538 to 871 °C at 2.8 °C/min	1000 to 1600 °F at 5 °F/min
3	871 to 935 °C at 1.7 °C/min	1600 to 1715 °F at 3 °F/min
4	Hold at 935±8 °C for 22.5±2.5 min	Hold at 1715 °F±15 °F for 22.5±2.5 min
5	935 to 871 °C at 1.7 °C/min	1715 to 1600 °F at 3 °F/min
6	871 to 538 °C at 2.8 °C/min	1600 to 1000 °F at 5 °F/min
7	538 °C to RT free cool	1000 °F to RT free cool

TABLE 2.—HIGH TEMPERATURE SIMULATED BRAZE THERMAL CYCLE

Step	Centigrade	Fahrenheit
1	RT to 538 °C at 5.6 °C/min	RT to 1000 at 10 °F/min
2	538 to 871 °C at 2.8 °C/min	1000 to 1600 °F at 5 °F/min
3	871 to 1000 °C at 1.7 °C/min	1600 to 1832 °F at 3 °F/min
4	Hold at 1000±5 °C for 22.5±2.5 min	Hold at 1832±10 °F for 22.5±2.5 min
5	1000 to 871 °C at 1.7 °C/min	1832 to 1600 °F at 3 °F/min
6	871 to 538 °C at 2.8 °C/min	1600 to 1000 °F at 5 °F/min
7	538°C to RT free cool	1000 to RT free cool

Two braze cycles were examined. They are listed in Tables 1 and 2. While the specimens could have been heated and cooled much faster, heating and cooling rates representative of a liner were chosen in an effort to mimic the actual likely braze cycle as closely as possible. No braze alloy was used to join pieces together in these trials. The samples only represent the changes in tensile properties that will occur in the base metal during a braze or diffusion bonding cycle. These results are representative of the bulk properties of the liner outside of the braze joint.

The simulated braze cycles were conducted in a vacuum furnace. The vacuum was typically <6.7 mPa (<5×10<sup>-5</sup> torr). The pressure in the chamber increased slightly with temperature due in part to the evaporation of Cu and Cr but never exceeded 13.4 mPa (1×10<sup>-4</sup> torr). The partial pressure of oxygen was always sufficiently low that no oxidation was observed. The samples were loosely shielded with tantalum foil to minimize the deposition of Cu and Cr onto the cool portions of the vacuum chamber.

A multistep programmable controller was used to control the temperature during the simulated-braze thermal cycle. Typically ten to twenty-five samples were heat treated together to minimize cycle-to-cycle variability in the heat treatments. Tungsten resistance heaters inside the furnace surrounded the samples and provided a uniform (±5 °C) hot zone approximately 10.1 cm high by 10.1 cm wide by 20.2 cm deep (4 by 4 by 8 in.). A control thermocouple was placed on the samples near the center. The thermocouple was in intimate contact with the middle sample during the thermal cycle and was considered representative of all specimens within the hot zone.

### End of Life Exposure

The anticipated life of a GRCop-84 liner for the RLV Second Generation Program was to be 500 missions, and each mission was assumed to be comparable to the current Space Shuttle mission. The total time accumulated on the liner would be 75 hr assuming a 9 min mission. Taking into account certification tests and a growth margin, a tentative life of 100 hr was assumed. The hot wall temperature was assumed to not exceed 500 °C (932 °F) based on the RS-83 program information available at the time.

A set of GRCop-84 samples were exposed for 100 hr at 500 °C. The samples were placed in commercially available Sen/Pak<sup>2</sup> heat treating envelopes to minimize oxidation. The envelopes were made from high chromium steel that acts to getter the oxygen inside the envelope. The envelopes were back-filled with argon to displace the air and sealed. Nitrogen was flowed into the box furnace used for

<sup>2</sup>Sentry Company, 62 Main St, Foxboro, MA 02035

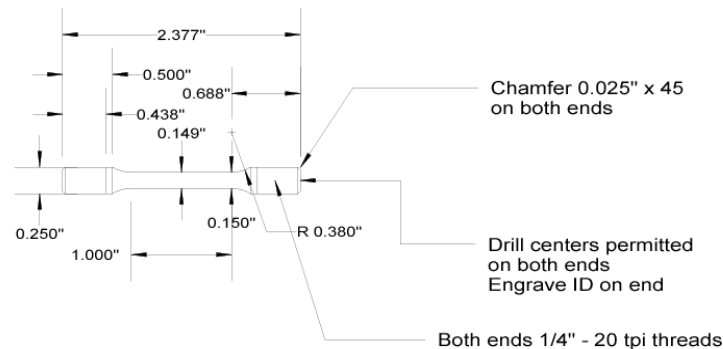
the exposure at a rate of 1 SCFM (28.3 LPM) to further reduce the oxygen partial pressure within the furnace and minimize oxidation. After the thermal exposure, a thin, adherent black oxide layer was observed on the surface. This oxide layer did not affect the results of the testing.

### Long-Term, High Temperature Exposures to Improve Creep Resistance

Creep properties of rolled GRCo-84 plate and sheet were generally inferior to that of extruded GRCo-84. One possible cause of this is the smaller grain size for recrystallized GRCo-84 annealed at 600 °C (Ref. 14). In an attempt to increase the grain size and restore the creep resistance of rolled GRCo-84, selected samples of plate and sheet were exposed to high temperatures for extended periods. In concert with the creep testing detailed elsewhere in this final report (Ref. 15), samples were tensile tested at 500 °C (932 °F), the same temperature at which the creep tests were conducted. Specimens from the 6.5 mm (0.25 in.) plate, 0.43 mm (0.017 in.) sheet and 0.58 mm (0.023 in.) sheet were heat treated at 600, 900, and 1000 °C (1112, 1652, and 1832 °F) for 1000 and 3000 min. In addition, specimens were heat treated for 100 and 300 min at 1000 °C.

### Tensile Testing

The round and sheet tensile test specimen designs are shown in Figure 1. Both conform to ASTM E8 (Ref. 16) and were found to give good results with failures consistently occurring at or near the center of the samples. For the sheet samples, some samples were reinforced in the region of the holes to prevent pullout by the pins. To reinforce the hole, stainless steel squares the width of the samples with a hole the same diameter as the specimen's hole were spot welded to the grip section.

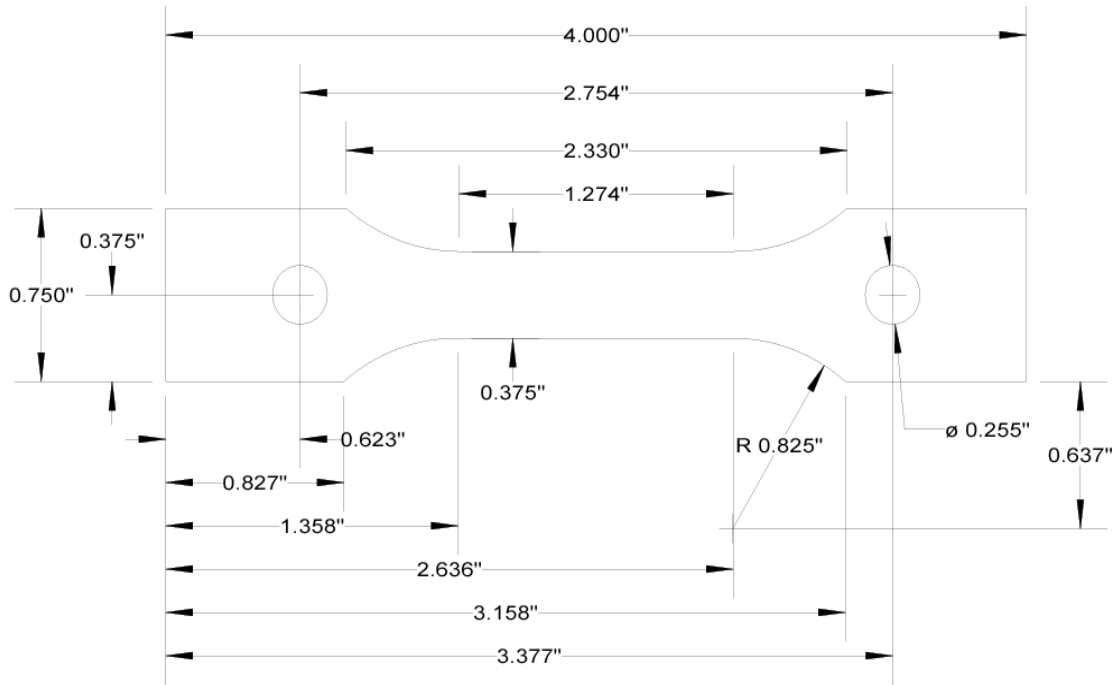


**NOTES:**

1. Scale = 1:1
2. Sample surfaces to be low stress ground or equivalent
3. Surface finish to be 32 RMS or finer (16 RMS desired)
4. Center of reduced section must be 0.149" +/- 0.001" diameter and taper up to 0.150" at the transition radii.
5. Ends of reduced section to be no more than 0.151" diameter maximum and no less than the diameter at the center of the reduced section
6. Threads may NOT extend into radii
7. Do NOT undercut radii
8. Threads and reduced sections to be concentric to within 0.002"
9. Sample ID to be engraved on at least one end
10. Radii at transition from threads to smooth section not critical

Drawing 7.3.6B  
 RLV Cu-8 Cr-4 Nb Specimen Design 6B  
 Modified Room And Elevated Temperature Tensile  
 David Ellis 216-433-8736 02/06/2004

Figure 1(a).—Typical round tensile test specimen design.



SCALE = 2:1

## Sheet Tensile Test Specimen

Figure 1(b).—Typical sheet tensile test specimen design.

Tensile testing was conducted using strain rate control. All tensile tests were conducted on Instron TT and 1125 series load frames upgraded using MTS hardware and Testworks 4 data acquisition and control software. The load frames used for room temperature and argon atmosphere elevated temperature tensile testing are shown in Figure 2.

The standard strain rate selected was  $8.3 \times 10^{-5}$  per second. To examine the strain rate sensitivity of GRCop-84, tests were conducted at room temperature and 400 °C (752 °F) using nominal strain rates of  $2.8 \times 10^{-5}$ ,  $8.3 \times 10^{-5}$ ,  $8.3 \times 10^{-4}$ , and  $8.3 \times 10^{-3}$  per second on annealed and 47 percent cold rolled sheet samples. Tensile testing of the tubes was conducted at a strain rate of 0.002 per second.

An extensometer was used for all air and argon atmosphere testing. The data from the extensometer was used for monitoring and controlling the strain rate during the test. At room temperature, an MTS Model 632.31E-24 clip-on extensometer with a 1.27 cm (0.5 in.) gauge length was used for all tests except the tubing. The tubing tensile tests used an MTS Model 632.31 extensometer with a 2.5 cm (1 in.) gauge length. For elevated temperature tensile testing, an MTS Model 632.59B-04 high temperature water-cooled extensometer was used (Fig. 3). The water-cooled extensometer had a 1.27 cm gauge length between the alumina probes. While the extensometers are capable of 20 percent strain, they were removed at 15 percent strain to prevent damage. Above 15 percent strain, the crosshead movement was used to determine and control the strain rate. At this point almost all samples were past the uniform deformation stage and well into the necking regime, so the change in control did not affect the yield strength or UTS.

For elevated temperature tensile testing, a Thermo Pro Model SN1G-0819M three zone resistance heating furnace was used to heat the samples, grips and several inches of the pull rod. The uniform hot zone typically extended 5 cm (2 in.) or more above and below the sample based upon the furnace temperature profile. Alumina fiberboard was placed on the top and bottom of the furnace, and insulation was packed around the pull rods to insulate the top and bottom of the furnace cavity. To minimize oxidation, argon was flowed into the furnace cavity during heating, testing and cool down. The flow rate was at least 0.2 lpm.



(a) Instron TT Series Load Frame



(b) Instron 1125 Load Frames

Figure 2.—Tensile test frames used for air and argon elevated temperature testing.

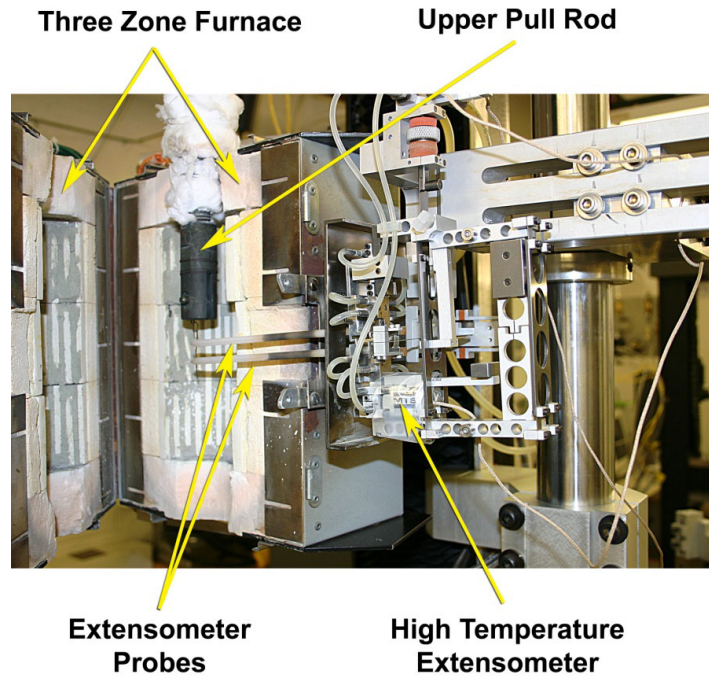


Figure 3.—High temperature extensometer.

The temperature of the specimen was measured using three 316 stainless steel sheathed type K thermocouple tied to the sample at the top, middle and bottom of the gauge section. A calibrated Doric thermocouple readout was used to visually monitor the sample temperature. The samples were heated at a rate of at least 1000 °C/h (1800 °F/h), allowed to stabilize at temperature over a period of less than 5 min and then tensile tested. The observed temperature gradients were less than 10 °C (18 °F) along the length of the reduced gauge section. The center of the specimen was held at the test temperature  $\pm 2$  °C (4 °F) throughout the test.

Data points were recorded every 0.01 percent strain during the test to generate the stress-strain curve. Results were provided as a Microsoft Excel (Microsoft Corporation) spreadsheet. The Testworks 4 software was also used to remove the slack from the test results and determine the 0.2 percent offset yield and ultimate tensile strengths. The elastic modulus is not reported because the extensometers used did not allow sufficiently high resolution over the first few tenths of a percent strain to provide the desired level of accuracy.

In addition to room and elevated-temperature testing, limited cryogenic tensile testing was conducted at NASA MSFC on baseline extruded GRCop-84. A standard 12.8 mm (0.505 in.) diameter gauge section bar again conforming to ASTM E8 (Ref. 16) (Fig. 4) was used for the cryogenic tensile tests. Testing was conducted in liquid nitrogen ( $-196$  °C/ $-321$  °F) and liquid hydrogen ( $-253$  °C/ $-423$  °F) by submersing the sample, fixtures and extensometer in the cryogenic fluid. After the sample was completely chilled to the center, the tests were conducted in a strain rate control mode using the standard strain rate of  $8.3 \times 10^{-5}$  per second.

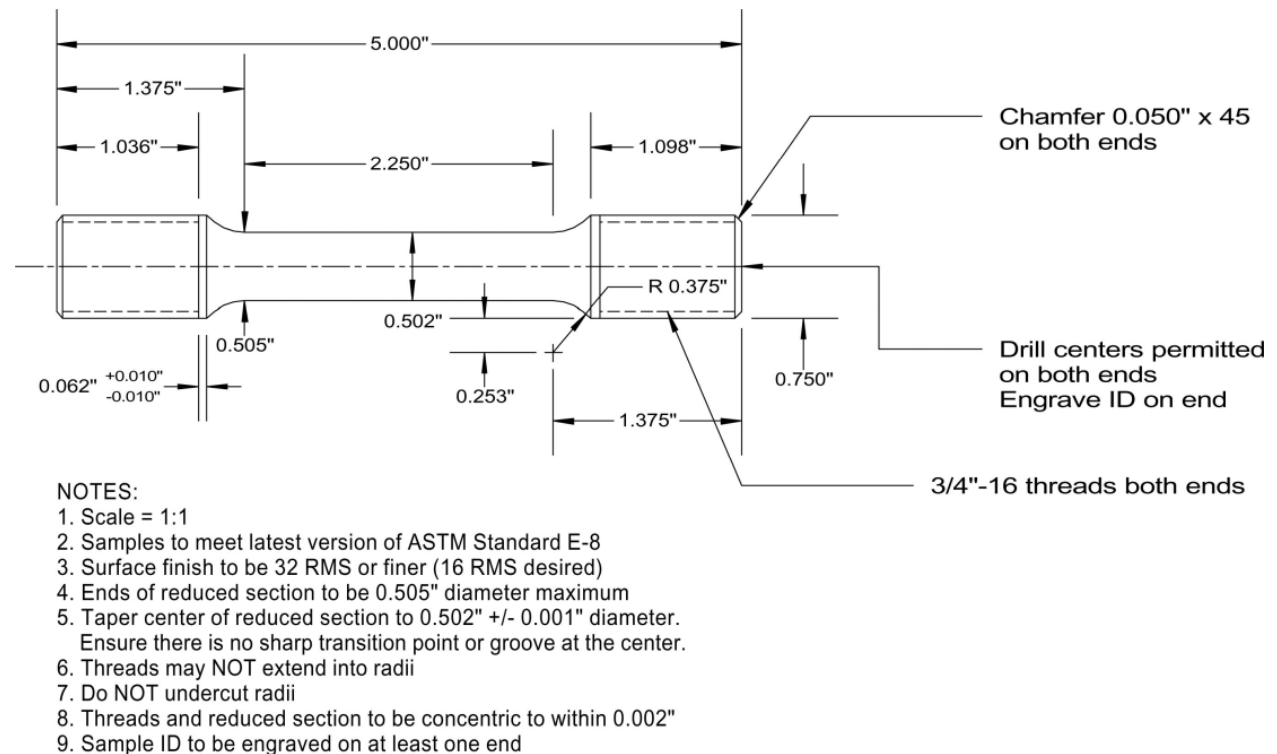


Figure 4.—Round specimen design for cryogenic tensile testing.

Limited testing of 58  $\mu\text{m}$  (0.0023 in.) thick GRCop-84 foil was also conducted. The same specimen design as shown in Figure 1(b) was used except the holes in the grip sections were removed. Hydraulic grips replaced the pin and clevis arrangement to hold the ends of the sample for room temperature testing. The clip-on extensometer was used for some but not all room temperature tensile tests because it was initially thought that the weight of the extensometer and the knife edges would tear or otherwise damage the sample.

For elevated-temperature testing, the foil sample had to be tested in vacuum to prevent complete oxidation of the foil during heating. To do this testing, the modified Instron TT series load frame shown in Figure 5 was used. The frame had the same upgrades to the control and data acquisition hardware and software as the other load frames. The test section including the furnace and specimen was encapsulated in a stainless steel vacuum chamber. Prior to heating the sample, a vacuum was established within the chamber that prevented oxidation.

The sample was heated using a solid tantalum heater that surrounded the sample and grips. The heater provided a uniform hot section approximately 150 mm (6 in.) in length. This allowed heating of the grips as well as the sample and minimized the thermal gradient. The chamber design did not allow the use of an extensometer in the tests. Instead, the movement of the crosshead and the initial gauge length were used to calculate the strain. Strain control was again used as the control mode even though it was realized that the accuracy of the control was degraded without the extensometer. The strain rate again was set to  $8.3 \times 10^{-5}$  per second.

The samples were gripped by bolting two flat plates together with the foil specimen sandwiched between the plates. The plates and attachments that allowed them to be attached to the pull rods were machined to center the foil and ensure uniaxial loading.

Prior to heating the sample, the chamber pressure was reduced to less than 7 mPa ( $5 \times 10^{-5}$  torr). The sample was heated at a rate of at least 1000  $^{\circ}\text{C}/\text{h}$  (1800  $^{\circ}\text{F}/\text{h}$ ) to the test temperature of 500  $^{\circ}\text{C}$ . As much of the load train below the specimen as possible was supported with the crosshead to prevent creep and premature failure of the foil samples. Once the temperature stabilized, usually within 5 min, the sample was tested in strain rate control.

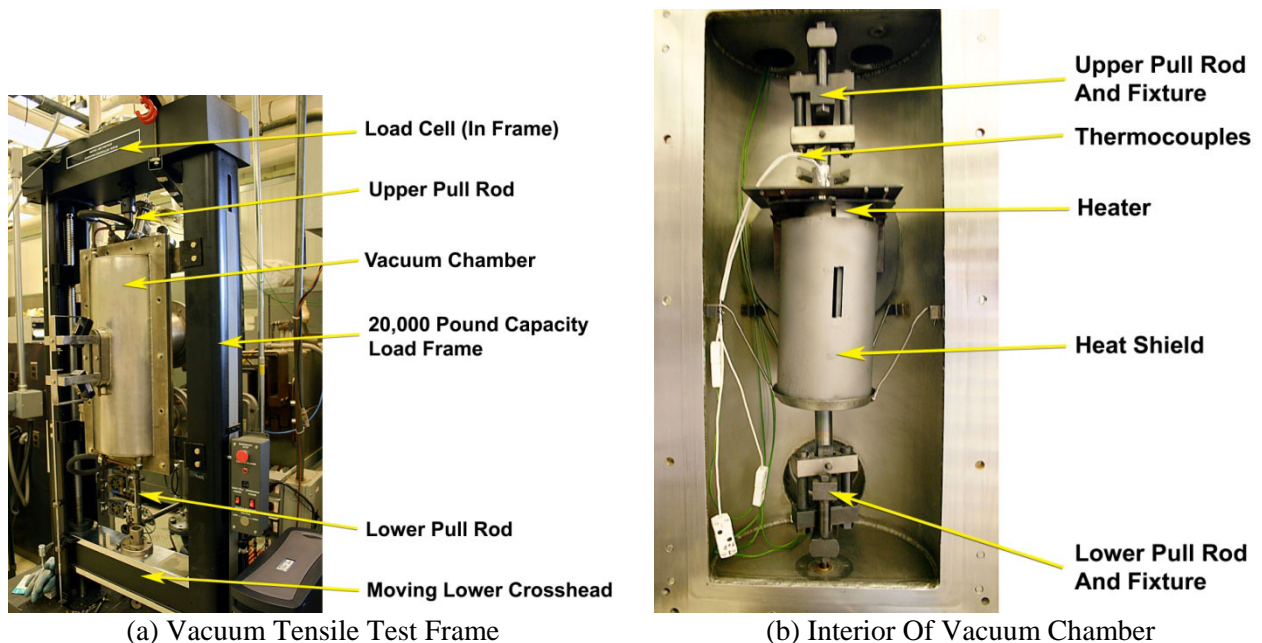


Figure 5.—Vacuum tensile test unit.

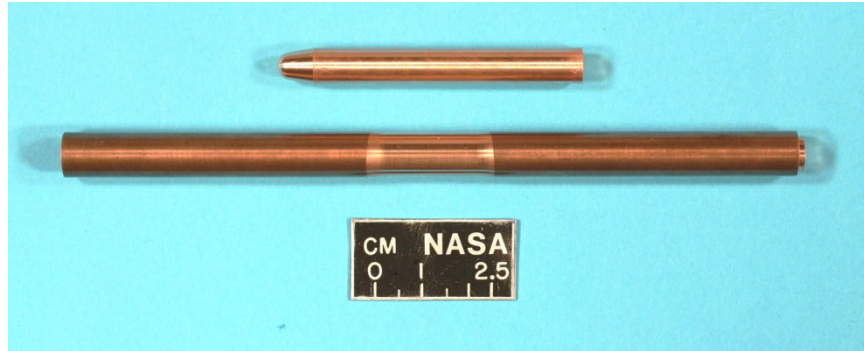


Figure 6.—Typical tubing tensile test specimen.

Tube testing presented issues since the tubing had to be gripped without crushing the ends and the center of the specimens had to have a reduced gauge section to prevent failure near the collets used to grip the specimens. Testing was limited to room temperature because of the fixturing used to grip the specimens. Room temperature testing also served to accentuate any differences in the annealing temperature. Samples approximately 152 mm (6 in.) long were cut from randomly selected tubes. A 25.4 mm (1 in.) long reduced section was created by removing 0.6 mm (0.02 in.) from the o.d. A smooth transition was provided to the ends. Solid copper bars were inserted into the i.d. to support the tubing and prevent crushing when the ends were gripped for tensile testing. A typical specimen and grip insert are shown in Figure 6.

Tube tensile testing was conducted at NASA GRC. The tensile tests were loaded in strain control at a strain rate of  $0.002 \text{ s}^{-1}$ . A 25 mm gage length clip-on extensometer was fixed to the reduced gage to provide strain data. At a strain value of 15 percent, the specimen was unloaded to zero load, the extensometer removed and the specimen reloaded in displacement control until failure occurred. The strain for the reload was calculated by converting displacement to strain using a calibration calculated in the original strain-controlled section.

## Results

The results of the testing are given below.

## Chemistry

The chemistry of the GRCop-84 was very well controlled by Crucible Research and did not vary much from powder lot to powder lot. As a result, all of the samples tested had essentially the same chemistry even though they were produced over several years of work. The range of chemistries is given in Table 3.

In addition to the primary alloying elements, Fe and O concentrations were controlled. Both elements can adversely affect the thermal conductivity of Cu and GRCop-84 (Refs. 17 and 18). Most of the powder and consolidated products had O contents in the 400 to 450 ppm range. Fe varied over time because there was a deliberate change in the Cr melt stock to reduce its level. Early material such as the baseline small extrusions had Fe contents in the 150 to 240 ppm range while later material such as the large extrusions and the plate and sheet made from them had Fe levels in the <20 to 60 ppm range. It is believed that the small change in Fe did not affect the mechanical properties since there were no detectable differences in similar product before and after the change.

No other elements were detected using the ICP AES when the sample was scanned for trace contaminants. From this, it was concluded that there was minimal contamination from the refractories used to melt the GRCop-84 or from the starting stock.

TABLE 3.—CHEMISTRY RANGE  
FOR GRCoP-84

Element	Minimum, wt. %	Maximum, wt. %
Cu	Bal.	
Cr	6.53	6.72
Nb	5.64	5.82
O	242 ppm	741 ppm
Fe	<20 ppm	240 ppm

TABLE 4.—CHEMISTRY OF GRCoP-84  
MATRIX AND PRECIPITATES

Element	Matrix, wt. %/at. %	Precipitate, wt. %/at. %
Cu	100/100	47.7/48.7
Cr	0/0	27.2/33.9
Nb	0/0	25.0/17.4
Cr:Nb	N/A	1.09/1.94

TABLE 5.—AVERAGE PARTICLE SIZE  
AND STANDARD DEVIATIONS

Powder lot	Mean diameter, μm	Standard deviation, μm
3B	30.3	22.4
3C	41.9	30.6
3D	42.8	33.8
3E	36.3	29.7

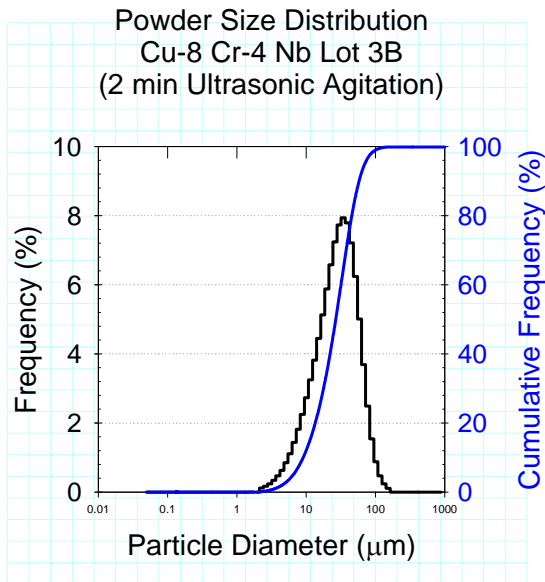
The results from the precipitate extraction sample which contains primarily Cr<sub>2</sub>Nb particles are presented in Table 4. The analysis shows that the matrix is essentially pure Cu. At the limits of detectability for the ICP AES unit, there were no Cr, Nb or other elements detected. The extracted precipitates show a substantial amount of Cu, but this is caused by the incomplete dissolution of the Cu matrix rather than the incorporation of Cu into the precipitates. If the extraction is run longer to remove the Cu coating from the precipitates, the precipitates are dissolved. This represented the best compromise achieved for dissolving the matrix and retaining the precipitates in the extraction process.

The atomic Cr to Nb ratio for the precipitates is near 2, the stoichiometric value for Cr<sub>2</sub>Nb and well within the compositional range for Cr<sub>2</sub>Nb (Ref. 19). The slightly lower value of 1.94 likely reflects the small amount of extra Cr added to the alloy for hydrogen embrittlement resistance that drives the Cr<sub>2</sub>Nb composition to the Cr-rich limit (Ref. 20). It may also reflect some of the fine Cr precipitates that are present in GRCoP-84. As will be shown, the nearly pure Cu matrix and hard Cr<sub>2</sub>Nb precipitates leads to GRCoP-84 sharing some characteristics with both pure copper (annealing behavior, ductility) and particulate reinforced composites (high strength, limited grain growth).

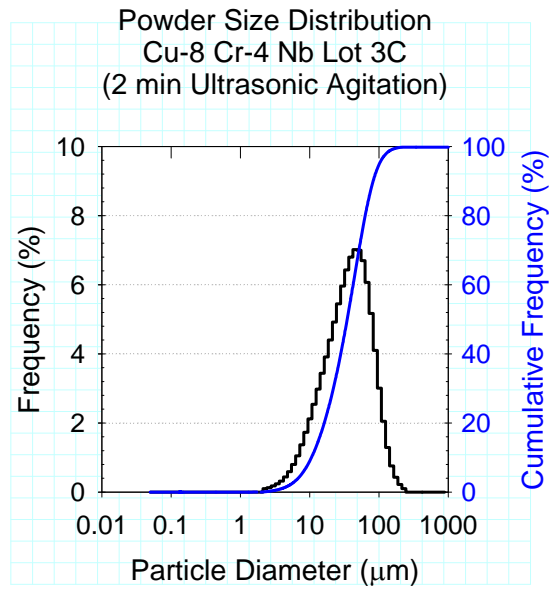
### Powder Size Distributions

The results of the powder sieve analyses provided by Crucible Research showed that over 70 percent of the powder particles were finer than 45 μm in diameter (–325 mesh). However, because so much of the powder was finer than the smallest sieve opening, these size distributions were not useful for determining the details of the powder sizes and their distributions. This led to the need to do a more detailed particle size analysis.

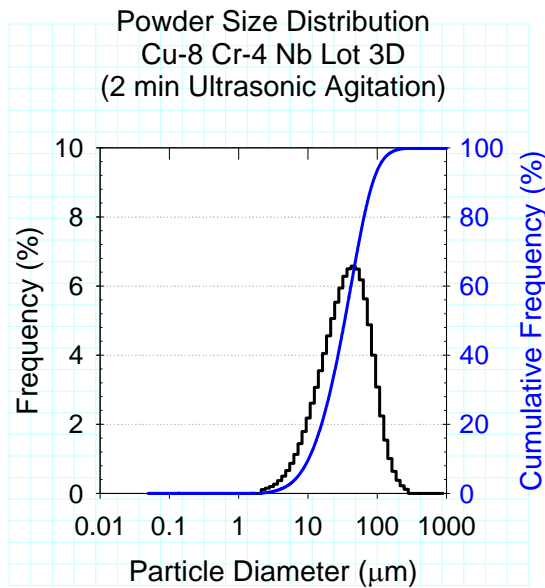
The average particle sizes as determined by Ricerca are shown in Table 5. The standard deviations of the powder sizes as reported by the Horiba unit are also reported. Mean particle sizes ranged from 30.3 to 42.8 μm. The individual particle size distributions for the four powder lots tested are given in Figure 7. All four powder lots exhibit typical log normal size distributions.



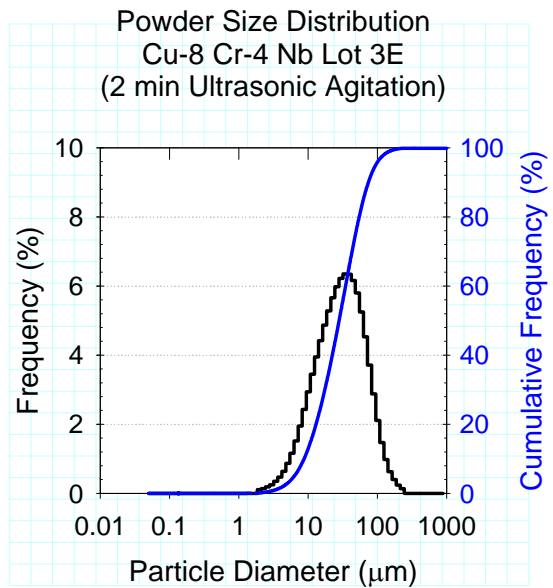
(a) Powder Lot 3B



(b) Powder Lot 3C



(c) Powder Lot 3D

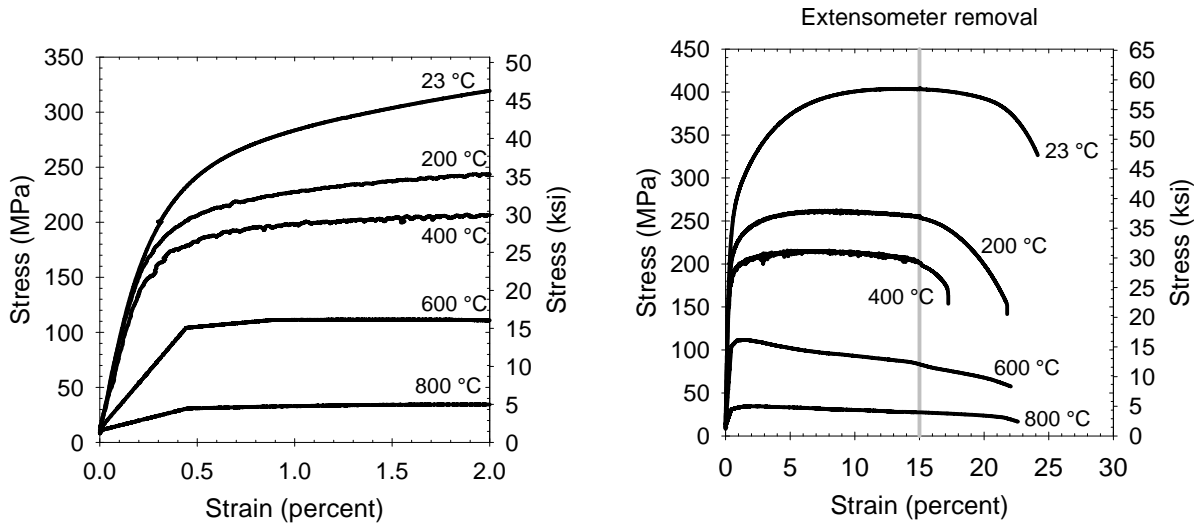


(d) Powder Lot 3E

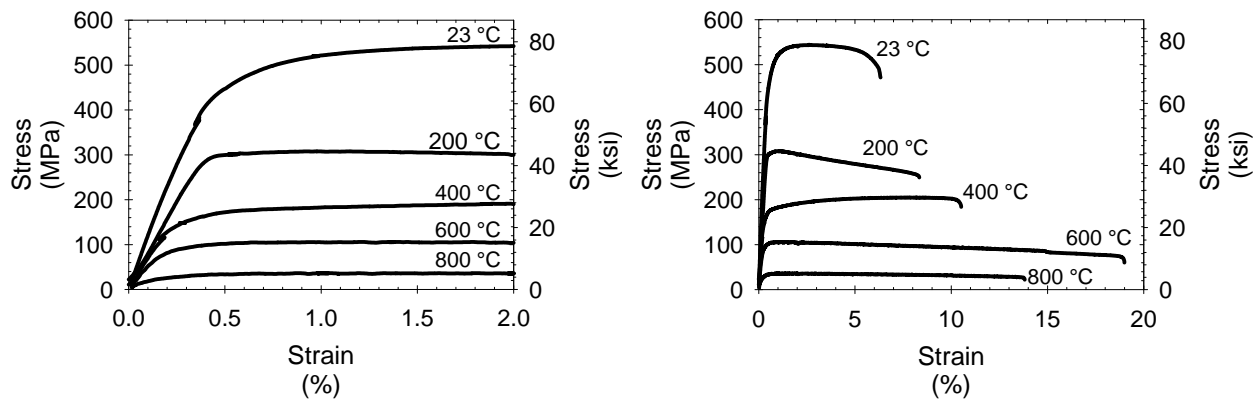
Figure 7.—Baseline particle size distributions.

## Stress-Strain Behavior

All GRCop-84 samples exhibited very similar stress-strain behavior regardless of the pedigree or heat-treatment. Typical stress-strain curves are shown in Figure 8. GRCop-84 has a minimal elastic region and quickly exhibits plastic deformation in the as-extruded, annealed and brazed conditions. Only cold-worked material shows any appreciable elastic region, and even that is limited as shown in Figure 8(b). After yielding GRCop-84 quickly reaches a stress near that of the ultimate tensile strength and remains at that level as considerable uniform plastic deformation occurs, typically 10 to 20 percent elongation prior to necking for samples without cold work. Once necking begins, the samples typically exhibit another 5 to 15 percent elongation prior to failure.



(a) Typical as-extruded GRCop-84 stress-strain curves with detail of 0 to 2 percent strain range  
(Also typical in shape for any annealed or brazed GRCop-84 regardless of form)



(b) Typical cold worked GRCop-84 stress-strain curves with detail of 0 to 2 percent strain range  
(All samples cold worked 47 percent)

Figure 8.—Typical GRCop-84 stress-strain curves at several temperatures.

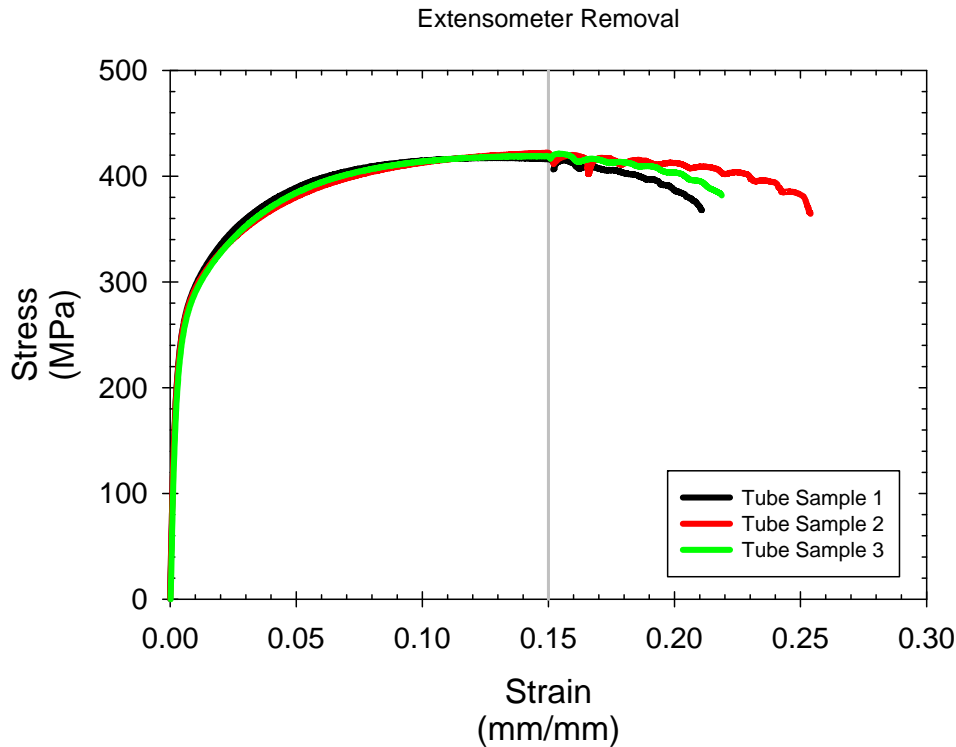


Figure 9.—Tube specimen room temperature stress-strain curves.  
(Strain rate = 0.002/sec)

Even heavily cold-worked samples typically show several percent uniform plastic deformation prior to necking and failure at room temperature. At elevated temperatures, they show behavior identical to annealed samples if the test temperature is sufficient to cause annealing. This typically occurs between 200 °C (392 °F) for heavily cold-worked samples and 600 °C (1112 °F) for minimally cold-worked samples. All samples tested above 600 °C exhibit the same tensile properties regardless of prior cold work.

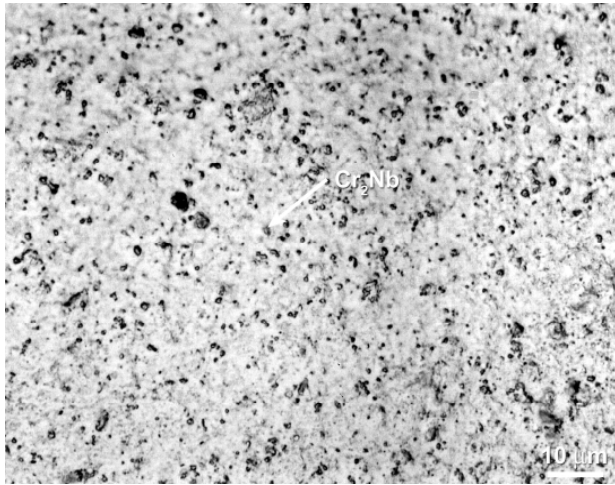
The stress-strain curves for the three production tubing samples tested at room temperature are shown in Figure 9. The results proved to be highly reproducible and consistent in form with the other specimens tested. The specimen design appeared to give very good results.

### **Baseline As-HIPed and As-Extruded GRCop-84**

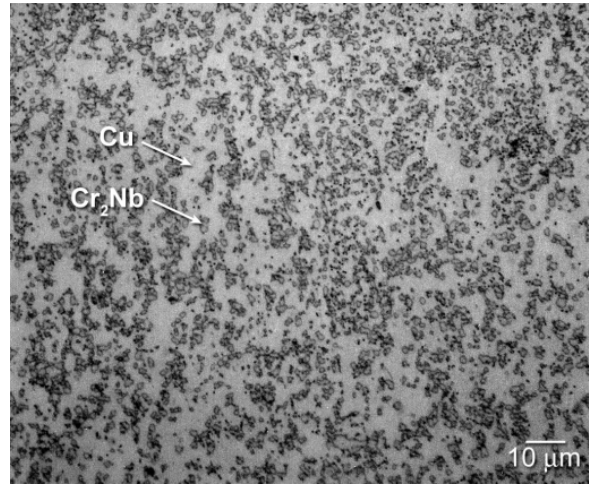
The baselines for the GRCop-84 tensile properties are the data sets generated under the RLV Focused program. The data were from powder extruded into bars or HIPed into a solid cylinder.

Typical optical micrographs of the as-extruded and as-HIPed specimens are shown in Figure 10. The samples show a good macroscopic distribution of Cr<sub>2</sub>Nb, but there are definitely variations of Cr<sub>2</sub>Nb volume fraction on a microscopic (~10 μm) scale. This is most likely related to the small variations in composition from powder particle to powder particle. The Cr<sub>2</sub>Nb particles seen in the optical micrographs tend to be agglomerations of smaller Cr<sub>2</sub>Nb particles that occur when the Cr<sub>2</sub>Nb precipitates in the liquid Cu (Ref. 21). Careful examination can reveal the presence of the smaller particles.

Typical SEM microstructures for as-extruded and as-HIPed GRCop-84 specimens are shown in Figure 11. The agglomerations are more easily seen in these micrographs. The banding of the Cr<sub>2</sub>Nb particles in the as-extruded specimens occurred as the particles were deformed and elongated in the extrusion direction during the extrusion process. The result was stringers of Cr<sub>2</sub>Nb. These stringers are coaxial with the test direction for the baseline as-extruded GRCop-84 tensile specimens.

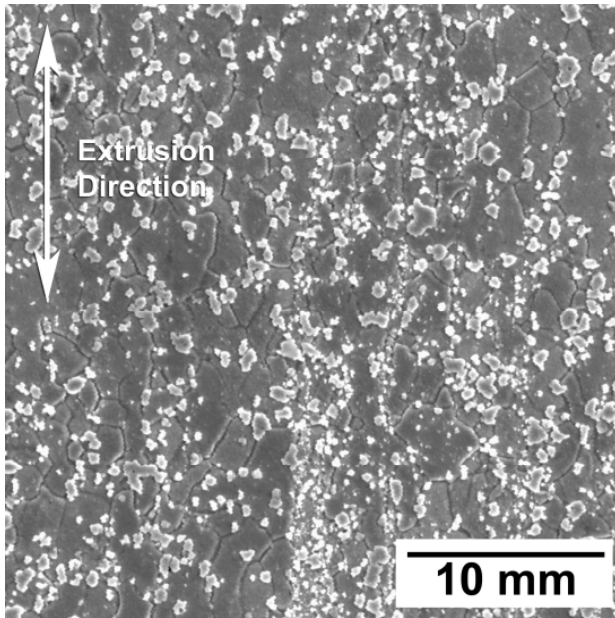


(a) As-Extruded  
(Extrusion direction perpendicular to page)

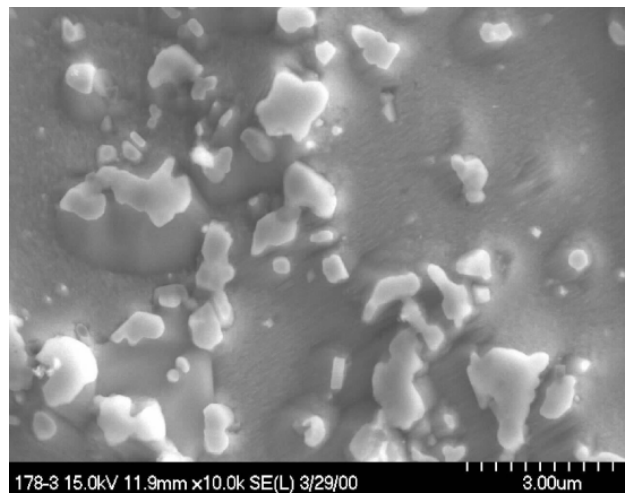


(b) As-HIPed

Figure 10.—Typical optical micrographs.



(a) As-Extruded



(b) As-HIPed

Figure 11.—Typical SEM micrographs.

While the HIP conditions did generally provide complete consolidation, there were some HIP cans that exhibited either leakage or trapped gases. The microstructure from those cans had porosity (Fig. 12) that was not seen in the extruded or well HIPed material. The data sets were culled to eliminate samples with known porosity problems, but there may have still been some samples with varying levels of porosity left in the data set. This porosity may help explain the lower high temperature elongation of the HIPed material.

Figure 12 also shows a prior powder boundary (PPB). In contrast to the extruded GRCo-84, PPBs are not broken up during the HIP process. They could act as sites for crack initiation in low cycle fatigue though they were not observed to do so during testing (Ref. 22). If the material is worked after consolidation by rolling, metal spinning or drawing, the PPBs will likely be broken up and not present any problem.

GRCo-84 is strengthened by a combination of fine grain size through a Hall-Petch type of strengthening mechanism and Orowan strengthening (Ref. 23). The grain size is controlled by the larger  $\text{Cr}_2\text{Nb}$  particles while the smaller particles pin dislocations. Some elemental Cr is also observed in the alloy due to the excess added to control hydrogen embrittlement. An example of individual  $\text{Cr}_2\text{Nb}$  and Cr particles observed using transmission electron microscopy is shown in Figure 13. The  $\text{Cr}_2\text{Nb}$  particles have heavily faulted Laves phase structures. Their high hardness (~2000 KHN) far exceeds the surrounding Cu matrix (Ref. 21). That makes them very effective at pinning both dislocations and grain boundaries.

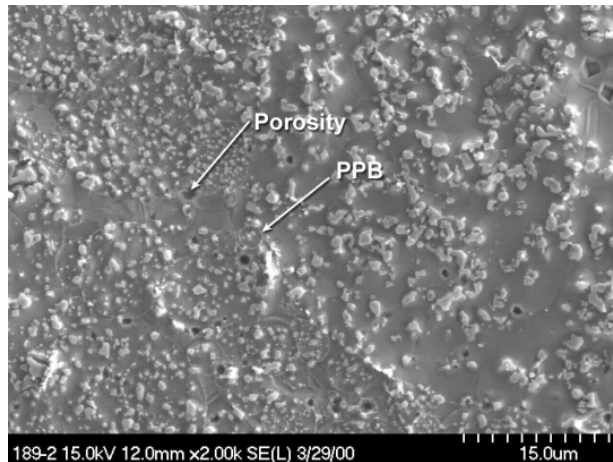


Figure 12.—Observed porosity in as-HIPed GRCo-84 caused by can leakage or trapped gas and prior particle boundary (PPB).

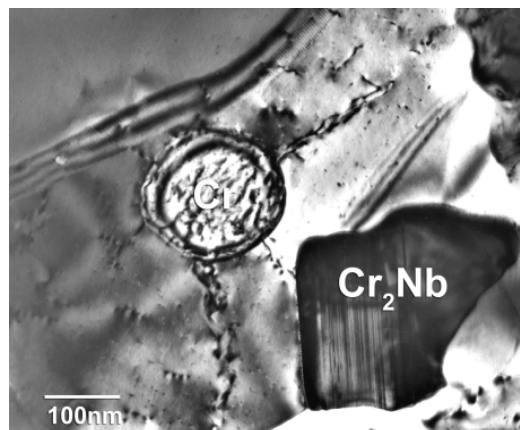


Figure 13.—TEM image of individual elemental Cr and  $\text{Cr}_2\text{Nb}$  particles.

Figure 14 shows the effect of temperature on the baseline tensile properties of extruded GRCo-84. The results of cryogenic testing at NASA MSFC are included as well as the results from room and elevated temperature tensile tests conducted at NASA GRC. Regression analysis requires that the temperatures be converted to absolute temperature, so Kelvin is used for the X-axis rather than Celsius.

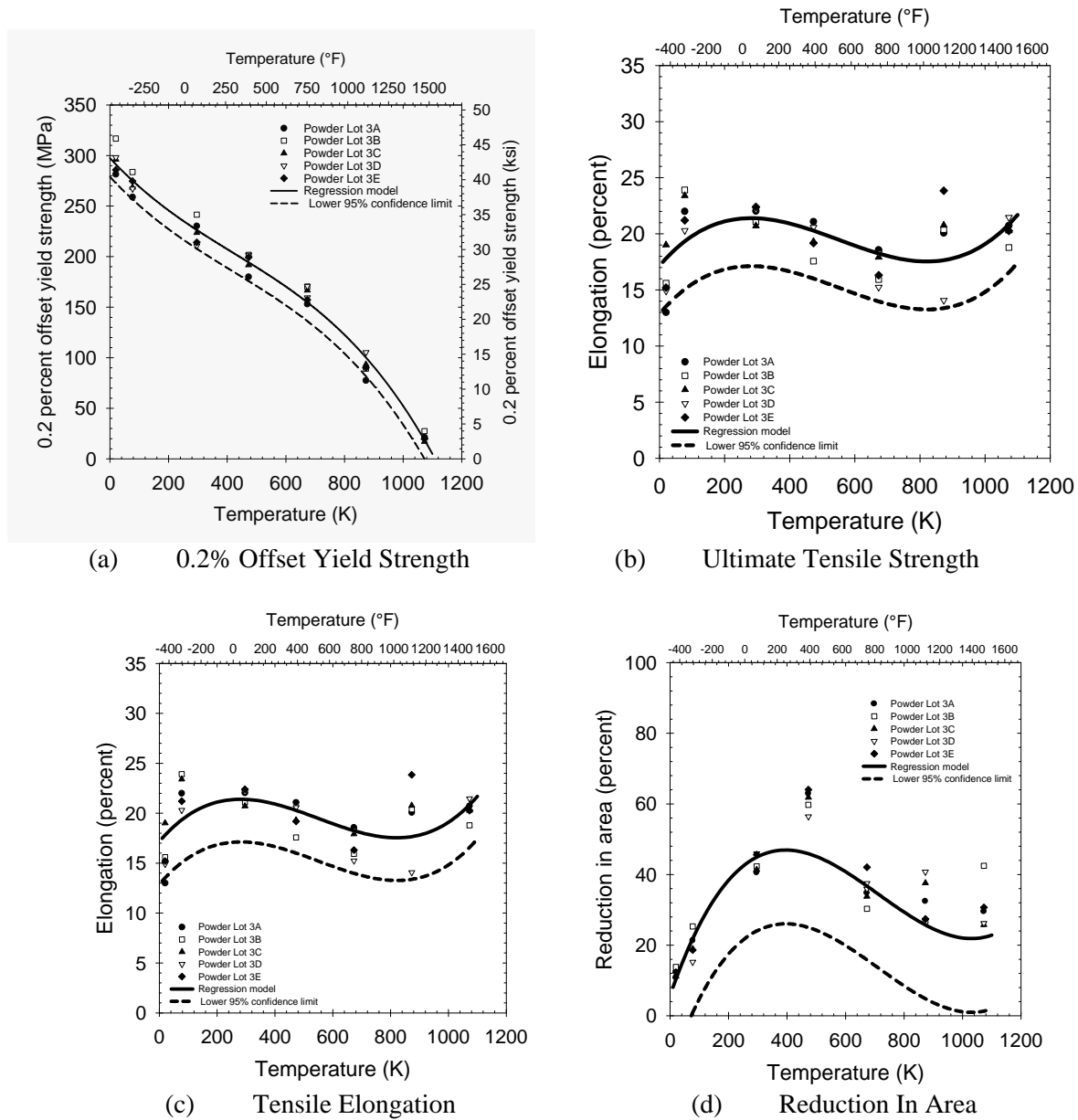


Figure 14.—Baseline tensile properties of extruded GRCo-84 with lower 95 percent confidence intervals.

Figure 15 shows the effect of temperature on the baseline tensile properties of HIPed GRCop-84. No cryogenic tensile data was available for HIPed material due to insufficient HIPed material for that testing.

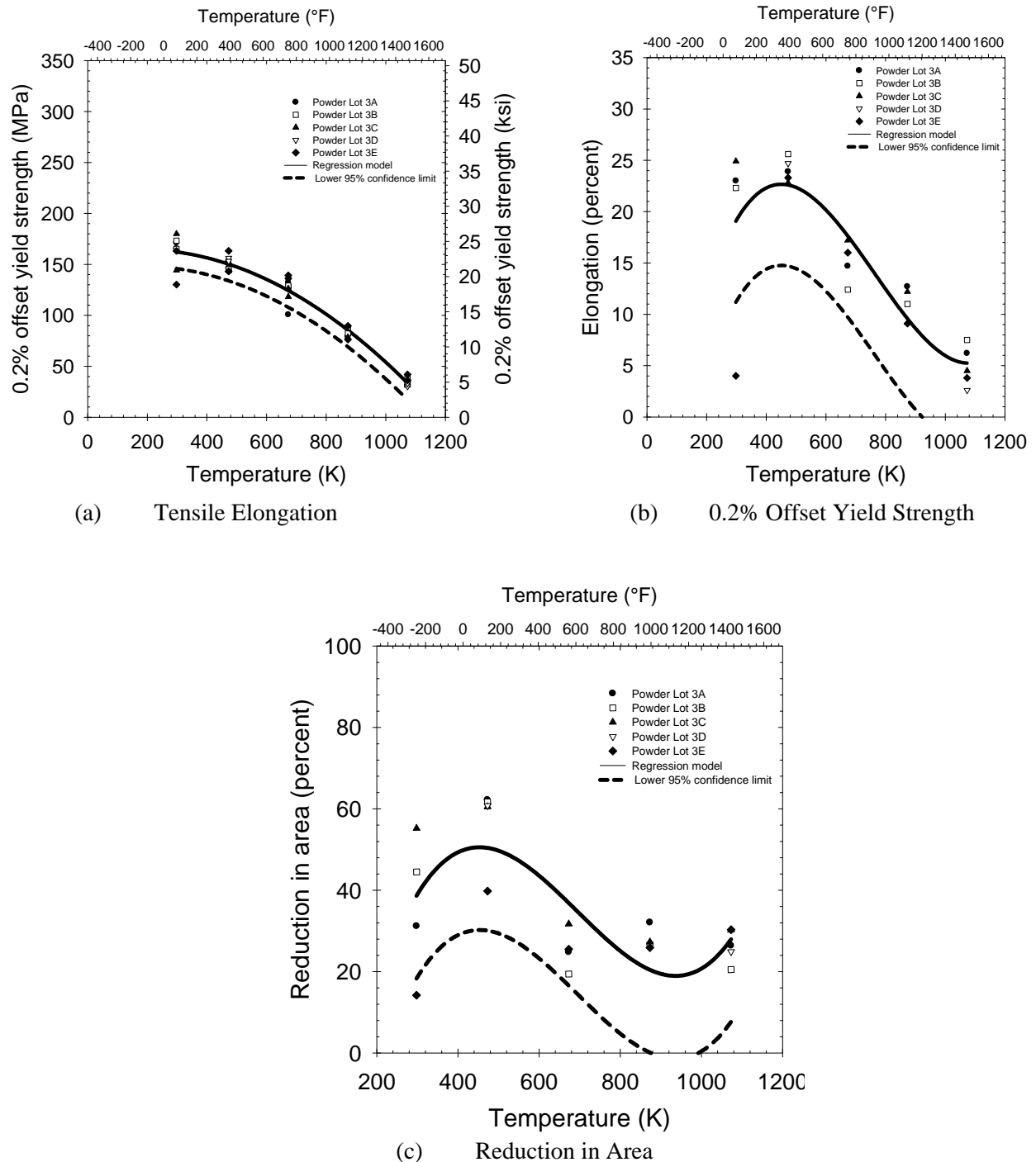


Figure 15.—Baseline tensile properties of HIPed GRCop-84 with lower 95 percent confidence intervals.

The large number of data points and five true repeats allowed for considerable statistical analysis and the assignment of upper and lower confidence intervals. Since tensile property minimums rather than ranges will be required for design purposes, it was decided to use lower one-sided confidence intervals instead of two-sided confidence intervals. The only effect was to change the  $t$  values by changing the probability  $(1-\alpha)$  value used. If necessary, the following equations can be easily modified to produce two-sided confidence intervals. Upper limits can also be assigned by adding rather than subtracting the final term,  $t(1-\alpha, \nu)S_{Y.X}$ .

A least squares polynomial regression analysis was conducted using temperature ( $T$ ) as the independent variable and the tensile property (0.2 percent offset yield strength, UTS, elongation, R.A.) as the dependent variable. The general form of the equation entertained was

$$Y = \beta_0 + \beta_1 T + \beta_2 T^2 + \beta_3 T^3 - t(1-\alpha, \nu)S_{Y.X} \quad (1)$$

where  $Y$  is the dependent variable of interest,  $T$  is the absolute temperature (K),  $\beta_0$  through  $\beta_3$  are the coefficients calculated from the regression,  $t(1-\alpha, \nu)$  is the value of the Student  $t$ -distribution associated with  $\nu$  degrees of freedom and  $1-\alpha$  cumulative probability, and  $S_{Y.X}$  is the standard error of estimate. Since a one-sided confidence interval is being used,  $1-\alpha$  rather than  $1-\alpha/2$  is used. The values of  $S_{Y.X}$  are calculated during regression.

The lower limits for the 0.2 percent offset yield strengths of GRCop-84 are given by the equations

*Extruded :*

$$\sigma_{0.2\% \text{ Offset}}(T) = 297.4 - 0.312T + 3.175 \times 10^{-4} T^2 - 2.506 \times 10^{-7} T^3 - t(1-\alpha, 31) \times 10.92 \quad (2a)$$

*HIPed :*

$$\sigma_{0.2\% \text{ Offset}}(T) = 159.9 + 5.65 \times 10^{-2} T - 1.62 \times 10^{-4} T^2 - t(1-\alpha, 19) \times 9.50 \quad (2b)$$

where  $T$  is in Kelvin,  $t(1-\alpha, \nu)$  is the value for the  $t$ -distribution with  $\nu$  degrees of freedom associated with  $1-\alpha$  cumulative probability, and  $\sigma_{0.2\% \text{ Offset}}(T)$  is in MPa. Adjusting the value of  $t(1-\alpha, \nu)$  allows calculation of differing confidence limits and both one and two sided confidence intervals. To achieve the regression values, it is only necessary to set the last term of each equation ( $t(1-\alpha, \nu)S_{Y.X}$ ) to 0. The same can be done with the other equations presented below.

The lower limits for the ultimate tensile strengths of GRCop-84 are given by the equations

*Extruded :*

$$\sigma_{UTS}(T) = 664.5 - 0.987 T + 3.850 \times 10^{-4} T^2 - t(1-\alpha, 32) \times 21.92 \quad (3a)$$

*HIPed :*

$$\sigma_{UTS}(T) = 448.5 - 0.405 T + 2.37 \times 10^{-5} T^2 - t(1-\alpha, 19) \times 30.30 \quad (3b)$$

where  $T$  is in Kelvin,  $t(1-\alpha, \nu)$  is the value for the  $t$ -distribution with  $\nu$  degrees of freedom associated with  $1-\alpha$  cumulative probability, and  $\sigma_{UTS}(T)$  is in MPa.

The lower limits for the elongations of GRCop-84 are given by the equations

$$\begin{aligned} & \textit{Extruded} : \\ \varepsilon(T) &= 17.16 + 0.034 T - 8.114 \times 10^{-5} T^2 + 4.907 \times 10^{-8} T^3 - t(1-\alpha, 31) \times 2.52 \end{aligned} \quad (4a)$$

$$\begin{aligned} & \textit{HIPed} : \\ \varepsilon(T) &= -17.27 + 0.206 T - 3.24 \times 10^{-4} T^2 + 1.42 \times 10^{-7} T^3 - t(1-\alpha, 19) \times 4.57 \end{aligned} \quad (4b)$$

where  $T$  is in Kelvin,  $t(1-\alpha, v)$  is the value for the  $t$ -distribution with  $v$  degrees of freedom associated with  $1-\alpha$  cumulative probability, and  $\varepsilon(T)$  is in percent.

The lower limits for the reduction in areas of GRCop-84 are given by the equations

$$\begin{aligned} & \textit{Extruded} : \\ RA(T) &= 5.73 + 0.239 T - 4.183 \times 10^{-4} T^2 + 1.956 \times 10^{-7} T^3 - t(1-\alpha, 31) \times 12.32 \end{aligned} \quad (5a)$$

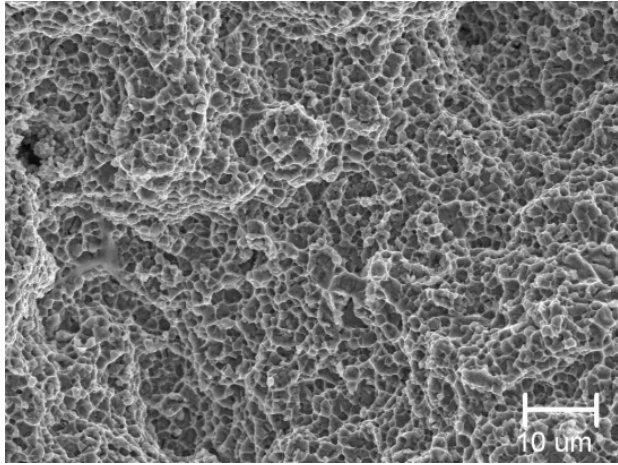
$$\begin{aligned} & \textit{HIPed} : \\ RA(T) &= -85.19 + 0.714 T - 1.17 \times 10^{-3} T^2 + 5.61 \times 10^{-7} T^3 - t(1-\alpha, 19) \times 11.76 \end{aligned} \quad (5b)$$

where  $T$  is in Kelvin,  $t(1-\alpha, v)$  is the value for the  $t$ -distribution with  $v$  degrees of freedom associated with  $1-\alpha$  cumulative probability, and  $RA(T)$  is in percent.

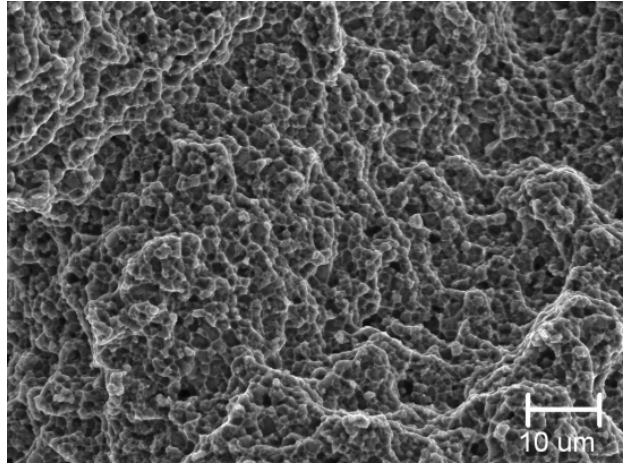
Limited fractography was done on the baseline GRCop-84 samples. Prior experience (Refs. 7 to 11, 24) had shown that microvoid coalescence and growth is consistently the failure mode for the ductile failure of GRCop-84 in tensile, creep and low cycle fatigue tests. Optical examination easily confirmed this, so most samples were not subjected to detailed fractography using an SEM. In addition, high temperature tensile testing tended to result in oxidized fracture surfaces that were not well suited for fracture analysis. Typically, only cryogenic, room temperature, 200 °C (392 °F) and 400 °C (752 °F) tensile specimens were suitable for SEM observation. Examples of typical fracture surfaces are shown in Figure 16.

As can be seen in Figure 16, the fracture surfaces show little if any discernable change over the temperature range shown. The dimpled surfaces are indicative of microvoid coalescence and growth. The size of the dimples varies somewhat between the specimens shown, but the differences are consistent with observed normal variations within a given set of specimens tested at a single temperature, so it is not considered significant. The dimples are sometimes observed to have Cr<sub>2</sub>Nb particles associated with them, but this is more likely because of the high volume fraction of Cr<sub>2</sub>Nb particles (14 vol.%) leading to the features being coincident rather than the Cr<sub>2</sub>Nb particles acting as initiation sites for the formation of voids. There is no evidence of a weak interface between the Cu matrix and the Cr<sub>2</sub>Nb that initiates the voids.

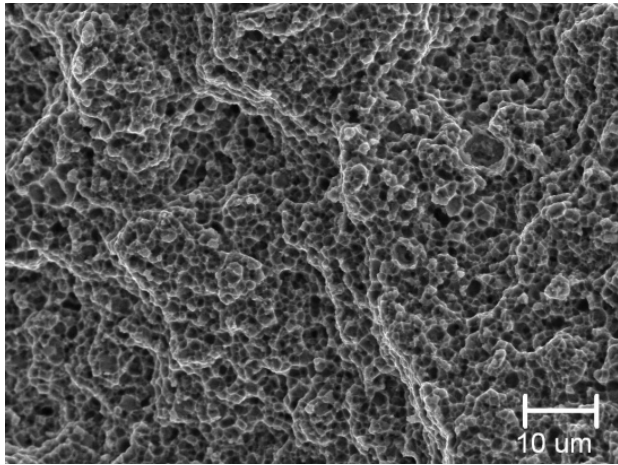
The 400 °C sample in Figure 16(e) shows a less well-defined surface due to oxidation during cooling of the sample, but most of the features remain sufficiently distinct that a major change in mechanism would have been detectable. Above 400 °C, the oxidation of the freshly created fracture surface is too great even in a flowing argon atmosphere to be usable for meaningful fractography. However, the general macroscopic morphology was visually observed to remain unchanged.



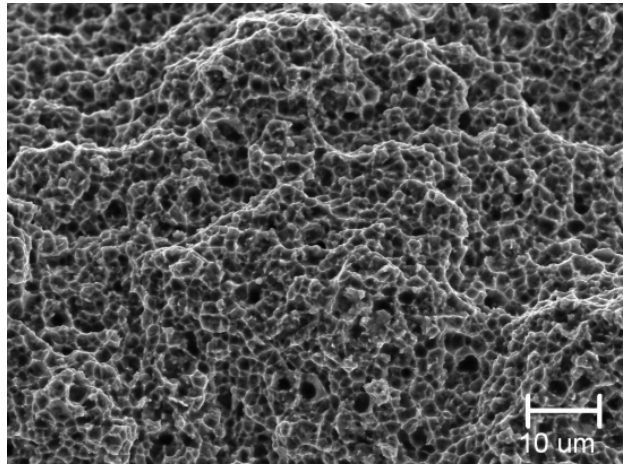
(a) Liquid Hydrogen ( $-253\text{ }^{\circ}\text{C}/-423\text{ }^{\circ}\text{F}$ )



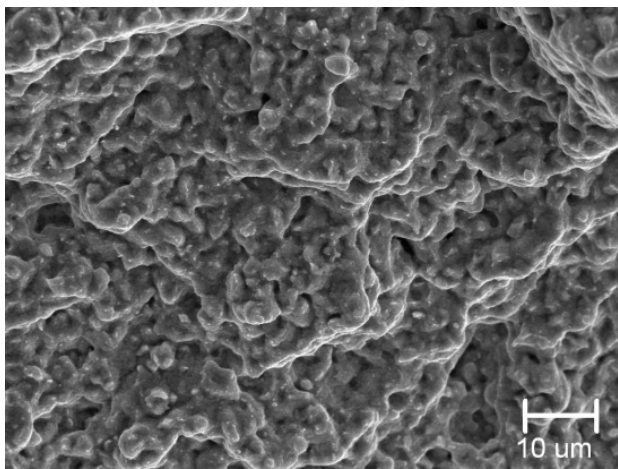
(b) Liquid Nitrogen ( $-196\text{ }^{\circ}\text{C}/-321\text{ }^{\circ}\text{F}$ )



(c)  $23\text{ }^{\circ}\text{C}$  ( $73\text{ }^{\circ}\text{F}$ )



(d)  $200\text{ }^{\circ}\text{C}$  ( $392\text{ }^{\circ}\text{F}$ )



(e)  $400\text{ }^{\circ}\text{C}$  ( $752\text{ }^{\circ}\text{F}$ )

Figure 16.—Typical tensile fracture surfaces for baseline as-extruded GRCop-84 samples.

## Effect of Simulated Braze Cycles on Baseline GRCop-84

The baseline extruded and HIPed materials were also given the low temperature simulated-braze cycle listed in Table 1 to determine the effect of a representative braze or diffusion bonding thermal cycle upon tensile properties. Again, due to the large number of samples and true repeats it was possible to do a rigorous and detailed statistical analysis and determine not only the averages but also lower confidence intervals.

The microstructure exhibited few if any detectable changes. An example of an extruded and brazed structure is shown in Figure 17. While the  $\text{Cr}_2\text{Nb}$  appeared to undergo some coarsening, the coarsening was relatively minor and both the particles and the Cu grains remained almost the same diameter. The dislocations present in the image are the result of ion milling to remove the surface oxide layer and are not representative of the actual dislocation density, which is low.

The results for the extruded material given a simulated-braze cycle appear in Figure 18. The results for the HIPed material given a simulated-braze cycle are shown in Figure 19. These results represent the baseline values for GRCop-84 given a simulated 935 °C (1715 °F) braze cycle.

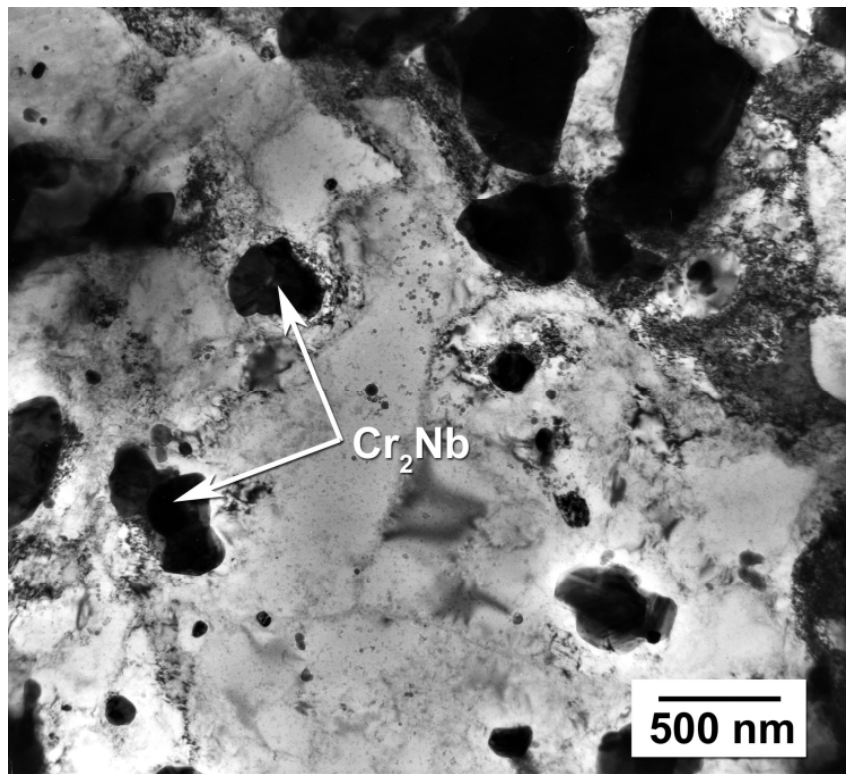


Figure 17.—Typical TEM image of extruded GRCop-84 specimen given a 935 °C (1715 °F) simulated braze.

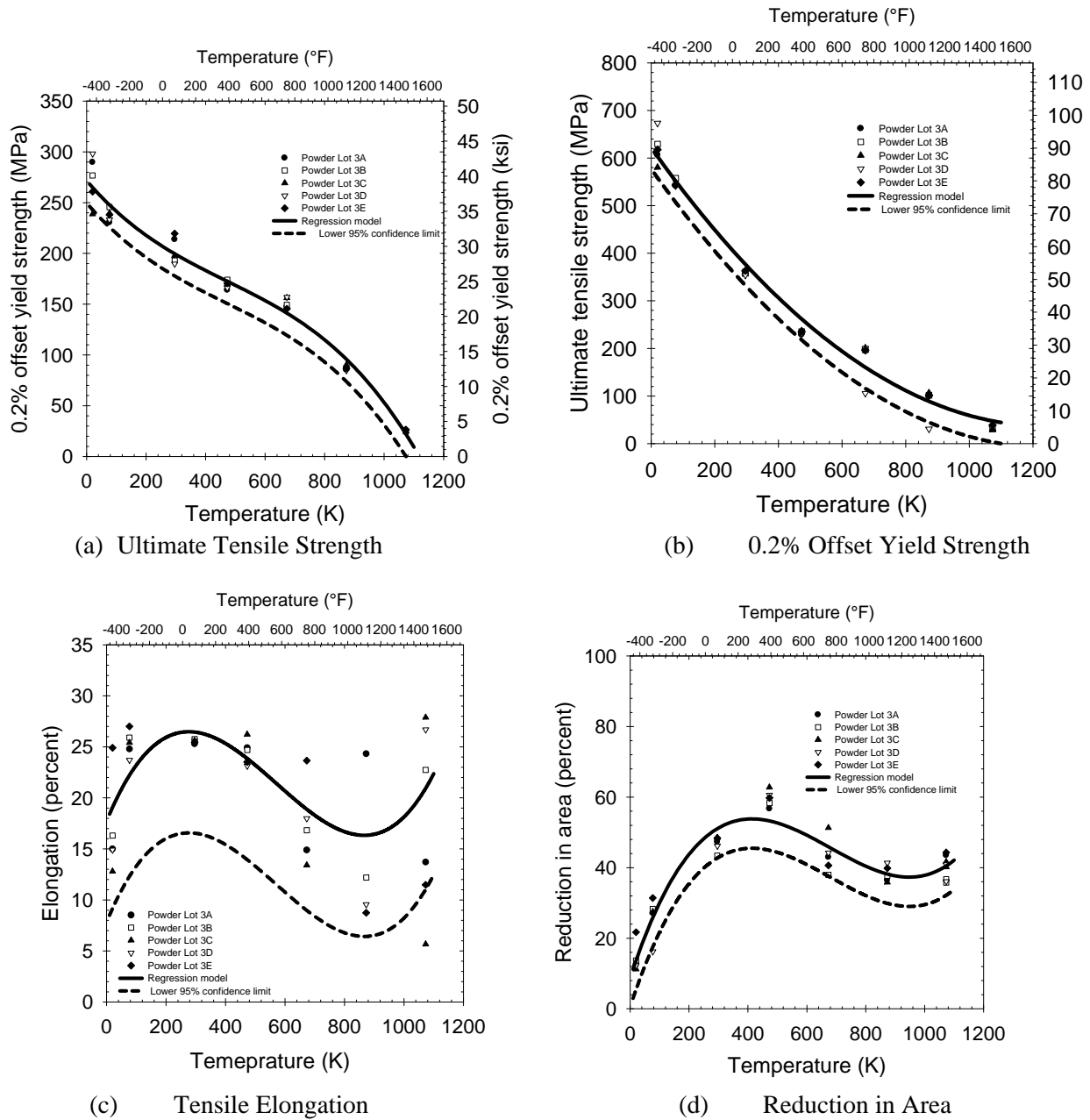
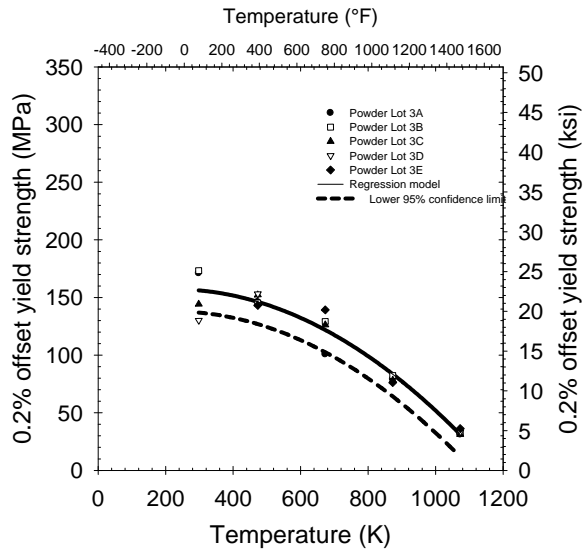
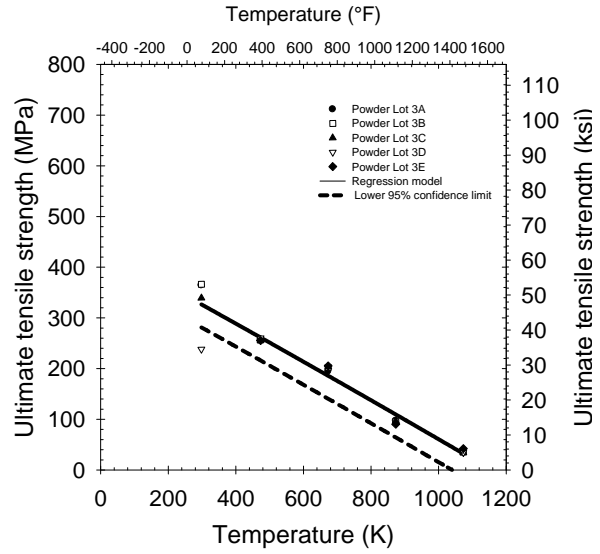


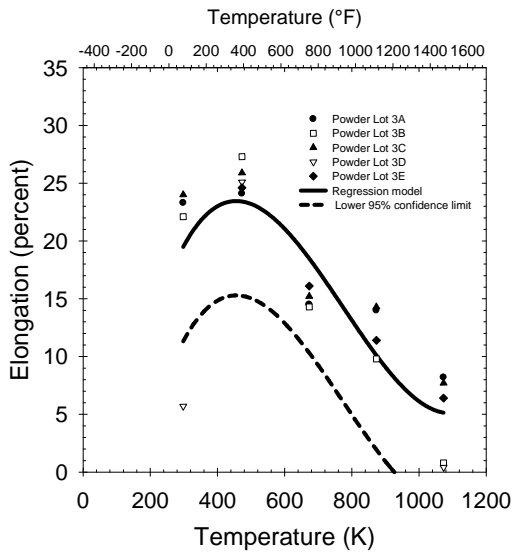
Figure 18.—Baseline tensile properties of extruded and 935 °C (1715 °F) brazed GRCop-84 with lower 95 percent confidence intervals.



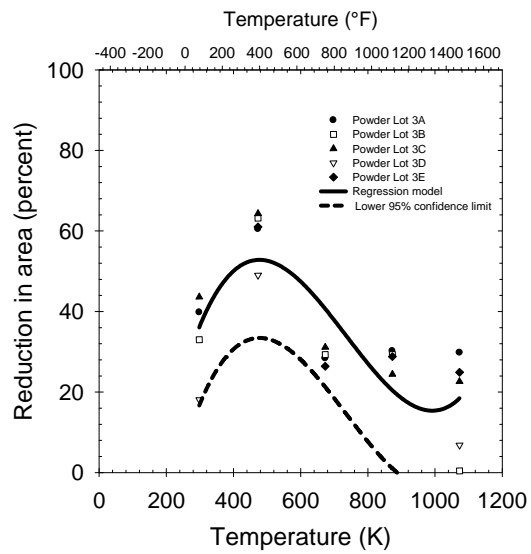
(a) Ultimate Tensile Strength



(b) 0.2% Offset Yield Strength



(c) Tensile Elongation



(d) Reduction in Area

Figure 19.—Baseline tensile properties of HIPed and 935 °C (1715 °F) brazed GRCop-84 with lower 95 percent confidence intervals.

The polynomial model given in Equation (1) was again entertained. Least squares regression analysis was used to fit the data to the model and calculated the standard error of estimate ( $S_{Y,X}$ ). The 0.2 percent offset yield strengths of brazed GRCop-84 are given by the equations

$$\begin{aligned} & \textit{Extruded} : \\ & \sigma_{0.2\% \textit{Offset}}(T) = 271.6 - 0.340T + 4.145 \times 10^{-4} T^2 - 2.929 \times 10^{-7} T^3 - t(1-\alpha, 31) \times 12.91 \end{aligned} \quad (6a)$$

$$\begin{aligned} & \textit{HIPed} : \\ & \sigma_{0.2\% \textit{Offset}}(T) = 148.7 + 0.077T - 1.74 \times 10^{-4} T^2 - t(1-\alpha, 19) \times 11.19 \end{aligned} \quad (6b)$$

where  $T$  is in Kelvin,  $t(1-\alpha, \nu)$  is the value for the  $t$ -distribution with  $\nu$  degrees of freedom associated with  $1-\alpha$  cumulative probability, and  $\sigma_{0.2\% \textit{Offset}}(T)$  is in MPa. Adjusting the value of  $t(1-\alpha, \nu)$  allows calculation of differing confidence limits and both one and two sided confidence intervals.

The ultimate tensile strengths of brazed GRCop-84 are given by the equations

$$\begin{aligned} & \textit{Extruded} : \\ & \sigma_{UTS}(T) = 621.8 - 0.939T + 3.763 \times 10^{-4} T^2 - t(1-\alpha, 32) \times 26.12 \end{aligned} \quad (7a)$$

$$\begin{aligned} & \textit{HIPed} : \\ & \sigma_{UTS}(T) = 436.3 - 0.365T - 1.09 \times 10^{-4} T^2 - t(1-\alpha, 19) \times 26.27 \end{aligned} \quad (7b)$$

where  $T$  is in Kelvin,  $t(1-\alpha, \nu)$  is the value for the  $t$ -distribution with  $\nu$  degrees of freedom associated with  $1-\alpha$  cumulative probability, and  $\sigma_{UTS}(T)$  is in MPa. Adjusting the value of  $t(1-\alpha, \nu)$  allows calculation of differing confidence limits and both one and two sided confidence intervals.

The elongations of brazed GRCop-84 are given by the equations

$$\begin{aligned} & \textit{Extruded} : \\ & \varepsilon(T) = 17.71 + 0.071T - 1.694 \times 10^{-4} T^2 + 9.882 \times 10^{-8} T^3 - t(1-\alpha, 31) \times 5.839 \end{aligned} \quad (8a)$$

$$\begin{aligned} & \textit{HIPed} : \\ & \varepsilon(T) = -18.49 + 0.214T - 3.32 \times 10^{-4} T^2 + 1.43 \times 10^{-8} T^3 - t(1-\alpha, 19) \times 4.72 \end{aligned} \quad (8b)$$

where  $T$  is in Kelvin,  $t(1-\alpha, \nu)$  is the value for the  $t$ -distribution with  $\nu$  degrees of freedom associated with  $1-\alpha$  cumulative probability, and  $\varepsilon(T)$  is in percent. Adjusting the value of  $t(1-\alpha, \nu)$  allows calculation of differing confidence limits and both one and two sided confidence intervals.

The reduction in area of GRCop-84 is given by the equations

$$\begin{aligned} & \textit{Extruded} : \\ & RA(T) = 8.73 + 0.255T - 4.427 \times 10^{-4} T^2 + 2.168 \times 10^{-7} T^3 - t(1-\alpha, 31) \times 4.90 \end{aligned} \quad (9a)$$

$$\begin{aligned} & \textit{HIPed} : \\ & RA(T) = -103.3 + 0.780T - 1.21 \times 10^{-3} T^2 + 5.49 \times 10^{-7} T^3 - t(1-\alpha, 19) \times 11.22 \end{aligned} \quad (9b)$$

where  $T$  is in Kelvin,  $t(1-\alpha, \nu)$  is the value for the  $t$ -distribution with  $\nu$  degrees of freedom associated with  $1-\alpha$  cumulative probability, and  $RA(T)$  is in percent. Adjusting the value of  $t(1-\alpha, \nu)$  allows calculation of differing confidence limits and both one and two sided confidence intervals.

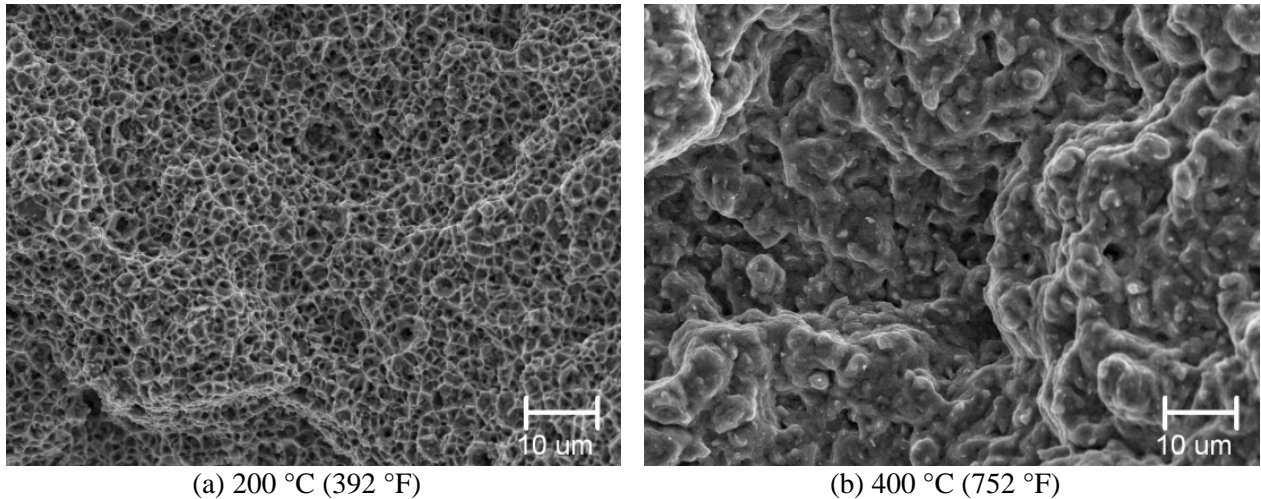


Figure 20.—Typical fracture surfaces of extruded and brazed GRCop-84 tensile tests.

Figure 20 shows typical fracture surfaces for GRCop-84 specimens subjected to a braze cycle. No differences were noted between the brazed samples and corresponding as-extruded and as-HIPed specimens.

### –270 Mesh Powder Extrusions

The tensile results for the small extrusions made from –270 mesh (<53 μm) powder are presented in Figure 21. Samples were exposed to both the 935 and 1000 °C braze cycles. The tensile results for the brazed –270 mesh powder GRCop-84 specimens are shown in Figure 22. For comparison, the as-extruded and 935 °C braze baseline data are also presented as appropriate.

The data were fit to Equation (1) using a least squares regression analysis. The results were:

#### Yield Strength

*As – Extruded :*

$$\sigma_{0.2\% \text{ Offset}}(T) = 202.0 + 5.39 \times 10^{-3} T + 5.17 \times 10^{-5} T^2 - 1.87 \times 10^{-7} T^3 - t(1 - \alpha, 6) \times 15.79 \quad (10a)$$

*935°C Braze :*

$$\sigma_{0.2\% \text{ Offset}}(T) = 304.0 - 0.671 T + 1.14 \times 10^{-3} T^2 - 6.96 \times 10^{-7} T^3 - t(1 - \alpha, 6) \times 5.95 \quad (10b)$$

*1000°C Braze :*

$$\sigma_{0.2\% \text{ Offset}}(T) = 196.7 - 0.118 T + 1.81 \times 10^{-4} T^2 - 2.05 \times 10^{-7} T^3 - t(1 - \alpha, 6) \times 1.11 \quad (10c)$$

### Ultimate Tensile Strength

*As – Extruded :*

$$\sigma_{UTS}(T) = 614.0 - 1.14 T + 1.01 \times 10^{-3} T^2 - 4.24 \times 10^{-7} T^3 - t(1 - \alpha, 6) \times 9.16 \quad (11a)$$

*935°C Braze :*

$$\sigma_{UTS}(T) = 716.3 - 1.62 T + 1.79 \times 10^{-3} T^2 - 8.11 \times 10^{-7} T^3 - t(1 - \alpha, 6) \times 13.88 \quad (11b)$$

*1000°C Braze :*

$$\sigma_{0.2\% \text{ Offset}}(T) = 589.7 - 1.10 T + 1.01 \times 10^{-3} T^2 - 4.45 \times 10^{-7} T^3 - t(1 - \alpha, 6) \times 9.60 \quad (11c)$$

### Elongation

*As – Extruded :*

$$\varepsilon(T) = 15.0 + 5.44 \times 10^{-2} T - 6.82 \times 10^{-5} T^2 + 2.51 \times 10^{-8} T^3 - t(1 - \alpha, 6) \times 3.93 \quad (12a)$$

*935°C Braze :*

$$\varepsilon(T) = 21.3 + 5.62 \times 10^{-2} T - 1.17 \times 10^{-4} T^2 + 6.54 \times 10^{-8} T^3 - t(1 - \alpha, 6) \times 3.10 \quad (12b)$$

*1000°C Braze :*

$$\varepsilon(T) = 40.3 - 8.18 \times 10^{-2} T + 8.91 \times 10^{-5} T^2 - 1.41 \times 10^{-8} T^3 - t(1 - \alpha, 4) \times 3.69 \quad (12c)$$

### Reduction In Area

*As – Extruded :*

$$RA(T) = -52.7 + 0.409 T - 6.15 \times 10^{-4} T^2 + 2.74 \times 10^{-7} T^3 - t(1 - \alpha, 6) \times 4.13 \quad (13a)$$

*935°C Braze :*

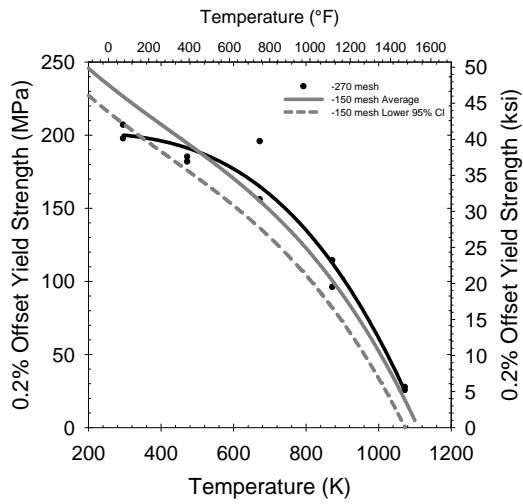
$$RA(T) = -39.0 + 0.370 T - 5.95 \times 10^{-4} T^2 + 2.84 \times 10^{-7} T^3 - t(1 - \alpha, 6) \times 3.04 \quad (13b)$$

*1000°C Braze :*

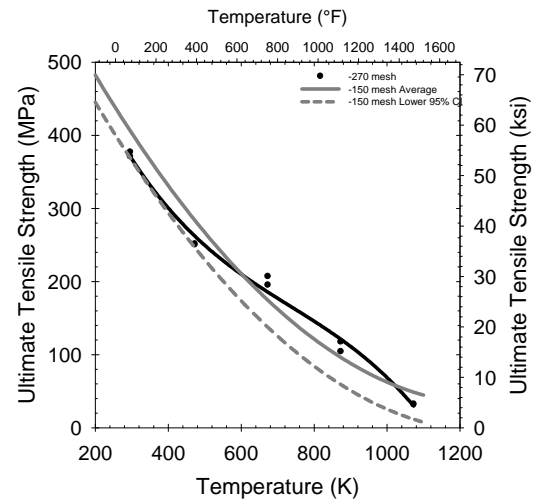
$$RA(T) = -40.9 + 0.492 T - 7.83 \times 10^{-4} T^2 + 3.67 \times 10^{-7} T^3 - t(1 - \alpha, 6) \times 2.96 \quad (13c)$$

An attempt was made to perform stepwise regression on the data sets to develop a model that combined all the data and that included the two braze cycles as independent variables. Collinearity was encountered with the data, which prevented development of a combined model.

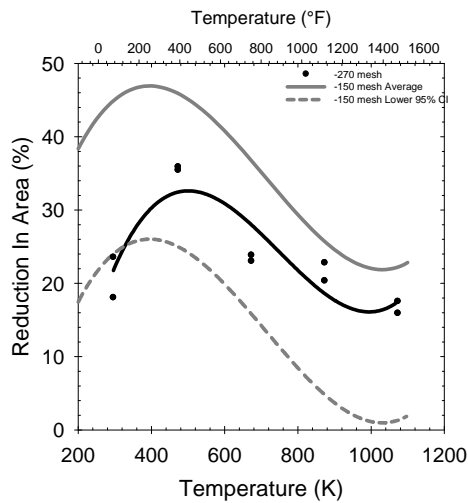
Since GRCop-84 is strengthened in part by a Hall-Petch mechanism (Ref. 23), finer powders with a higher cooling rate and finer grain size should exhibit a higher yield strength. However, at room temperature, Figures 21(a) and 22(a) indicate that the yield strength of the –270 mesh powder is not greater than the –150 mesh powder.



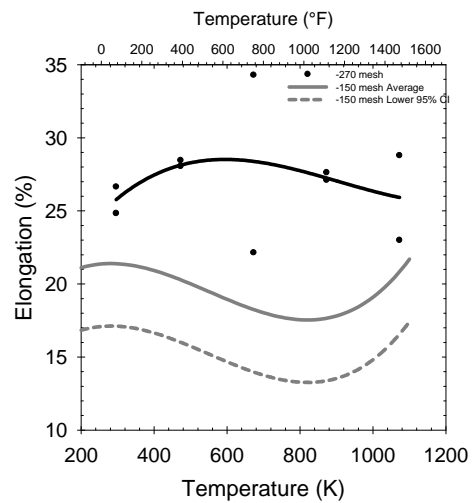
(a) 0.2% Offset yield Strength



(b) Ultimate Tensile Strength

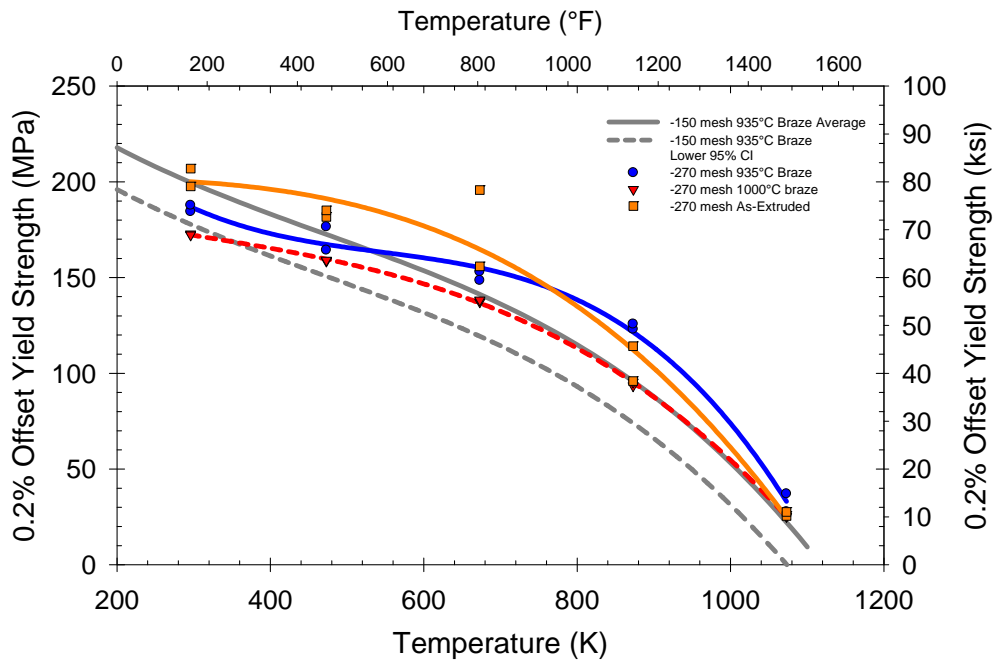


(c) Tensile Elongation

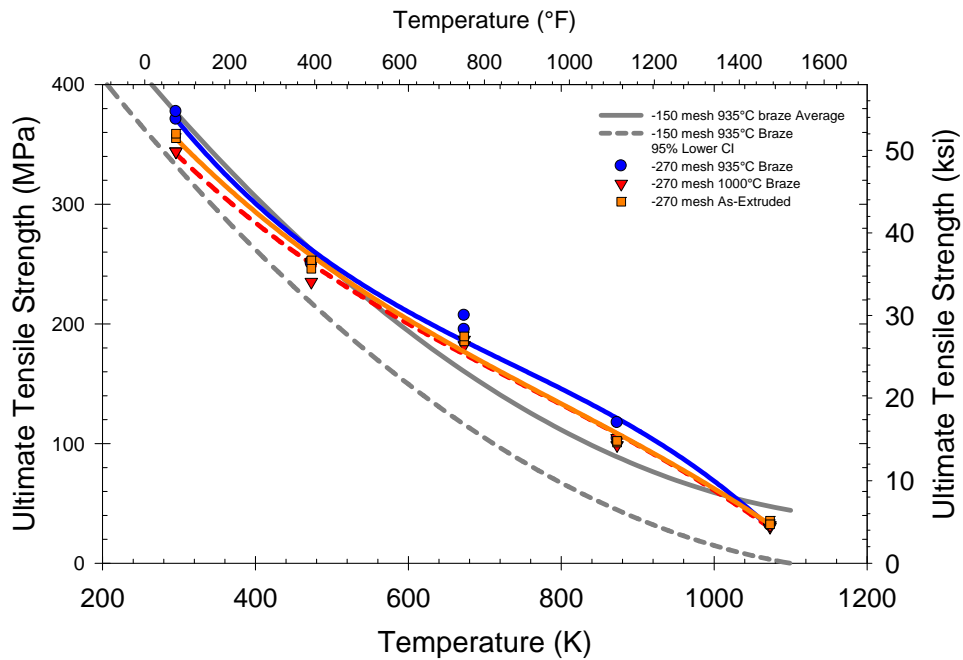


(d) Reduction in Area

Figure 21.—Tensile properties of as-extruded -270 mesh GRCop-84.



(a) 0.2% Offset Yield Strength



(b) Ultimate Tensile Strength

Figure 22.—Tensile properties of brazed -270 mesh GRCop-84.

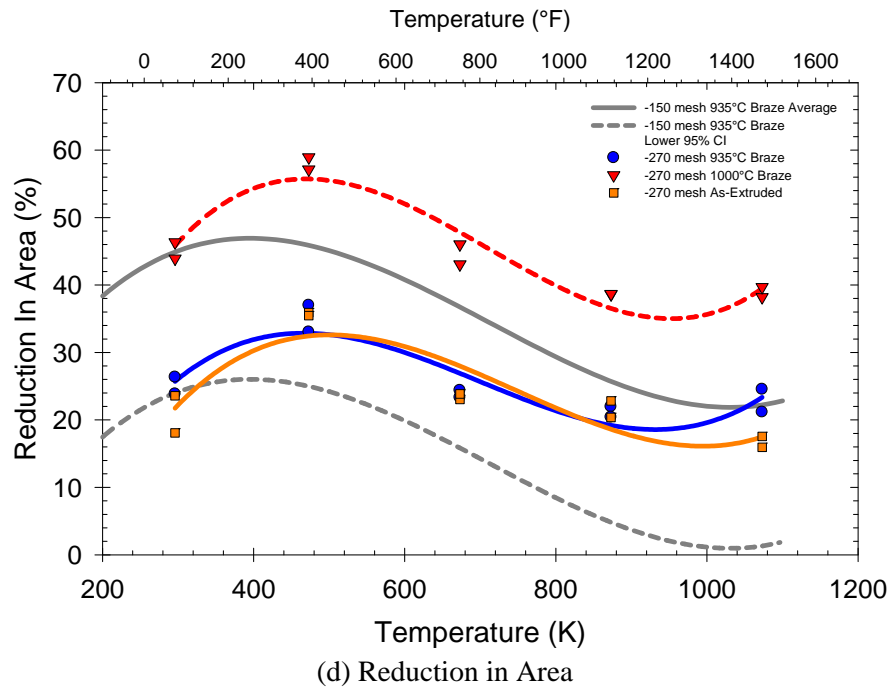
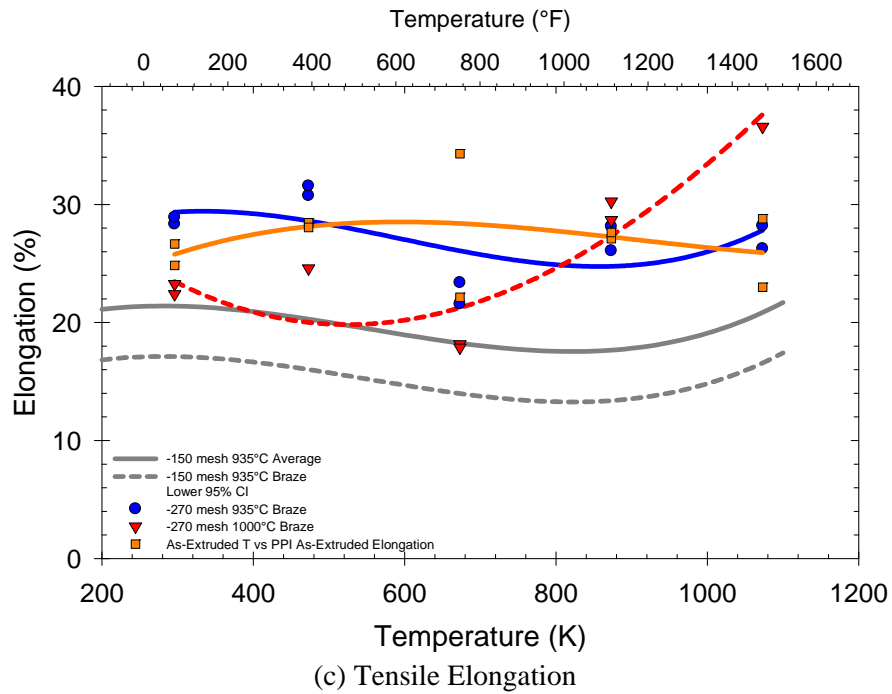


Figure 22.—Concluded.

One possible reason for the general similarity in strength is that –150 and –270 mesh GRCo-84 powders were produced in the same manner. The as-produced powder had essentially the same initial powder size distribution. The powders were then sieved to the desired maximum powder size without any of the smaller powder particles being removed. The –270 mesh powder distribution would therefore be a truncated version of the –150 mesh powder size distribution.

As an example, using the powder size distribution for Powder Lot 3D in Figure 7(c), removing the portion of the powder above 51.47  $\mu\text{m}$  completely would reduce the average powder particle size from 45.8 to 27.1  $\mu\text{m}$ , a reduction of 18.7  $\mu\text{m}$  or 41 percent. The other powder lots would have had a smaller reduction given their smaller initial powder size. If it is assumed that the portion of the tensile strength from Hall-Petch strengthening is proportional  $d^{-1/2}$  then an upper limit of the additional Hall-Petch strengthening can be set at 30 percent or about 21 MPa. More likely, the effects would be less and fall within the normal scatter of the testing as appears to have generally occurred in this testing.

The yield strength of the –270 mesh GRCo-84 samples falls below the –150 mesh powder GRCo-84 lower confidence interval for the as-extruded condition. Similarly, the 1000 °C simulated braze cycle –270 mesh powder GRCo-84 yield strength falls below the 935 °C simulated braze cycle –150 mesh GRCo-84 lower 95 percent confidence limit. The unusually low room temperature strength of the –270 mesh powder specimens in both the as-extruded and brazed conditions cannot be explained. The good intermediate temperature strength would indicate that the low temperature tensile strengths should be as good as or better than the –150 mesh powder. No root cause for this difference was ever discovered. Additional testing is underway to understand the effects of powder size on tensile and creep properties, and those results will be reported separately at a future date.

Ductility as measured by the tensile elongation was good. The values exceeded the values for the baseline as-extruded and 935 °C braze materials. The reduction in area, on the other hand, was generally lower than the baseline material values. The cause for this discrepancy was not established in this work but will be investigated in future work.

The effects of the simulated-braze cycles was to lower the yield strength of the brazed material compared to the as-extruded material. As expected, the effects were greater for the 1000 °C braze than the 935 °C braze. The maximum change was about 50 MPa for the 1000 °C braze specimens tested at room temperature. There were no easily discerned changes in the microstructure, but it is likely that the Cu grains and Cr<sub>2</sub>Nb particles underwent some coarsening which would decrease their ability to strengthen the material. The same trend and approximate order of magnitude changes are observed in the UTS results.

The effects of the 935 °C braze on ductility was minimal. The elongation and reduction in areas of the as-extruded and 935 °C braze specimens were very similar. In contrast the 1000 °C braze produced a variable change in elongation and nearly doubled the average reduction in area.

Based upon these results the change from –150 to –270 mesh powder did not have a beneficial effect upon the GRCo-84 tensile properties. Most of the differences were small and generally fell within the two-sided 95 percent confidence limit indicating no statistically significant difference occurred. Additional refinement of the powder size may result in improvements.

## Large Extrusions

The tensile properties of the first two large extrusions are presented in Figure 23. The lower 95 percent confidence interval for the baseline extruded GRCop-84 is also provided for comparison. Due to loss of identification by the machining vendor, it is uncertain which samples were long transverse and which were short transverse. Based on the data generated, the large extrusion appears to be isotropic in the long transverse and short transverse directions, so the loss of identification, while highly undesirable, is not critical. The decision was made based on time and available resources not to repeat the machining and testing.

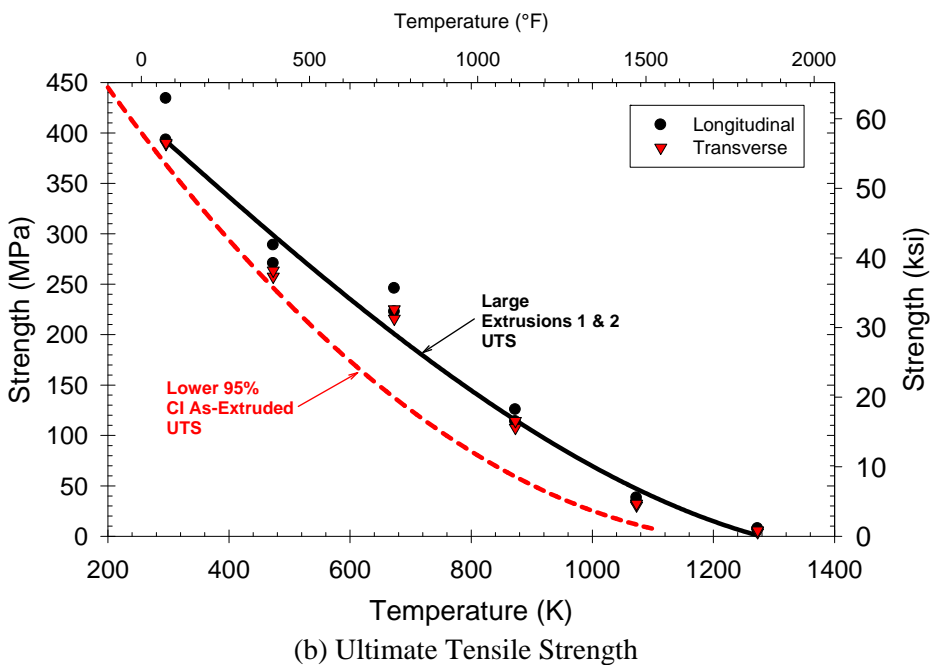
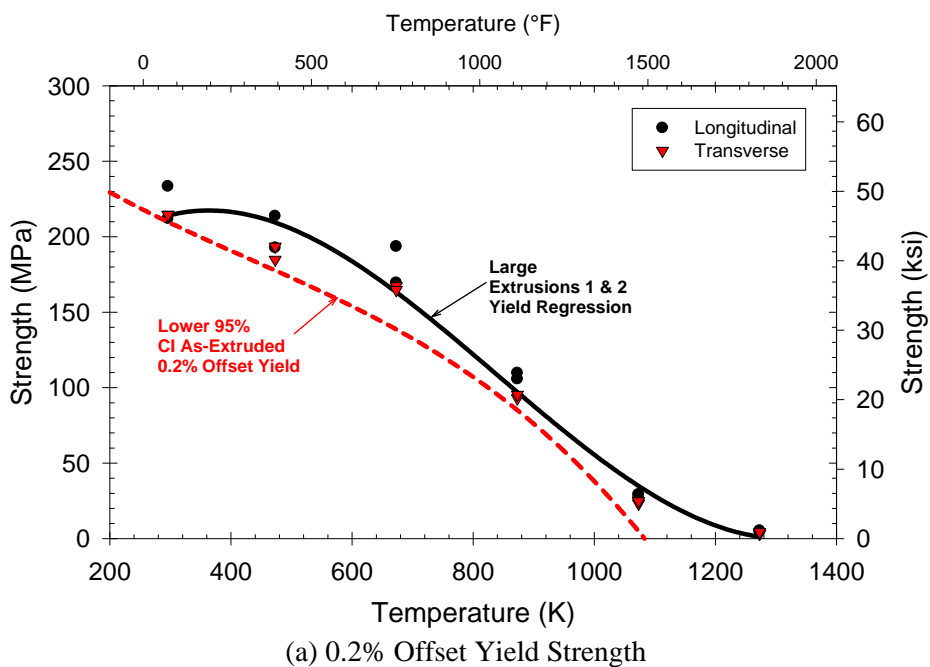


Figure 23.—Tensile properties of large GRCop-84 extrusions 1 and 2.

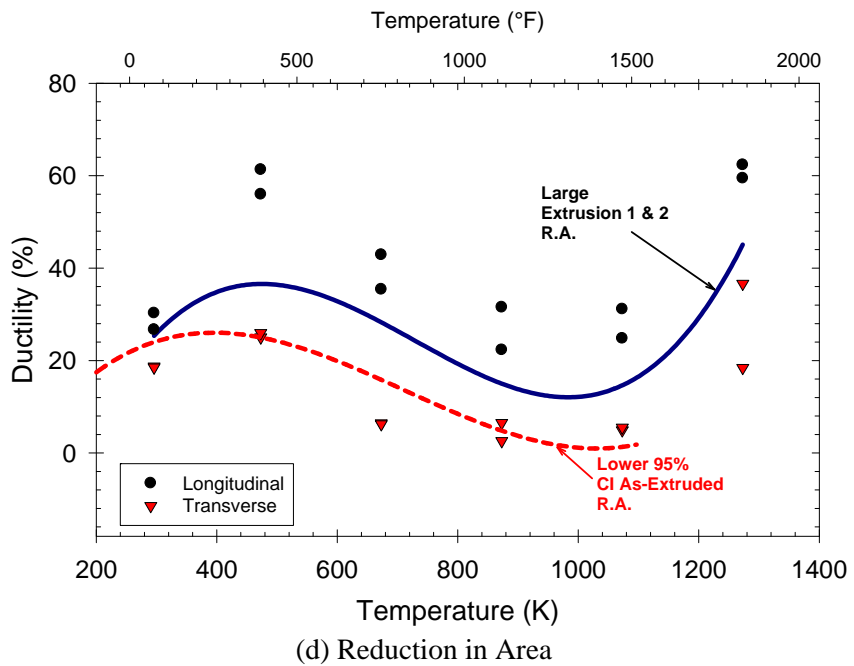
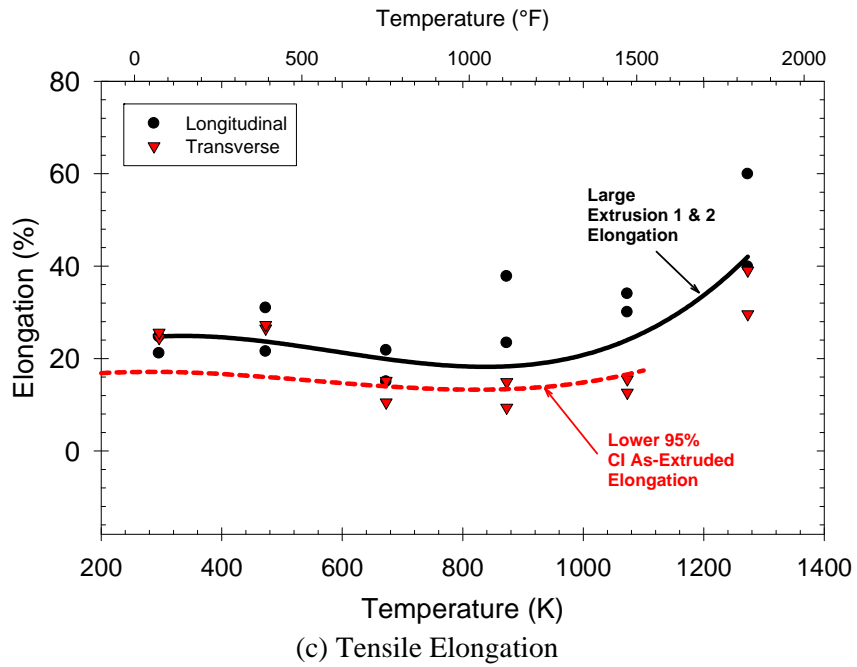


Figure 23.—Concluded.

Initially a t-test was used to compare the longitudinal and transverse tensile strengths at each test temperature. The results showed that the average values of the two data sets were not statistically significantly different at a 95 percent confidence level. The lack of a difference indicates that the material does not have a preferred orientation or texture. However, it was noted that the transverse results were usually lower than the longitudinal results. Given the small number of tests, the power of the test and the ability to discern small differences was brought into question.

Given results from the creep testing that indicate the possibility of a hard and soft direction (Ref. 15), it was decided to repeat the analysis for the yield strength using the methodology used to discern differences between processing methods in creep tests. A model of the form

$$YS = \beta_0 + \beta_1 T + \beta_2 T^2 + \beta_3 T^3 + B_1 \beta_4 T + B_1 \beta_5 T^2 + B_1 \beta_6 T^3 \quad (14)$$

where YS is the 0.2 percent offset yield strength (MPa),  $T$  is the temperature (K),  $B_1$  is a blocking variable equal to 0 if the sample is oriented longitudinally and 1 if it is oriented transversely, and  $\beta_0$  through  $\beta_6$  are the coefficients fit to the model during the forward stepwise linear regression.

Forward stepwise regression was performed using SigmaStat<sup>3</sup> Version 3.5. The results are shown in Table 6.

TABLE 6.—FORWARD STEPWISE REGRESSION ANALYSIS FOR LARGE EXTRUSION YIELD STRENGTH

R = 0.990      R<sup>2</sup> = 0.981      Adjusted R<sup>2</sup> = 0.978  
Standard Error of Estimate = 12.541

***Analysis of Variance***

Group	DF	SS	MS	F	P
Regression	3	162264.153	54088.051	343.923	<0.001
Residual	20	3145.359	157.268		

***Variables in Model***

Variable	Coefficient	Standard Coefficient	Standard Error	F-to-Remove	P
Constant	97.854		38.116		
T	0.724	2.932	0.179	16.298	<0.001
T <sup>2</sup>	-0.00127	-8.197	0.000249	26.105	<0.001
T <sup>3</sup>	0.000000506	4.379	0.000000105	8.036	0.010

***Variables not in Model***

Variable	F-to-Enter	P
B1 T	2.182	0.155
B1 T <sup>2</sup>	1.038	0.321
B1 T <sup>3</sup>	0.522	0.478

<sup>3</sup> Systat Software, Inc., 1735, Technology Drive, Ste 430. San Jose, CA 95110

The total degrees of freedom were raised to 23 using this technique. There is a strong dependence of the yield strength upon temperature as expected, but none of the variables with the blocking variable  $B_1$  appear in the model. In fact, the probabilities associated with the variables indicate a very strong probability that they should be excluded. This indicates that the initial conclusion that there is no statistical dependency of the yield strength upon orientation is correct. The plot of the data still indicates that there may be an underlying phenomenon such as crystallographic texture (Ref. 25) that causes a small but noticeable difference. If there is such a phenomenon, it does not manifest itself at a level that creates a statistical difference.

The longitudinal and transverse tensile strengths are above the lower 95 percent confidence interval for the baseline as-extruded GRCop-84 data taken from the small extrusions. This is important because it confirms that the strength of GRCop-84 is not significantly affected by changes in the reduction in area during extrusion over the range of approximately 6:1 to 29:1.

The data from the longitudinal and transverse data sets were pooled for the least squares regression analysis. The model given in Equation (1) was used again. The regression equations for the as-extruded large extrusion tensile properties including the lower confidence limit that were developed are

$$\sigma_{0.2\% \text{ Offset}}(T) = 205.5 + 0.113 T - 2.46 \times 10^{-4} T^2 - 1.48 \times 10^{-8} T^3 - t(1 - \alpha, 16) \times 11.38 \quad (15)$$

$$\sigma_{UTS}(T) = 730.8 - 1.55 T + 1.65 \times 10^{-3} T^2 - 7.60 \times 10^{-7} T^3 - t(1 - \alpha, 16) \times 20.98 \quad (16)$$

$$\varepsilon(T) = 14.6 + 7.38 \times 10^{-2} T - 1.60 \times 10^{-4} T^2 + 9.26 \times 10^{-8} T^3 - t(1 - \alpha, 16) \times 8.16 \quad (17)$$

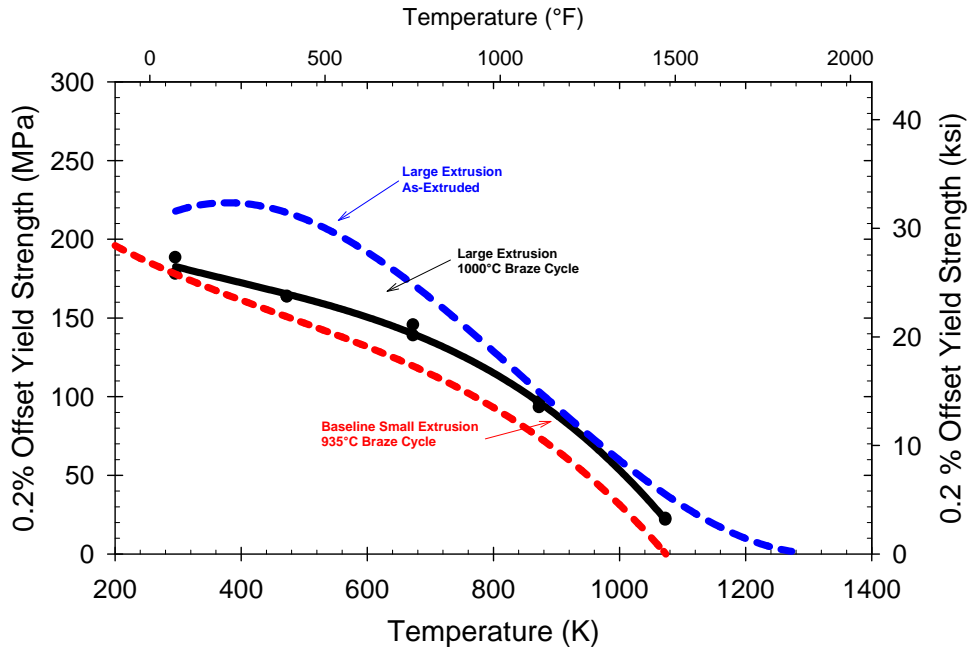
$$RA(T) = -96.5 + 0.688 T - 1.09 \times 10^{-3} T^2 + 5.14 \times 10^{-7} T^3 - t(1 - \alpha, 16) \times 15.0 \quad (18)$$

As shown in Figure 23(c), the ductility of the large extrusions appears to differ in the longitudinal and transverse directions. However, there is no statistical difference between the two data sets. This is a reflection of the relatively low power of the test to determine the significance of the difference. Additional testing is required to confirm if the observed difference is truly significant or not.

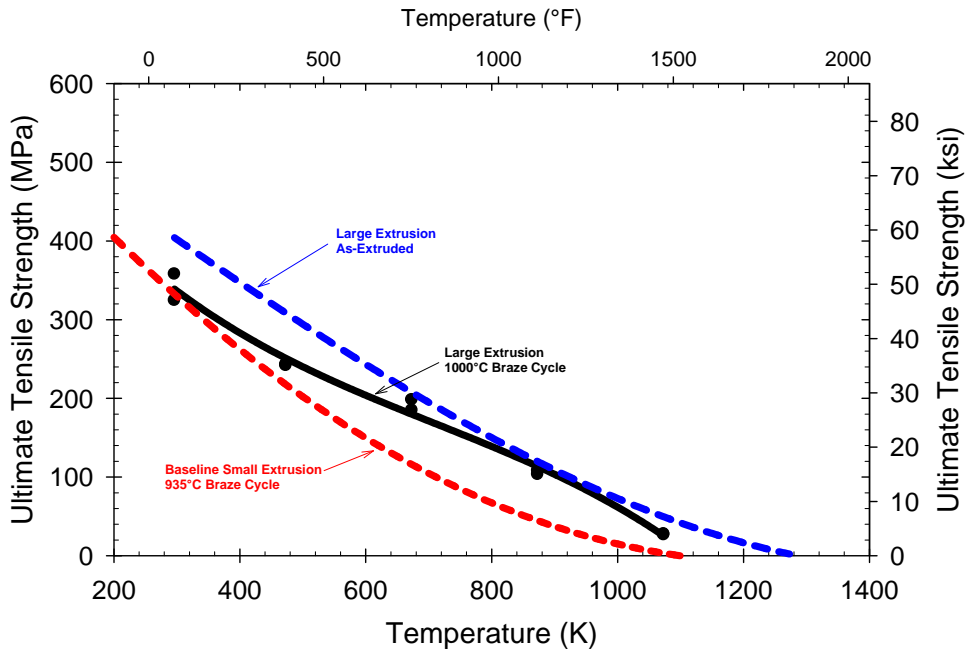
The transverse ductility values are at or below the 95 percent confidence interval as shown in Figures 23(c) and (d). The results are still consistent with the baseline results, but they are sufficiently low to warrant future analysis of the transverse samples to determine the cause of the lower elongations and reductions in areas. Crystallographic texture such as has been observed in the small extrusions (Ref. 25) can at least partially account for these differences. The stringers observed in the as-extruded material also could contribute to the observed differences.

The results for large extrusion samples subjected to a 1000 °C simulated-braze cycle are shown in Figure 24. All of these specimens come from the transverse directions. Data for the reduction in area was lost. For comparison, the results for the lower 95 percent confidence interval for the baseline small extrusion samples given a 935 °C simulated-braze cycle and the average as-extruded curves are also presented. The data show that the 1000 °C braze cycle reduced the tensile strength of the large extrusions by up to almost 75 MPa (10.9 ksi). One sample falls below the lower 95 percent confidence limit for the brazed baseline small extrusions, but the average values are close indicating that there are not significant differences between the response of the large and small extrusions.

The 1000 °C braze cycle tensile elongations are lower than the average values for the as-extruded large extrusions, but they are slightly better than just the transverse specimens' tensile elongation. Compared to the baseline small extrusions given a 935 °C braze cycle the brazed large extrusion values are generally better. The exception is at 400 °C where the brazed large extrusion values are at or below the brazed small extrusion lower confidence limit.

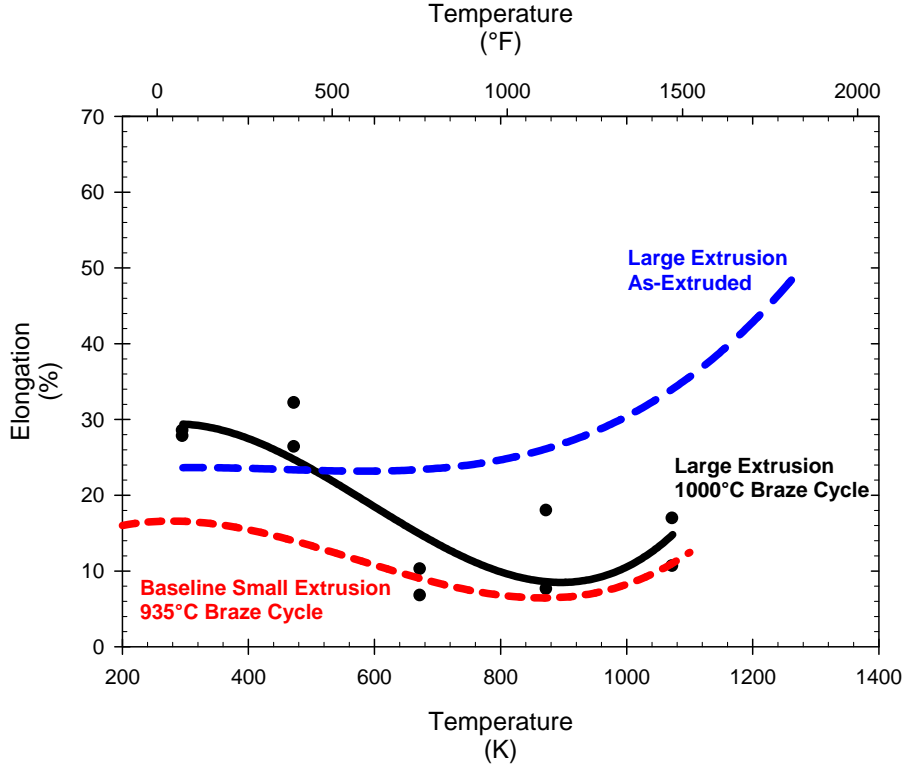


(a) 0.2% Offset yield Strength



(b) Ultimate Tensile Strength

Figure 24.—Tensile properties of large GRCop-84 extrusions 1 and 2 following 1000 °C simulated braze cycle.



(c) Tensile Elongation

Figure 24.—Concluded.

As with the as-extruded data, the 1000 °C braze data was fit to Equation (1) using least squares regression. The regression equations generated are

$$\sigma_{0.2\% \text{ Offset}}(T) = 226.7 - 0.217 T + 3.11 \times 10^{-4} T^2 - 2.67 \times 10^{-7} T^3 - t(1 - \alpha, 6) \times 4.17 \quad (19)$$

$$\sigma_{UTS}(T) = 590.6 - 0.148 T + 1.17 \times 10^{-3} T^2 - 5.50 \times 10^{-7} T^3 - t(1 - \alpha, 6) \times 14.19 \quad (20)$$

$$\varepsilon(T) = 11.4 + 0.141 T - 3.26 \times 10^{-4} T^2 + 1.84 \times 10^{-7} T^3 - t(1 - \alpha, 6) \times 6.57 \quad (21)$$

To quantify the effects of the braze cycle on the tensile properties of the large extrusion, a forward stepwise regression analysis was conducted. Equation (14) was used as the basis for the model.  $B_1$  was set to 1 for samples with a braze cycle and 0 for the as-extruded specimens. It proved necessary to force the  $T$ ,  $T^2$  and  $T^3$  terms to be included in the model. Otherwise, only the  $T^3$  term entered the model. The implication of this was that the as-extruded material was directly proportional to  $T^3$  which was not what was determined in Equations (15) to (18). The resulting regression equations are

$$\begin{aligned} \sigma_{0.2\% \text{ Offset}}(T) = & 212.6 + 4.49 \times 10^{-2} T - 1.01 \times 10^{-4} T^2 - 9.87 \times 10^{-8} T^3 \\ & - 0.127 B_1 T + 1.21 \times 10^{-4} B_1 T^2 \end{aligned} \quad (22)$$

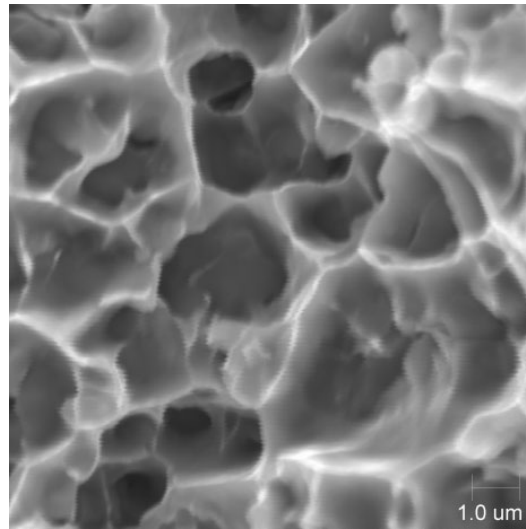
$$\begin{aligned} \sigma_{UTS}(T) = & 684.0 - 1.36 T + 1.44 \times 10^{-3} T^2 - 6.90 \times 10^{-7} T^3 \\ & - 0.154 B_1 T + 1.47 \times 10^{-4} B_1 T^2 \end{aligned} \quad (23)$$

$$\varepsilon(T) = 13.6 + 9.62 \times 10^{-2} T - 2.12 \times 10^{-4} T^2 + 1.23 \times 10^{-7} T^3 - 9.02 \times 10^{-6} B_1 T^2 \quad (24)$$

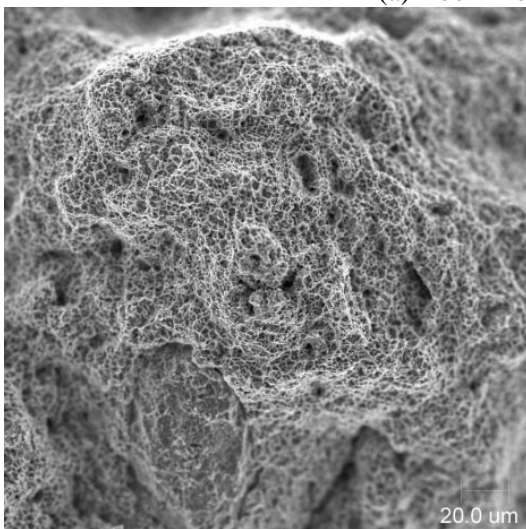
The fit for the yield strength and ultimate tensile strength models are good with the  $R^2$  values being 0.982 and 0.979, respectively. The model for the elongation suffers from poor fit with the  $R^2$  value being only 0.336. It is likely that the large scatter in the elongation data is the cause of this lack of fit. It is preferable to use the individual models (Eqs. (17) and (21)) to predict the elongation. The real strength of the models is their ability to quantitatively determine the effects of the 1000 °C braze cycle upon the tensile properties. This allows a designer to estimate the decrease from giving a large GRCop-84 to this or a similar thermal cycle for purposes of either design or manufacturing assessment.

Examining the data for both the as-extruded and brazed large extrusions, the material appears to have a minimum in ductility in the 400 to 600 °C temperature range. This is consistent with the small extrusion data and Cu-Cr alloys (Ref. 26). While not desirable, it demonstrates that the GRCop-84 is behaving similarly after extruding with both a small and a large reduction in area and is consistent with other Cu-based alloys.

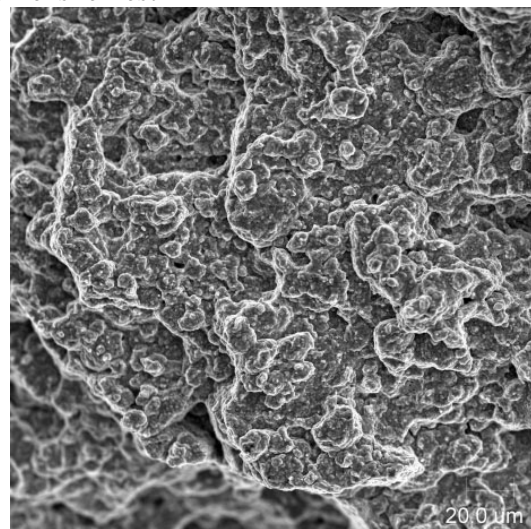
Fracture surfaces for several typical samples are shown in Figure 25. The fracture surfaces are consistent with the baseline tensile tests and show evidence of microvoid coalescence and growth during tensile testing.



(a) Room Temperature Tensile Test



(b) 200 °C (392 °F) Tensile Test



(c) 400 °C (752 °F) Tensile Test

Figure 25.—Typical fracture surfaces for large extrusion samples.

Polished cross-sections of select longitudinal tensile test specimens are shown in Figure 26. In all cases, the applied stress was in the vertical direction. Backscattered electron (BSE) imaging was used to highlight the voids found throughout the specimens. Considerable void formation is seen throughout the reduced section of the sample and extends well back (>10 mm) from the fracture surface. Relatively uniform damage is seen for room temperature and 600 °C (1112 °F) for both the as-extruded material and the samples given a 1000 °C (1832 °F) simulated braze cycle.

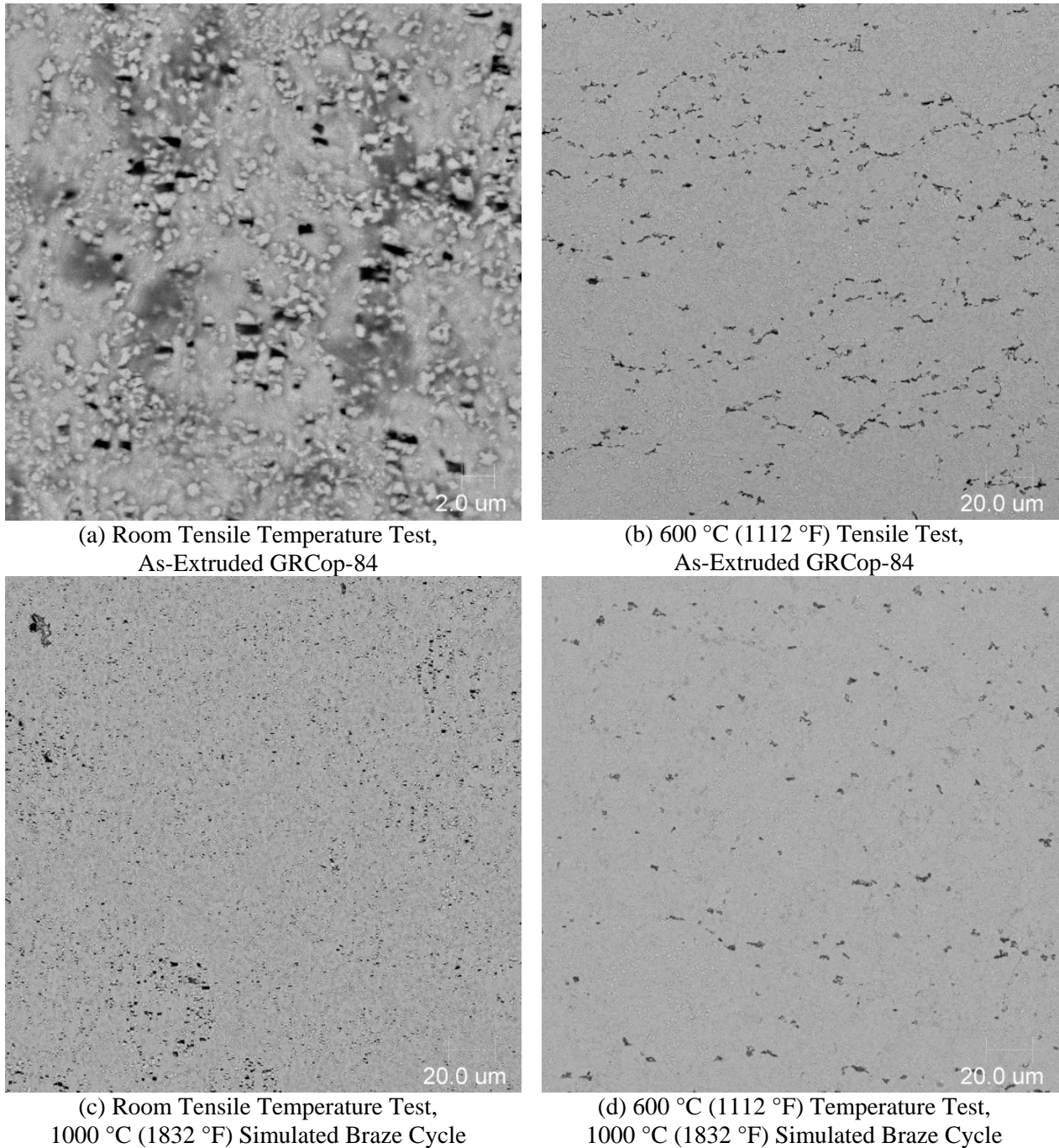
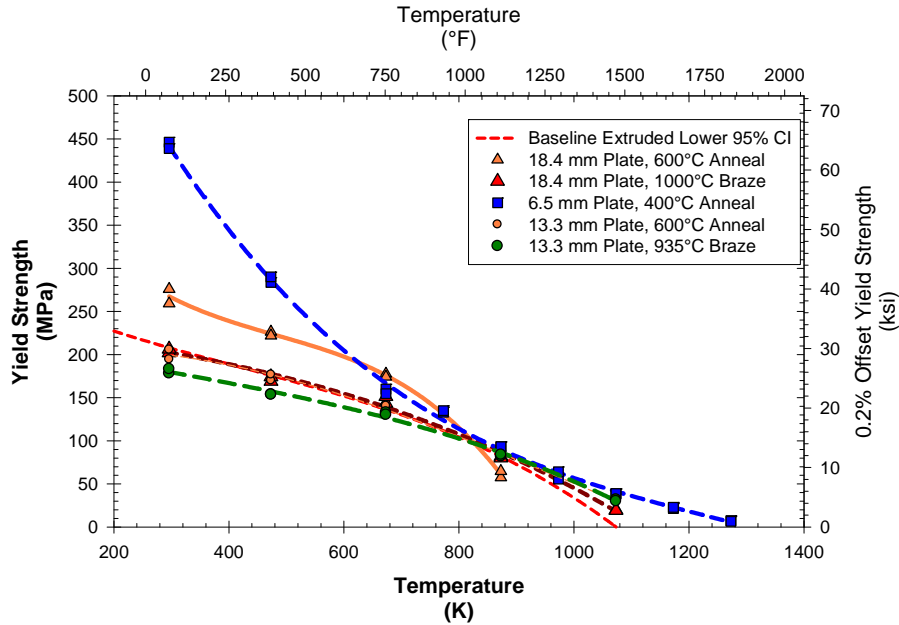


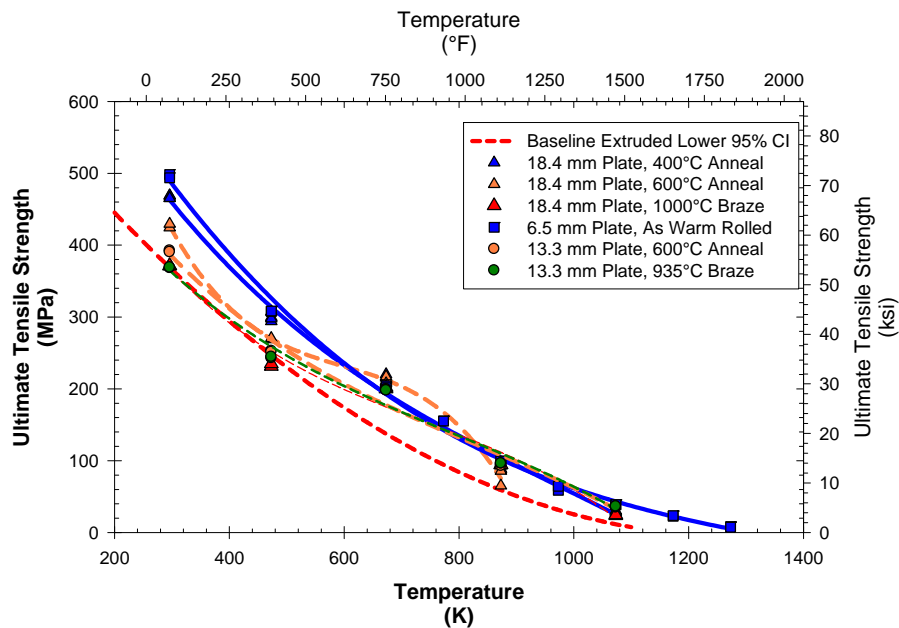
Figure 26.—Polished cross-sections of longitudinal tensile test specimens showing uniform damage.  
(All images used backscattered electron imaging)

## Rolled Plate

Three thicknesses of plate were produced and tested—18.4 mm (0.725 in.), 13.3 mm (0.525 in.) and 6.48 mm (0.255 in.). Two of the plates were annealed after warm rolling to remove residual stresses. The 18.4 mm plate was originally annealed at 400 °C (752 °F) for 15 min. (the old annealing cycle). Samples were re-annealed at 600 °C (1112 °F) for 30 min. (the new annealing cycle) and tested. Both data sets are presented in Figure 27. Also in Figure 27 are the tensile properties of 13.3 mm plate given a 600 °C/30 min anneal and 6.48 mm plate in the as-warm rolled condition with no anneal. For comparison purposes, the curve for the lower 95 percent confidence interval for the baseline as-extruded properties is also presented.

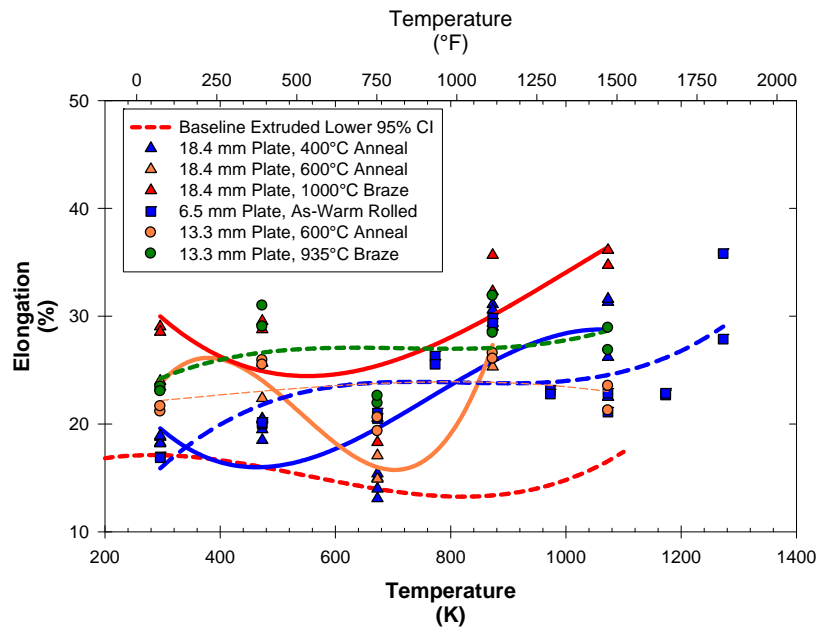


(a) 0.2% Offset Yield Strength

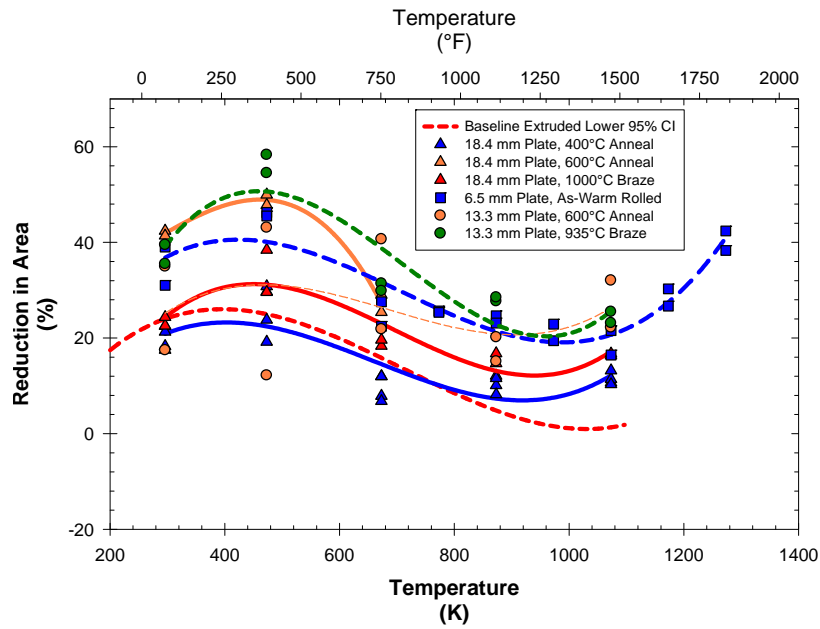


(b) Ultimate Tensile Strength

Figure 27.—Tensile properties of GRCop-84 plate.



(c) Tensile Elongation



(d) Reduction In Area

Figure 27.—Concluded.

To assess the effect of a simulated braze cycle, samples from the 13.3 mm plate were given the low temperature (935 °C/1715 °F) braze cycle in Table 1 while samples from the 18.4 mm plate were given the high temperature (1000 °C/1832 °F) simulated-braze cycle. The braze cycles were selected based upon changing requirements for the liner preform thickness and the anticipated braze cycle. The results of the tensile testing of those specimens are also presented in Figure 27.

Statistical analysis of the longitudinal and long transverse data sets showed that there was no statistical difference between the two directions. That is consistent with the data from the large extrusions. The  $\geq 79$  percent reduction in thickness during warm working of the extrusion to make the plate appears to break up the Cr<sub>2</sub>Nb agglomerations and refines the microstructure. Turning the plates during rolling also appeared to minimize the development of anisotropy.

The 400 °C heat treatment did not appear to anneal the plate. The 600 °C anneal for the 18.4 mm plate appears to still leave some residual cold work, but the 13.3 mm plate annealed for the same time and temperature appears to be fully annealed. This indicates that the time was insufficient for the thicker plate. This is further substantiated by the 1000 °C braze data.

The data sets for the 13.3 mm plate 600 °C anneal, 13.3 mm plate 935 °C braze and 18.4 mm plate 1000 °C braze conditions were fitted to Equation (1) using least squares regression analysis. The results are as follows

$$\sigma_{0.2\% \text{ Offset}, 600\text{C Anneal}}(T) = 196.6 + 0.112T - 3.87 \times 10^{-4} T^2 + 1.29 \times 10^{-7} T^3 - t(1 - \alpha, 6) \times 5.40 \quad (25)$$

$$\sigma_{0.2\% \text{ Offset}, 935\text{C Braze}}(T) = 228.3 - 0.0614T - 7.35 \times 10^{-5} T^2 - 4.83 \times 10^{-8} T^3 - t(1 - \alpha, 6) \times 11.38 \quad (26)$$

$$\sigma_{0.2\% \text{ Offset}, 1000\text{C Braze}}(T) = 218.8 - 0.149T + 9.14 \times 10^{-5} T^2 - 1.08 \times 10^{-7} T^3 - t(1 - \alpha, 6) \times 4.33 \quad (27)$$

$$\sigma_{UTS, 600\text{C Anneal}}(T) = 720.9 - 1.49T + 1.39 \times 10^{-3} T^2 - 5.58 \times 10^{-7} T^3 - t(1 - \alpha, 6) \times 18.04 \quad (28)$$

$$\sigma_{UTS, 935\text{C Braze}}(T) = 736.9 - 1.76T + 1.97 \times 10^{-3} T^2 - 8.89 \times 10^{-7} T^3 - t(1 - \alpha, 6) \times 21.50 \quad (29)$$

$$\sigma_{UTS, 935\text{C Braze}}(T) = 660.7 - 1.33T + 1.26 \times 10^{-3} T^2 - 5.33 \times 10^{-7} T^3 - t(1 - \alpha, 6) \times 17.26 \quad (30)$$

$$\varepsilon_{600\text{C Anneal}}(T) = 20.9 + 3.13 \times 10^{-3} T + 6.44 \times 10^{-6} T^2 - 6.98 \times 10^{-9} T^3 - t(1 - \alpha, 6) \times 3.18 \quad (31)$$

$$\varepsilon_{935\text{C Braze}}(T) = 55.0 - 0.127T + 1.58 \times 10^{-4} T^2 - 5.26 \times 10^{-8} T^3 - t(1 - \alpha, 6) \times 5.04 \quad (32)$$

$$\begin{aligned} \varepsilon_{1000C\ Braze}(T) = & 11.9 + 0.0650 \times 10^{-3} T - 9.20 \times 10^{-5} T^2 + 4.28 \times 10^{-8} T^3 \\ & - t(1 - \alpha, 6) \times 4.12 \end{aligned} \quad (33)$$

$$\begin{aligned} RA_{600C\ Anneal}(T) = & -29.0 + 0.311 T - 5.06 \times 10^{-4} T^2 + 2.46 \times 10^{-7} T^3 \\ & - t(1 - \alpha, 6) \times 12.7 \end{aligned} \quad (34)$$

$$\begin{aligned} RA_{935C\ Braze}(T) = & -71.3 + 0.633 T - 1.02 \times 10^{-3} T^2 + 4.80 \times 10^{-7} T^3 \\ & - t(1 - \alpha, 6) \times 6.9 \end{aligned} \quad (35)$$

$$\begin{aligned} RA_{1000C\ Braze}(T) = & -47.6 + 0.416 T - 6.83 \times 10^{-4} T^2 + 3.28 \times 10^{-7} T^3 \\ & - t(1 - \alpha, 6) \times 4.3 \end{aligned} \quad (36)$$

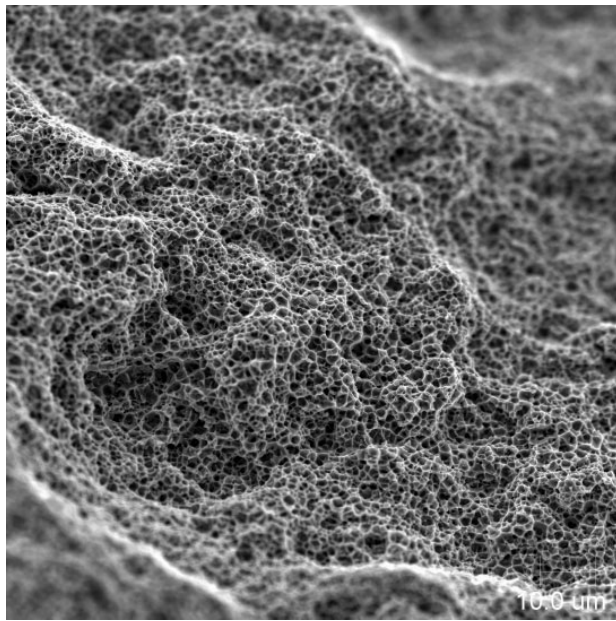
The fit of the regression models for the strengths was very good ( $R^2 > 0.98$ ), but the fit of the regression models to the elongation and reduction in area were not as good as can be visibly observed in Figures 27(c) and 27(d). The models for the 600 °C annealed material in particular had poor fits ( $R^2 \leq 0.1$ ). The fit of the model for the 1000 °C braze elongation was also poor with  $R^2 = 0.17$ . The other models had reasonable fits with  $R^2$  ranging from 0.53 to 0.78.

Fractography was performed on the plate samples. Typical fracture surfaces are shown in Figure 28. The highest temperature tensile test fracture surfaces are not shown because the surfaces oxidized too much for good analysis. Even the 600 °C fracture surfaces showed considerable oxidation though the larger features were still visible enough to provide useful information. However, optical examination at low magnification (7X to 60X) showed that the fracture surface morphology remained consistent with the fracture surfaces presented. The fractures are all ductile with the predominant failure mode being microvoid coalescence and growth. The size and morphology of both the fracture surfaces and the dimples on the surface appears to remain consistent with the baseline samples.

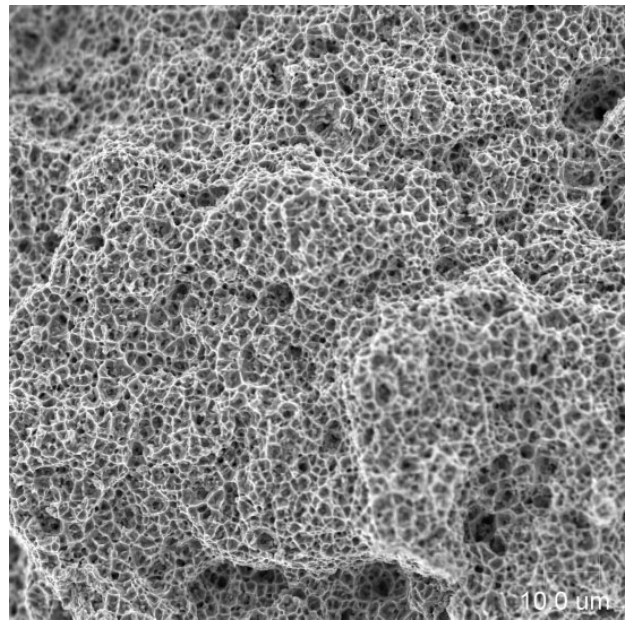
The largest observed change occurs in the plate samples given the high temperature simulated-braze cycle. Figure 29 shows large particles on the surface. EDS analysis identified the particles as elemental Cr. Since an excess of Cr is added to the alloy to minimize the Nb activity and prevent hydrogen embrittlement (Refs. 20 and 27), there is some elemental Cr in the alloy. Normally the Cr is present as very fine precipitates such as the one shown in Figure 13 that serve to help strengthen the alloy. During long high temperature exposures, they can undergo considerable coarsening as demonstrated by the observed particles that exceeded 5  $\mu\text{m}$  in many cases.

It appears that the Cr-Cu matrix interface is not quite as strong as the  $\text{Cr}_2\text{Nb}$ -Cu matrix interface. As a result, the large particles act as a site for premature failure. The effect on strength appears to be minimal based on the UTS results, but it does appear to adversely affect the reduction in area.

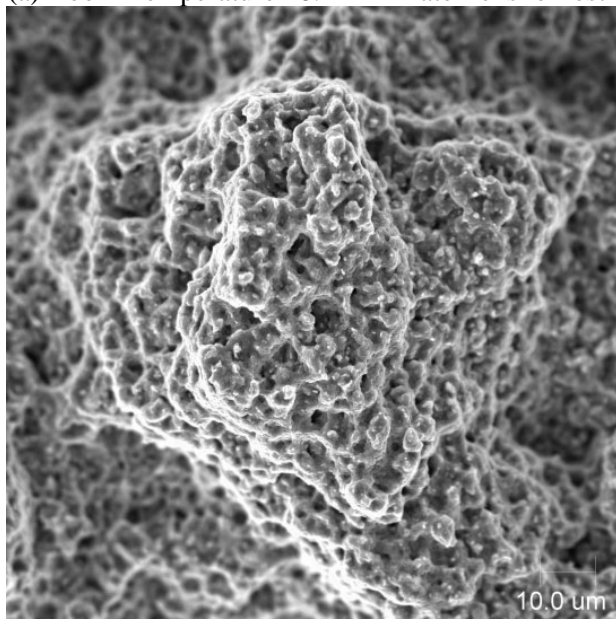
Figure 30 shows typical polished longitudinal cross-sections for several test conditions. The applied stress is in the vertical direction in all images. As with the large extrusions, the sections reveal damage in the form of voids extending well back from the fracture surface. While an effort was made to find Cr particles, no conclusive observations were made in the polished cross-sections. Given the small number of elemental Cr particles observed on the fracture surfaces, this was not a surprising result. Assuming that the Cr particles act as sites for failure initiation, they would tend to be more prevalent on the fracture surfaces than in a random cross-section such as is shown in Figure 30.



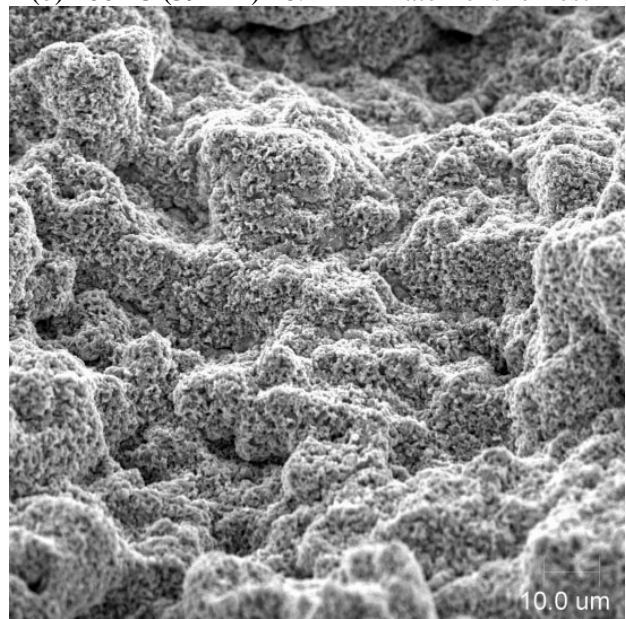
(a) Room Temperature 18.4 mm Plate Tensile Test



(b) 200 °C (392 °F) 18.4 mm Plate Tensile Test



(c) 400 °C (752 °F) 18.4 mm Plate Tensile Test



(d) 600 °C (1112 °F) 18.4 mm Plate Tensile Test

Figure 28.—Typical fracture surfaces of GRCop-84 plate.

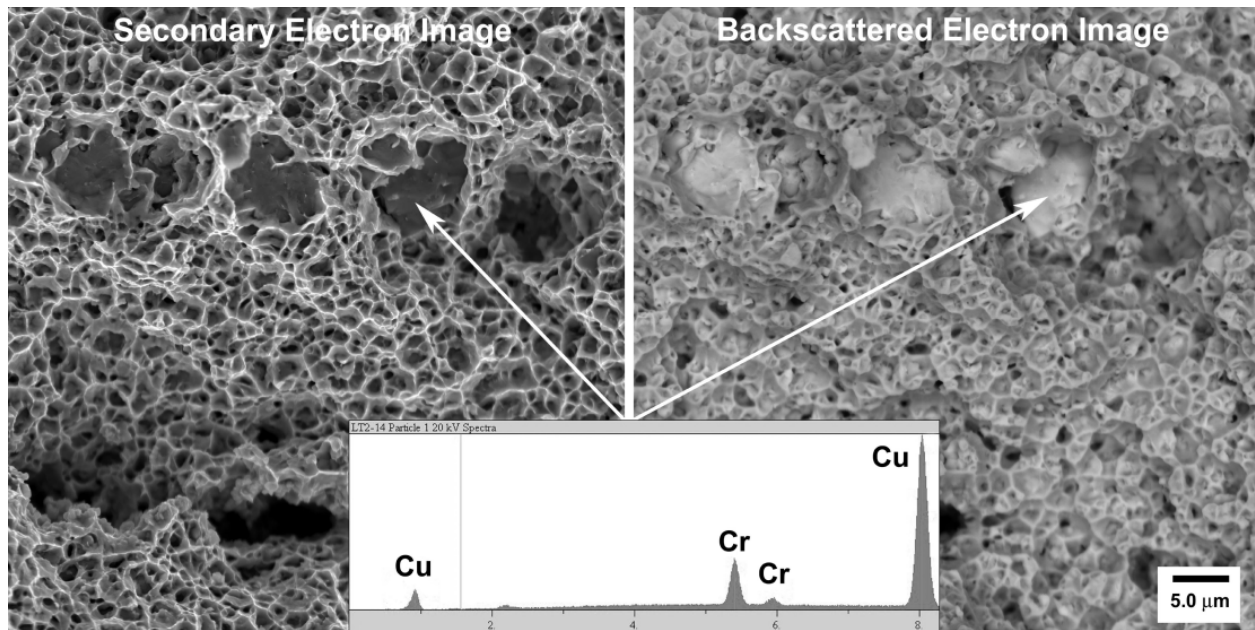
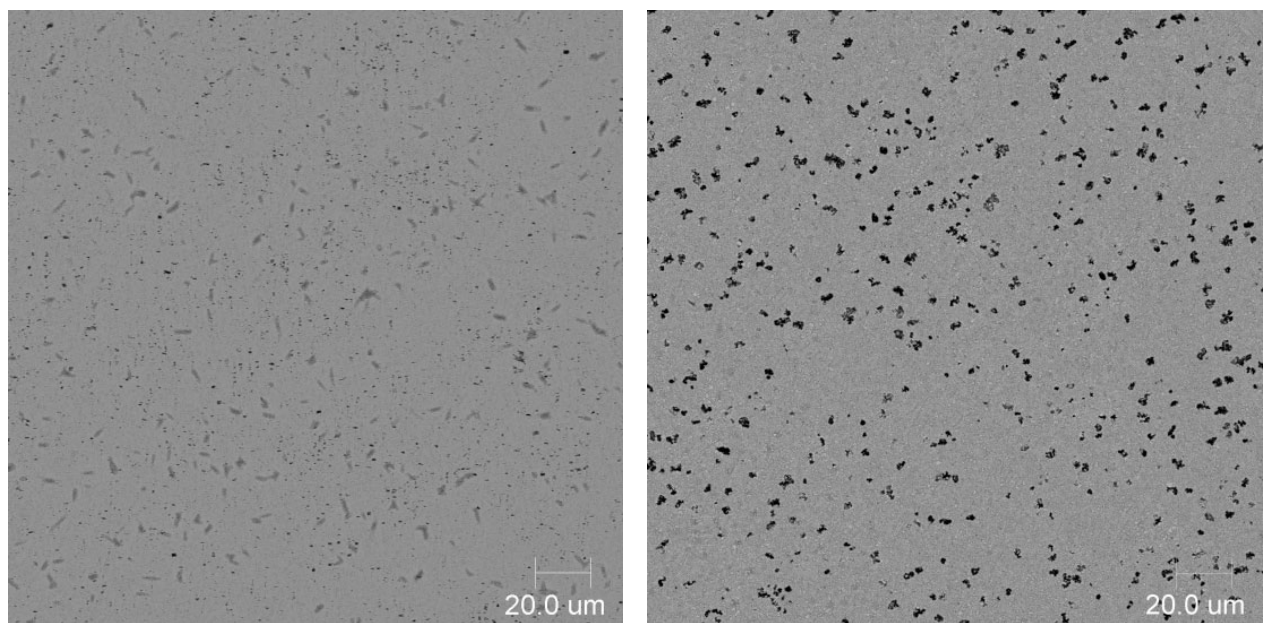


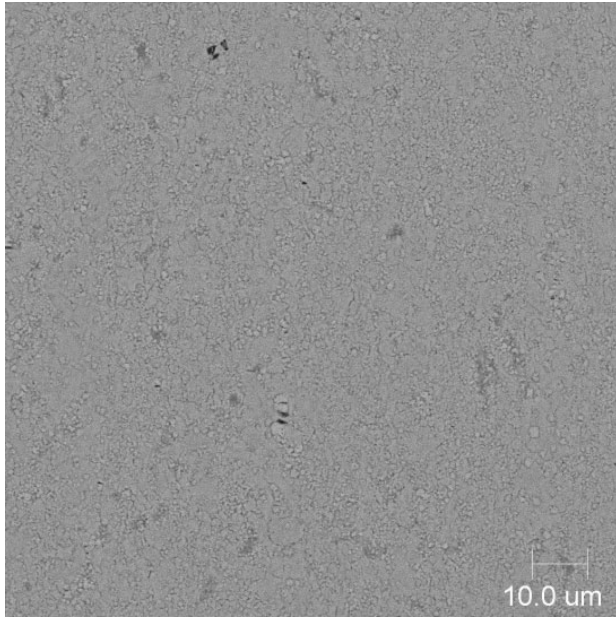
Figure 29.—Example of large Cr particles observed on fracture surface of plates given high temperature (1000 °C) simulated braze cycle.



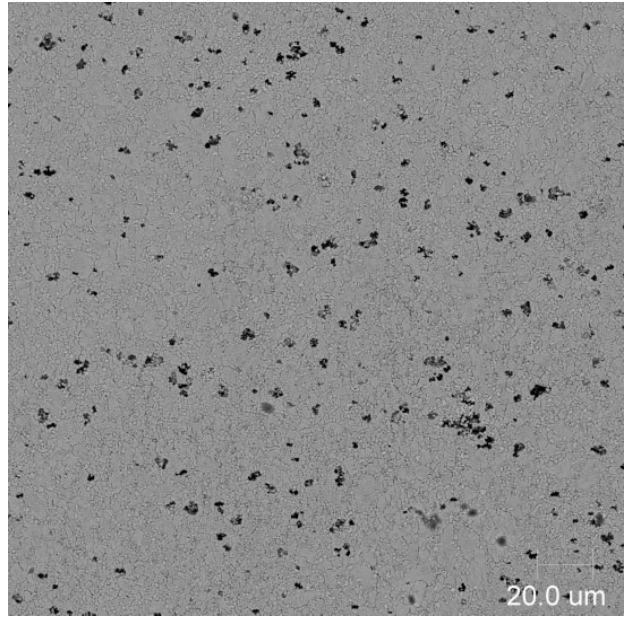
(a) Room Temperature Tensile Test,  
400 °C (752 °F) Annealed 18.4 mm Plate

(b) 600 °C (1112 °F) Tensile Test,  
400 °C (752 °F) Annealed 18.4 mm Plate

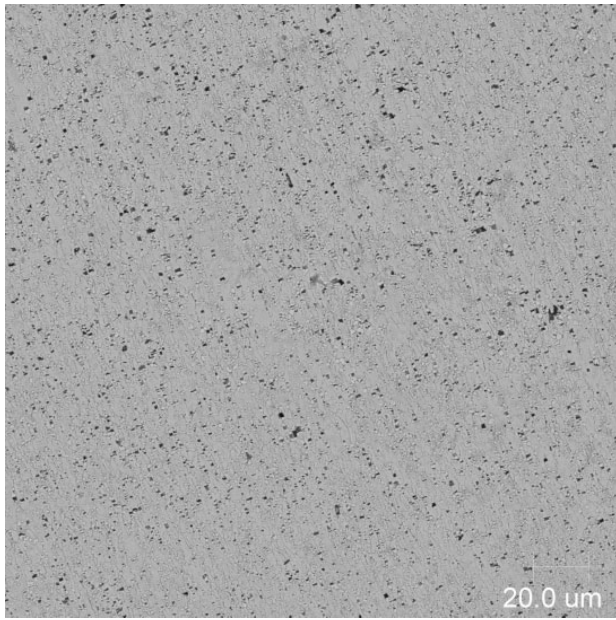
Figure 30.—Polished longitudinal cross-sections showing damage throughout reduced section.  
(All images used backscattered electron imaging)



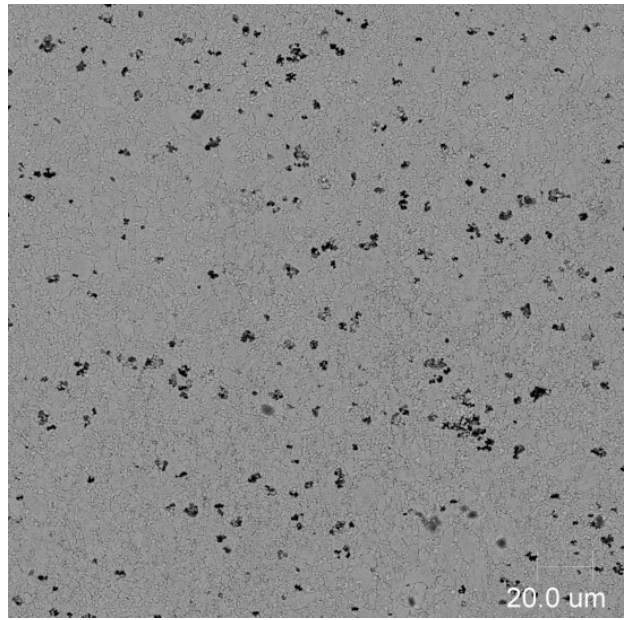
(c) Room Temperature Tensile Test,  
600 °C (1112 °F) Annealed 18.4 mm Plate



(b) 600 °C (1112 °F) Tensile Test,  
600 °C (1112 °F) Annealed 18.4 mm Plate



(e) Room Temperature Tensile Test,  
1000 °C (1832 °F) Brazed 18.4 mm Plate



(b) 600 °C (1112 °F) Tensile Test,  
1000 °C (1832 °F) Brazed 18.4 mm Plate

Figure 30.—Concluded.

## GRCop-84 Sheet

GRCop-84 sheet was produced in several thicknesses and levels of cold work. The nominal thicknesses of the sheets were 1.09, 0.58, 0.43, 0.36, and 0.25 mm (0.043, 0.023, 0.017, 0.014, and 0.010 in.).

The 1.09 mm sheet was provided with a 23 percent cold reduction and with two different annealing cycles. The first set of sheets were given an annealing cycle of 400 °C (752 °F) for 15 min. which does not produce a complete anneal (Ref. 14). Later sheets were provided with a complete anneal using 600 °C (1112 °F) for 30 min. The annealed 1.09 sheet was used as the feedstock for subsequent cold rolling to the other sheet thicknesses tested. The remaining sheet was provided in a cold-worked condition with the amount of cold work increasing as the thickness decreased.

### Effect of Annealing Temperature on Room Temperature Tensile Properties

The room temperature tensile properties of 23 percent cold rolled 1.09 mm thick GRCop-84 sheet following a 30 min. anneal at various temperatures are presented in Figure 31. Additional details and analysis are presented elsewhere in the GRCop-84 task final report (Ref. 14). There appears to be some strengthening occurring in the samples annealed at 200 and 300 °C (392 and 573 °F). It is believed that very fine Cr or Cr<sub>2</sub>Nb particles are precipitating or that Cu subgrains are organizing and acting similar to grain boundaries to provide additional Hall-Petch strengthening, but no definitive proof was seen in the TEM observations of the samples.

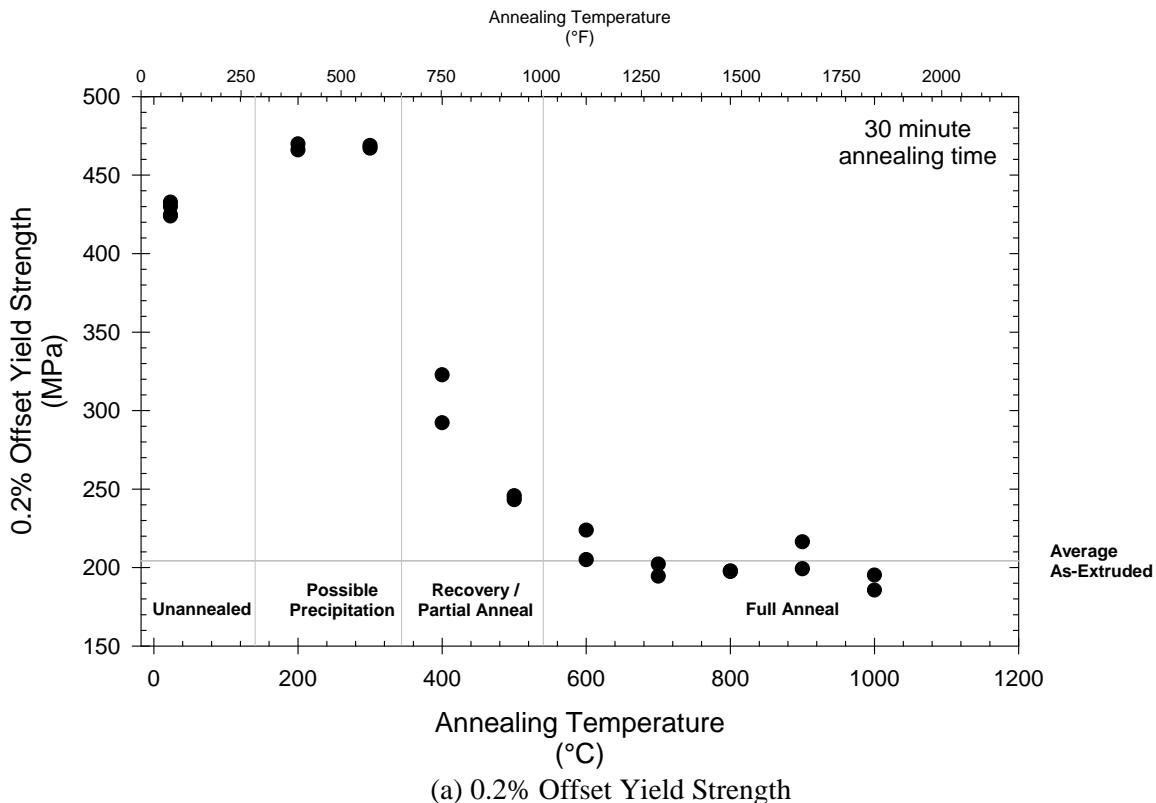
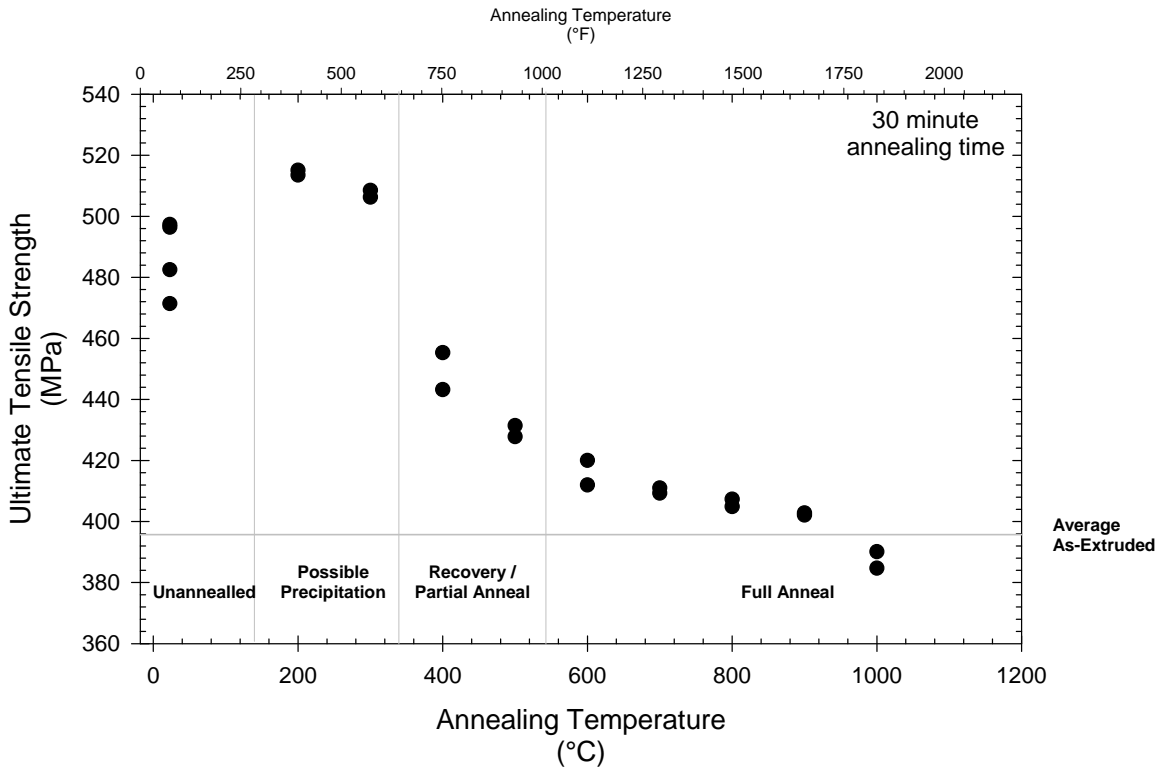
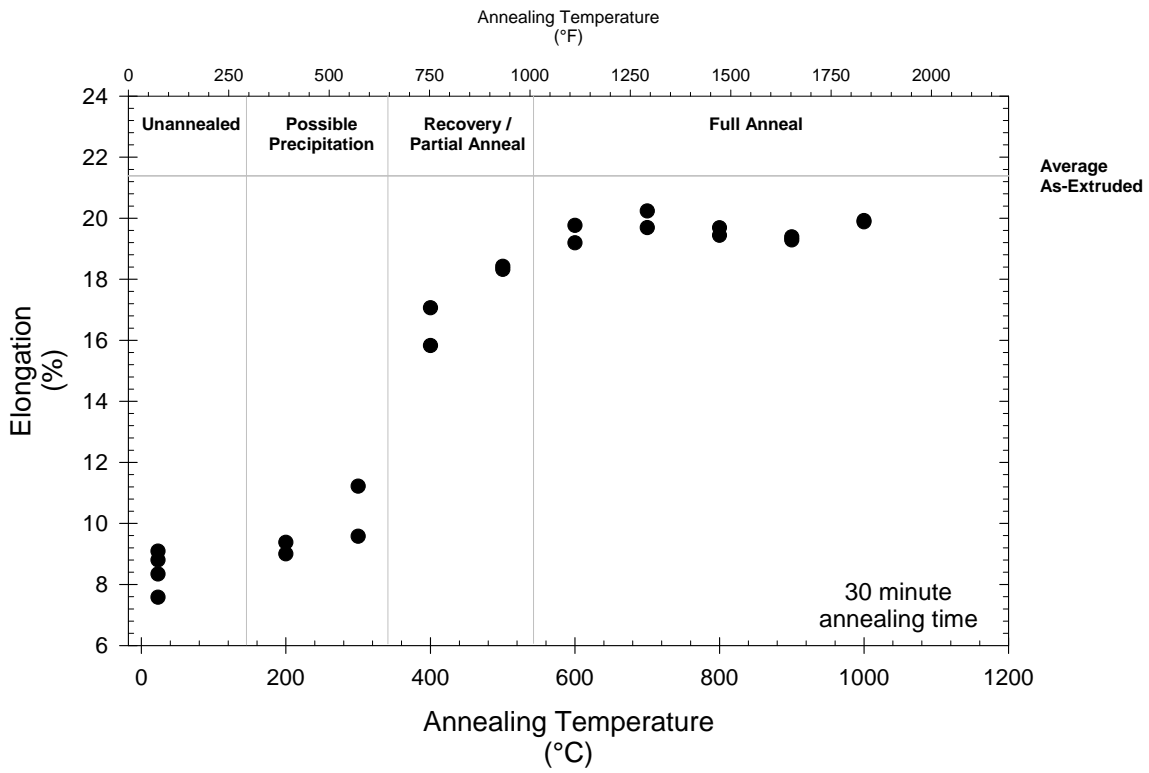


Figure 31.—Room temperature tensile properties following annealing at various temperatures.



(b) Ultimate Tensile Strength



(c) Tensile Elongation

Figure 31.—Concluded.

Representative fracture surfaces are presented in Figure 32. Annealing temperature does not appear to have any discernable effect on the failure mode or the dimple morphology and size. Even comparing the as-cold rolled and annealed specimens there were no major changes in the fracture surfaces.

Based upon these results it was determined that a 600 °C (1112 °F) annealing temperature was needed to ensure a complete anneal. Prior work to set the 400 °C anneal was with 30 to 35 percent cold worked GRCop-84, and apparently this difference in work was sufficient to greatly affect the annealing temperature. Easily observed grain growth occurred in samples given an 800 to 1000 °C anneal, so these were not deemed suitable (Ref. 14). Using 600 °C instead of the higher temperatures also has commercial benefits since lower temperature annealing costs less.

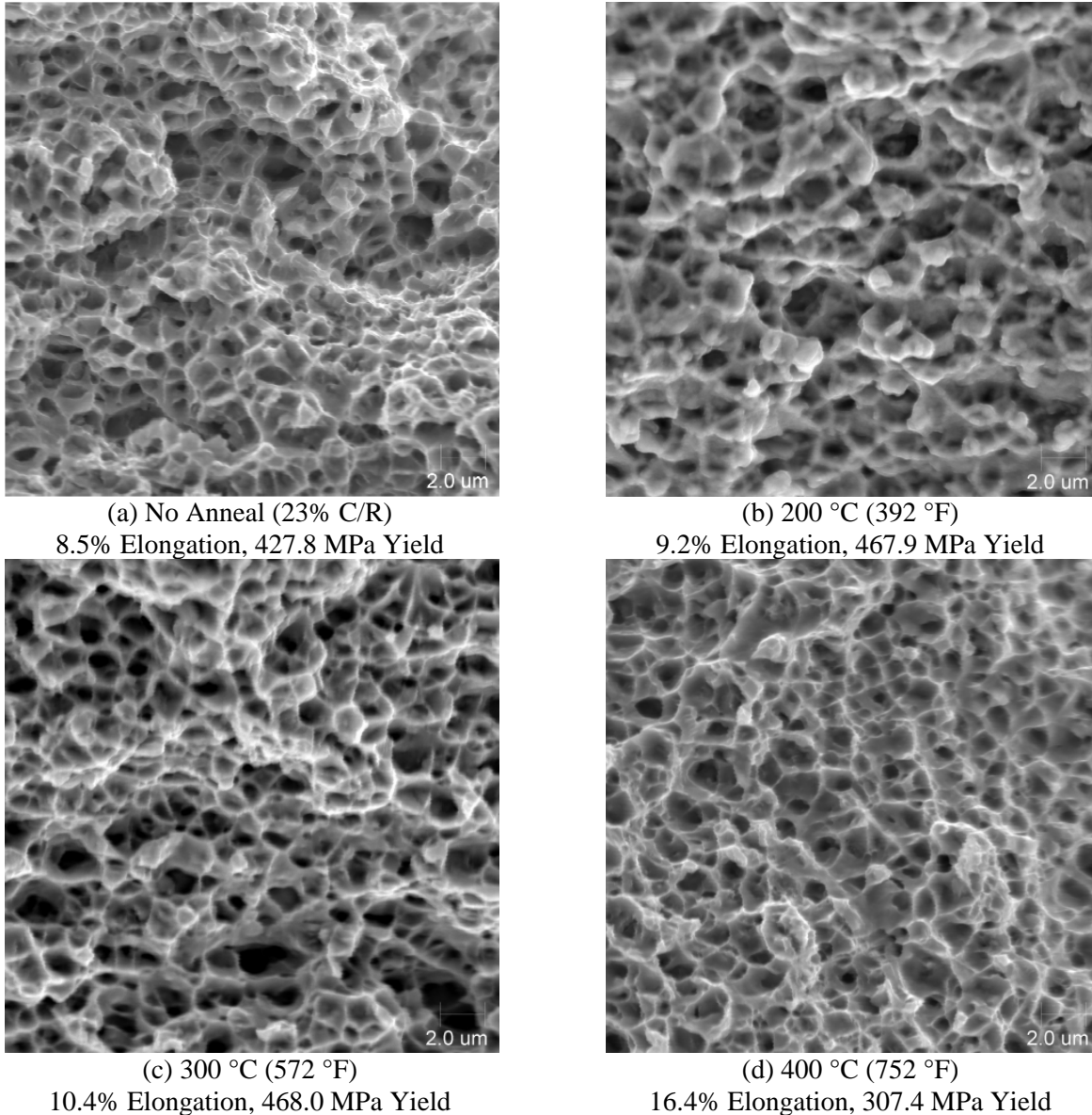
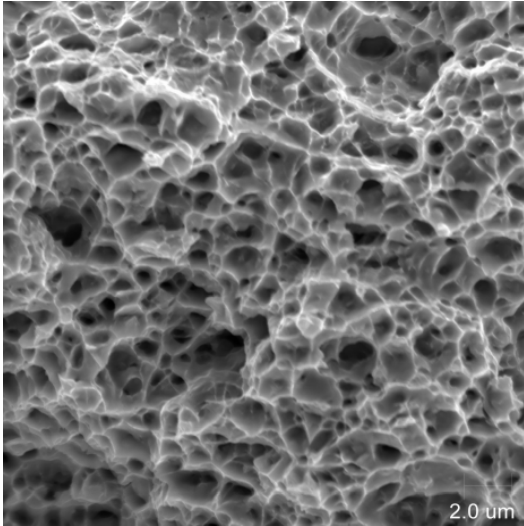
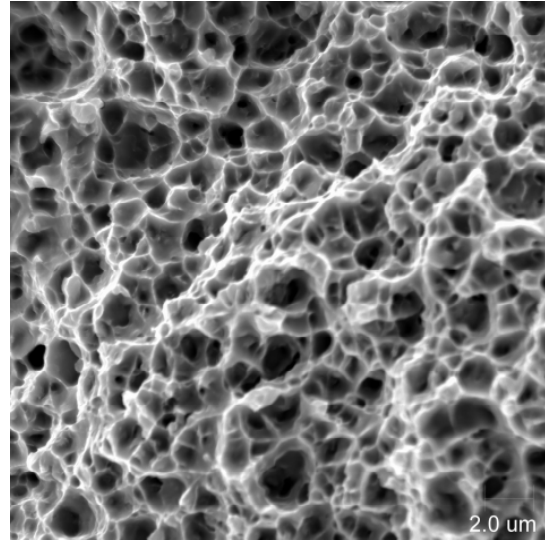


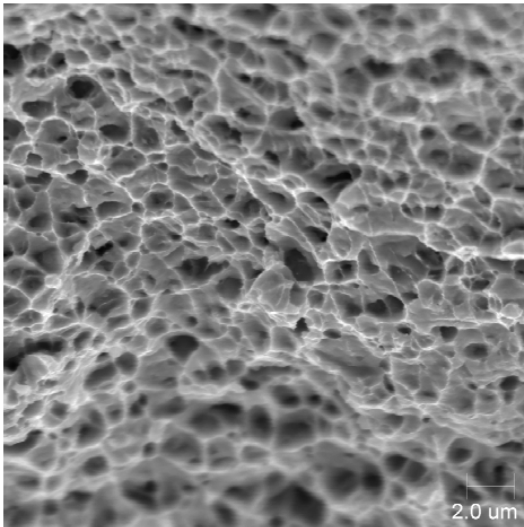
Figure 32.—Representative fracture surfaces of samples annealed for 30 min at various temperatures.



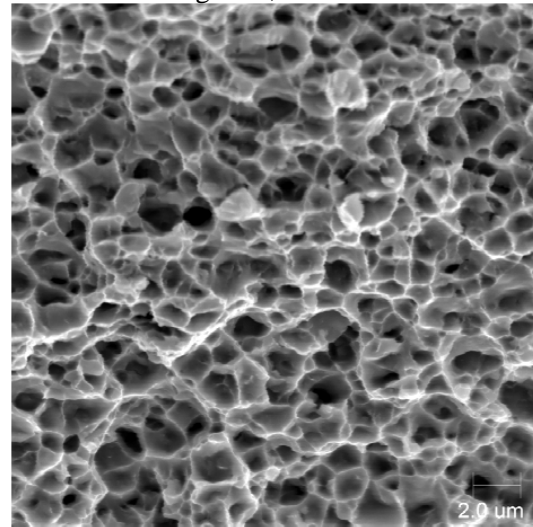
(e) 500 °C (932 °F)  
18.4% Elongation, 244.5 MPa Yield



(f) 600 °C (1112 °F)  
19.5% Elongation, 214.4 MPa Yield

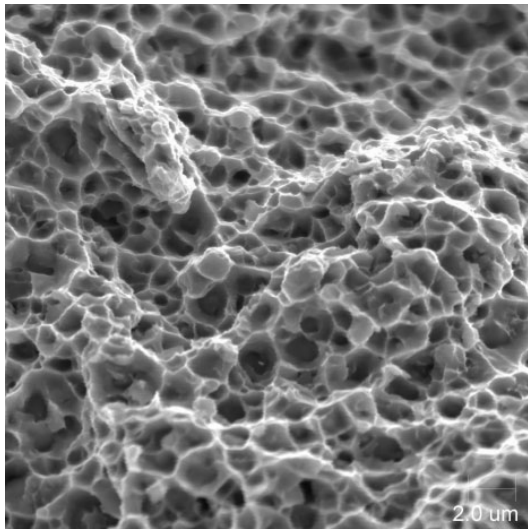


(g) 700 °C (1292 °F)  
20.0% Elongation, 198.3 MPa Yield

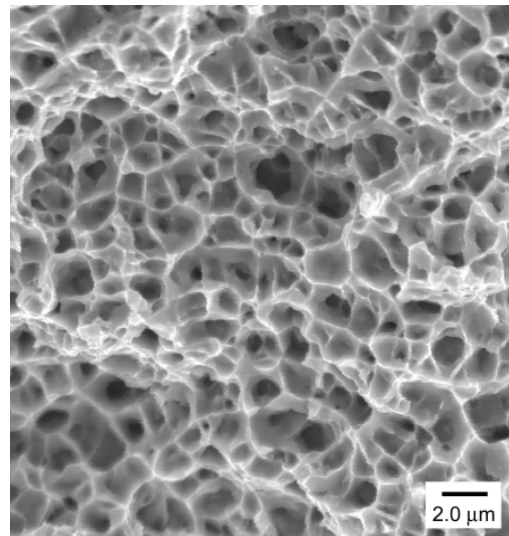


(h) 800 °C (1472 °F)  
19.6% Elongation, 197.6 MPa Yield

Figure 32.—Continued.



(i) 900 °C (1652 °F)  
19.3% Elongation, 207.8 MPa Yield



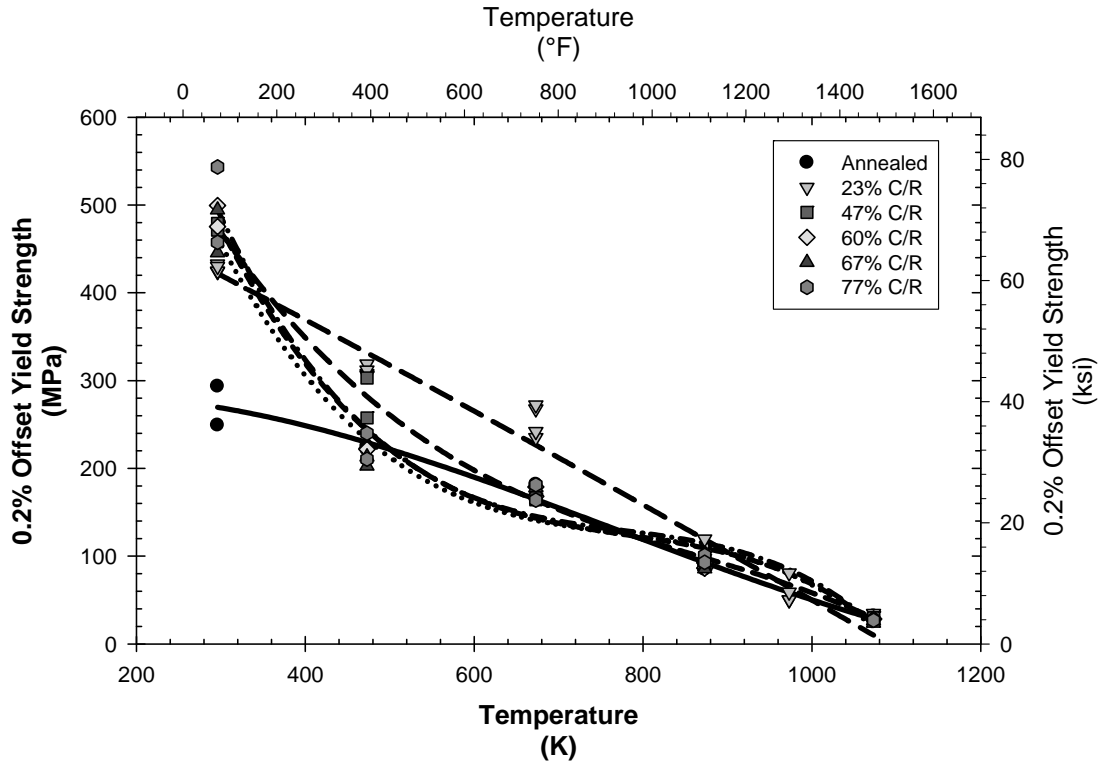
(j) 1000 °C (1832 °F)  
19.9% Elongation, 190.3 MPa Yield

Figure 32.—Concluded.

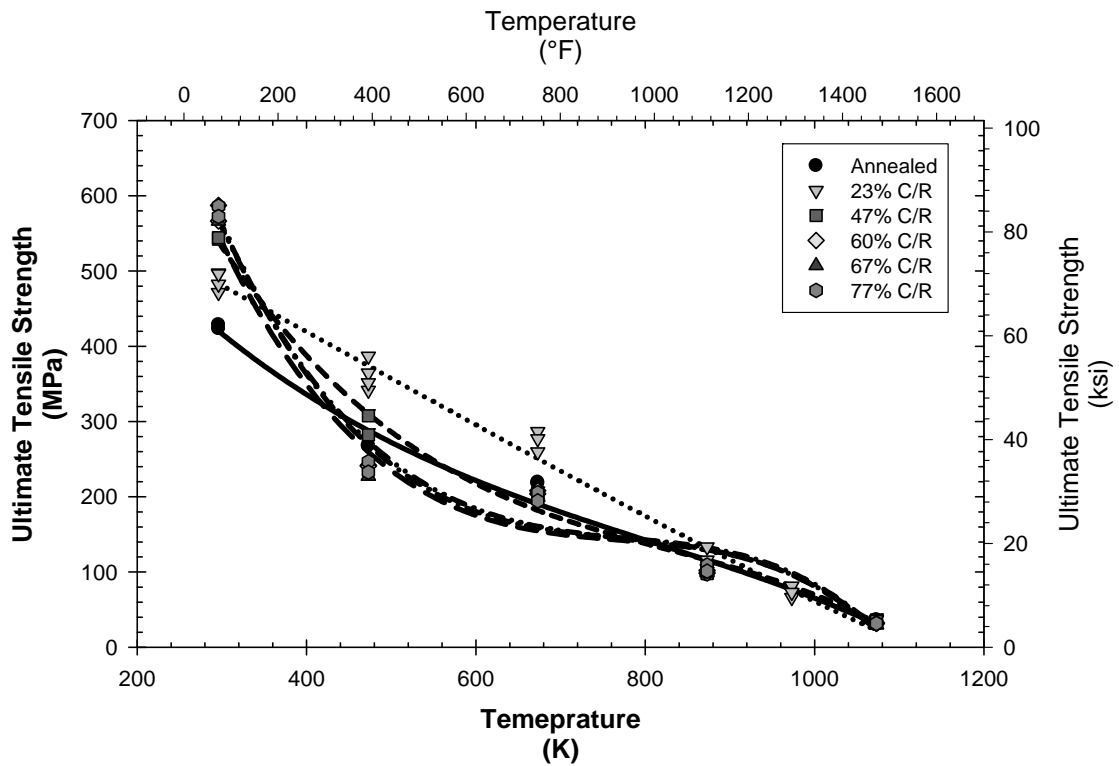
### Cold Rolled Sheet

Samples of 1.09 mm thick GRCop-84 sheet were tested in the as-annealed condition following a 600 °C (1112 °F)/30 min. anneal and following annealing and additional cold-rolling reductions of 23, 47, 60, 67, and 77 percent. Tensile testing was conducted at room temperature (nominally 23 °C/73 °F) and elevated temperatures of 200, 400, 600, 700, and 800 °C (392, 752, 1112, 1292, and 1472 °F). The results are presented in Figure 33. Because the differences at room temperature, 200 and 400 °C are difficult to distinguish, the results are plotted in Figure 34 as strength and elongation as a function of cold work at a constant temperature. For the room temperature tests, the foil sample results described in detail in the next section are also included. These specimens had a 90 percent cold reduction. Only results from tests that used an extensometer are included. At temperatures of 600 °C and above, the test results collapse to essentially the same value for all conditions. This is consistent with a full anneal occurring during the heating of the samples which typically took between 24 and 36 min.

Looking at Figures 33 and 34, the effect of cold work decreased markedly with increasing test temperature as the material recovered and annealed. At room temperature any cold work raises the yield strength to between 423 and 543 MPa, an increase of about 150 to 270 MPa relative to the fully annealed 1.09 mm thick sheet. Above room temperature the difference rapidly decreases as shown in Figure 34. By 600 °C the effects of cold work disappear as the GRCop-84 specimens anneal completely during heating to the test temperature. Because of this, there was no statistically detectable effect of cold work when the data for all temperatures was considered.

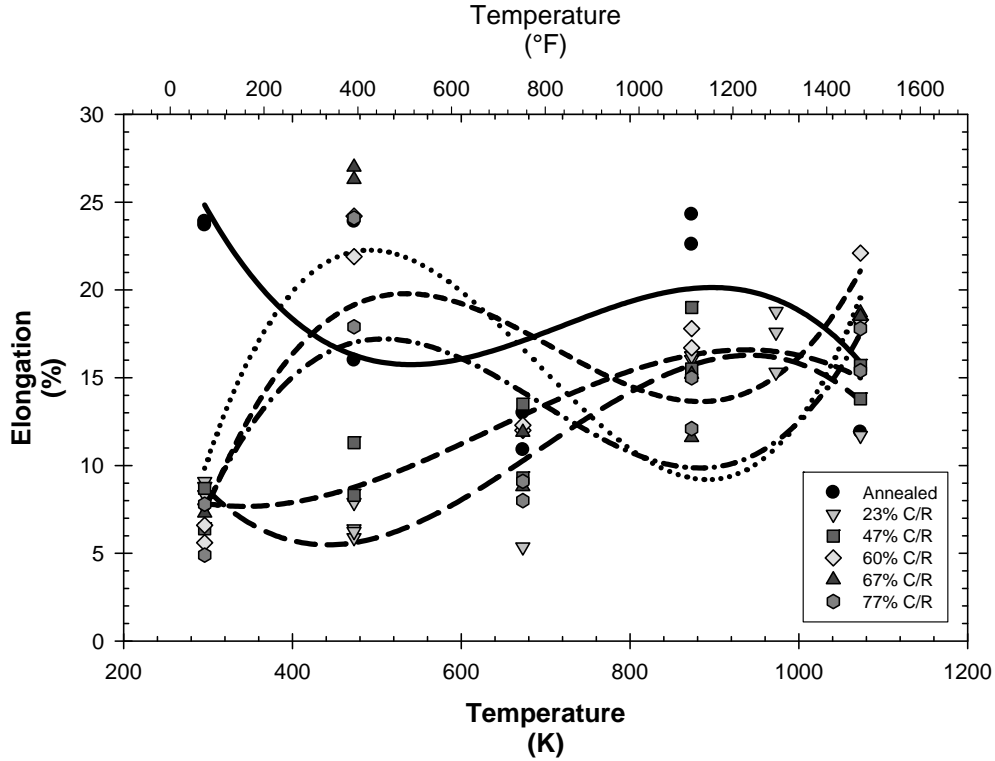


(a) 0.2% Offset Yield Strength



(b) Ultimate Tensile Strength

Figure 33.—Effect of temperature and cold work on tensile properties.



(c) Tensile Elongation

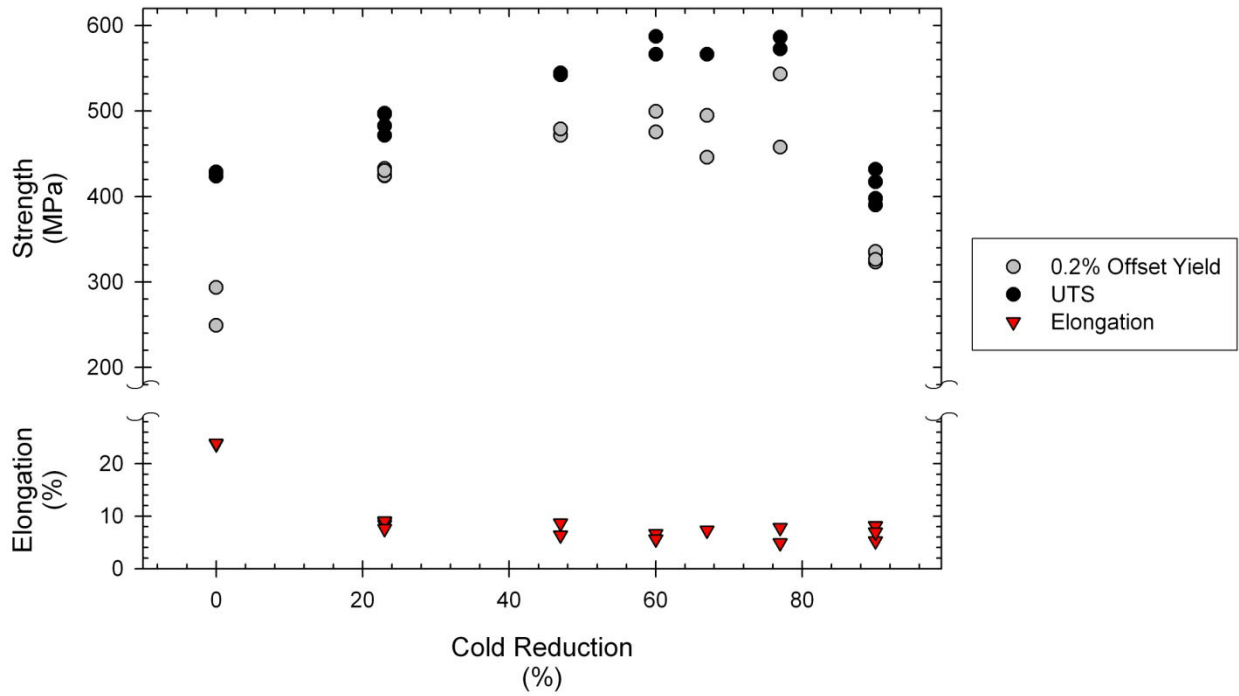
Figure 33.—Concluded.

Cold work clearly plays a role in the room temperature tensile properties, so a model using just the room temperature data was developed. The analysis was done as a simple polynomial regression of the room temperature data using the percent of cold work as the dependent variable. The results showed that a third order polynomial had a small advantage over a second order polynomial for the fit of the data as measured by  $R^2$  but gave results that passed the normality test much better. Based on this difference, the third order polynomial was selected over the second order polynomial. The resulting equations for the tensile properties are

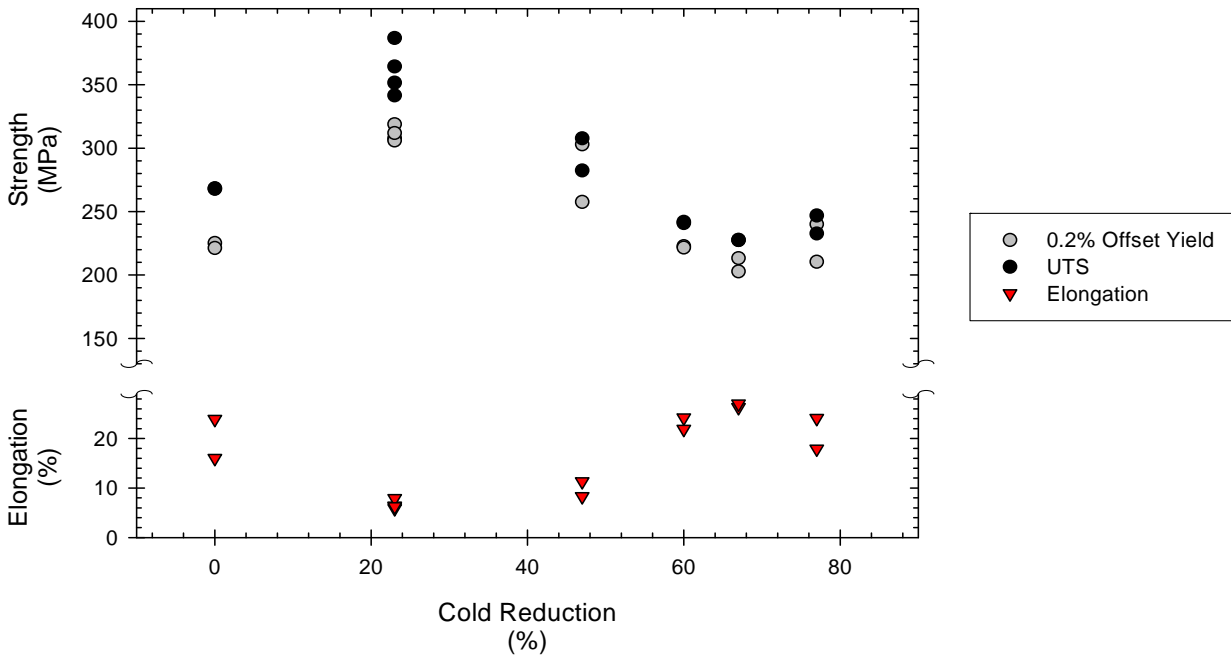
$$\sigma_{0.2\% \text{ Offset}, RT} = 270.9 + 10.51 W - 0.184 W^2 + 1.11 \times 10^{-3} W^3 \quad (37a)$$

$$\sigma_{UTS, RT} = 426.3 + 2.30 W - 2.13 \times 10^{-2} W^2 + 3.31 \times 10^{-4} W^3 \quad (37b)$$

$$\epsilon_{RT} = 23.7 + 1.08 W - 2.15 \times 10^{-2} W^2 + 1.36 \times 10^{-4} W^3 \quad (37c)$$

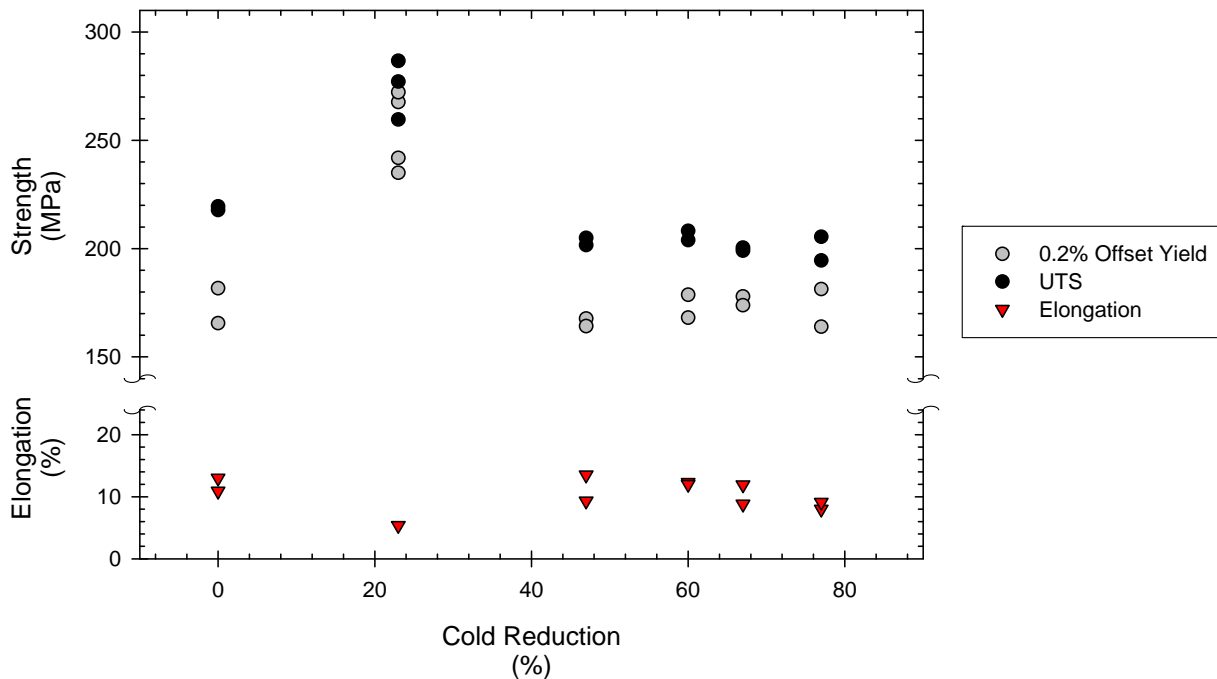


(a) Room Temperature



(b) 200 °C (392 °F)

Figure 34.—Effect of cold work on tensile properties at selected temperatures.



(c) 400 °C (752 °F)

Figure 34.—Concluded.

### Tensile Properties of GRCop-84 Foil

A sample of GRCop-84 was cold rolled using a Sendzimir mill to determine the maximum cold reduction possible through rolling. The piece was reduced 90 percent without cracking or otherwise failing before the mill could not further reduce the thickness. Samples were tested at room temperature in air and at 500 °C (932 °F) in vacuum. Both the longitudinal and long transverse directions were examined. After testing five samples using crosshead control, an extensometer was placed on the last four samples. The samples did not fail at the knife edge as feared, so it was possible to more accurately determine the stress-strain curve. No extensometer was used with the 500 °C tests due to physical limitations of the test frame vacuum chamber.

Figure 35 shows room temperature stress-strain curves with and without the extensometer. As one would expect, the major difference observed with and without the extensometer was in the elastic region. The samples tested with an extensometer attached have a higher slope since machine compliance is not included in the calculation of the strain. All samples show at least 5 percent elongation and some approach 10 percent elongation at failure.

Table 7 summarizes the results for the longitudinal and long transverse directions as well as the composite average for all nine tests. The number of tests for each direction and the overall average is given as well.

A difference that was statistically significant at the 95 percent confidence level was observed between the room temperature longitudinal and long transverse ultimate tensile strengths (UTS). The average long transverse UTS was 39.4 MPa (5.7 ksi) greater than the longitudinal UTS. Observations of the microstructure shown in Figure 36 did not show any substantial differences. Likewise x-ray pole figures prepared for the foil did not reveal significant texture. The basis for the difference is not known, and it is the one of the few cases where measurable anisotropy has been observed for GRCop-84. Even the 77 percent cold-rolled sheet did not show this behavior.

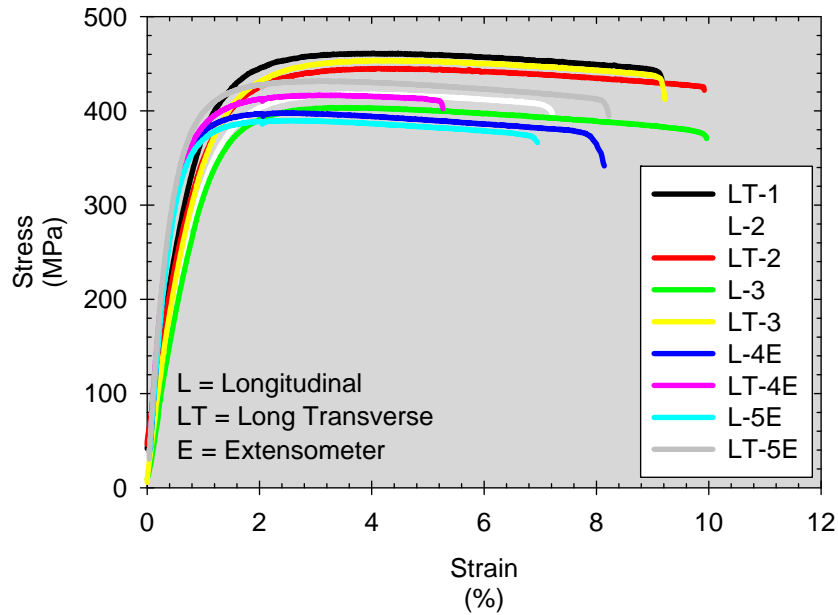
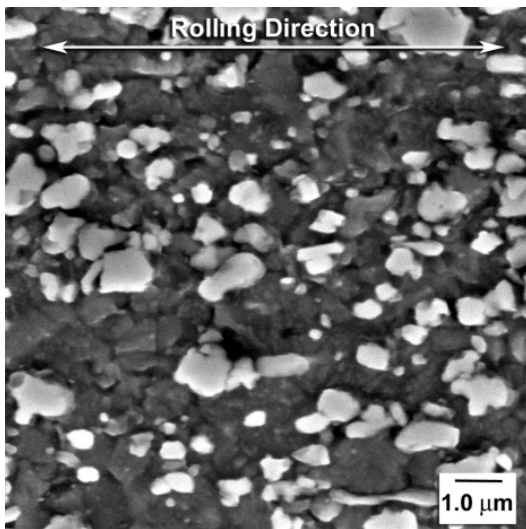


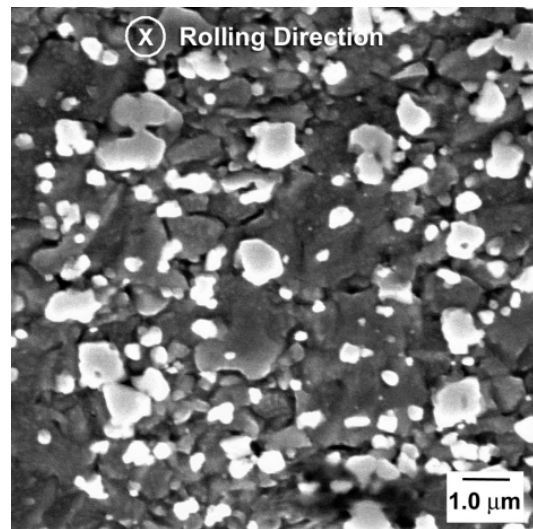
Figure 35.—Stress strain curves for nine GRCop-84 foil samples.

TABLE 7.—AVERAGE ROOM TEMPERATURE TENSILE VALUES FOR 90 PERCENT COLD ROLLED GRCop-84 FOIL

Orientation		0.2% Offset Yield (MPa)	Ultimate Tensile Strength (MPa)	Elongation (%)	Modulus (GPa)
Long Transverse (4 Tests)	Average	324.1	441.7	8.3	92.0
	Standard Deviation	13.1	17.7	1.8	1.7
Longitudinal (5 Tests)	Average	316.2	402.3	8.0	79.0
	Standard Deviation	17.6	12.0	1.4	0.5
Average (9 Tests)	Average	320.6	424.2	8.2	85.5
	Standard Deviation	14.8	25.3	1.6	7.6



(a) Longitudinal



(b) Long Transverse

Figure 36.—Microstructure of 90 percent cold rolled GRCop-84 foil.

TABLE 8.—DIFFERENCES IN PROPERTIES BETWEEN 77 PERCENT COLD WORKED SHEET AND 90 PERCENT COLD WORKED FOIL

<b>Reduction</b>	<b>Yield Strength (MPa)</b>	<b>UTS (MPa)</b>	<b>Elongation (%)</b>
77	457.5	572.5	7.8
77	543.3	586.4	4.9
<b>Average</b>	<b>500.4</b>	<b>579.5</b>	<b>6.4</b>
<b>Std. Dev.</b>	<b>60.7</b>	<b>9.8</b>	<b>2.1</b>
90	323.0	416.9	5.2
90	334.2	431.7	8.2
90	335.7	397.8	8.1
90	326.4	389.8	6.9
<b>Average</b>	<b>329.8</b>	<b>409.1</b>	<b>7.1</b>
<b>Std. Dev.</b>	<b>6.1</b>	<b>18.9</b>	<b>1.4</b>
<b>Difference</b>	<b>170.6</b>	<b>170.4</b>	<b>-0.8</b>

While it appears likely that the modulus of the foil differs between the longitudinal and long transverse direction, the difference is not statistically significant. The primary reason for this is the poor power available to compare the two means. With only two degrees of freedom the differences would have to be much greater to become statistically significant. Additional testing with an extensometer could resolve this question with only a few tests for each direction.

It was observed that the yield and ultimate tensile strengths of GRCop-84 foil worked 90 percent is much less than that of GRCop-84 sheet cold worked 77 percent as shown in Table 8. The differences in the average strengths are 171 MPa, but the elongations remain nearly constant. The strength and ductility values are similar to GRCop-84 sheet cold worked 23 percent and annealed for 30 min. at 400 °C (752 °F) (Fig. 31). The microstructures in Figure 36 do not show the anticipated pancake-shaped grains.

Given that the recrystallization temperature of GRCop-84 appears to be dependent on the amount of cold work and that the microstructure does not show evidence of large deformations, it is hypothesized that the foil underwent partial annealing during cold rolling. The increase in temperature of the foil during rolling due to the large amount of work introduced into the material likely assisted this process even though the foil did not appear to achieve a temperature greater than 200 °C (352 °F) and generally was cooler. This is consistent with the work by Yokelson and Balicki (Ref. 28) on the annealing of pure copper. Their work indicated that copper cold worked 90 percent would begin to anneal at 200 °C. It is also consistent with the observations of this study that increasing cold work lowers the temperature required to anneal or at least recover cold worked GRCop-84.

Figure 37 shows a typical fracture surface for a room temperature tensile test. While the GRCop-84 has been extensively cold-worked, the fracture surface remains a ductile failure through the coalescence and growth of microvoids. This continues the observed trend of uniformly ductile failure modes regardless of the processing of GRCop-84. This gives confidence that the alloy will always deliver predictable failure in service with some plastic deformation prior to failure.

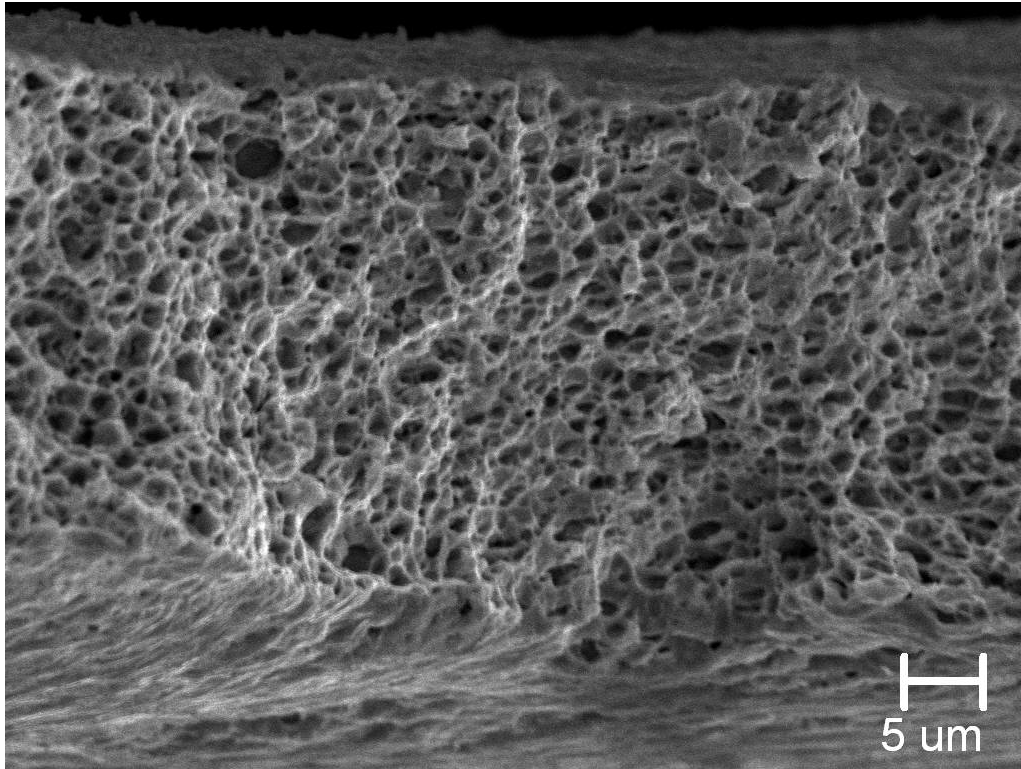


Figure 37.—Typical room temperature fracture surfaces of 90 percent cold rolled GRCop-84 foil.

TABLE 9.—AVERAGE 500 °C (932 °F) TENSILE VALUES FOR 90 PERCENT COLD ROLLED GRCop-84 FOIL

Orientation		0.2% Offset Yield (MPa)	Ultimate Tensile Strength (MPa)	Elongation (%)
<b>Long Transverse</b> (4 Tests)	<b>Average</b>	96.3	110.8	11.2
	<b>Standard Deviation</b>	12.0	12.6	1.7
<b>Longitudinal</b> (5 Tests)	<b>Average</b>	89.8	103.0	12.7
	<b>Standard Deviation</b>	22.3	25.3	1.4
<b>Average</b> (9 Tests)	<b>Average</b>	93.1	106.9	11.9
	<b>Standard Deviation</b>	16.9	18.9	1.7

The testing of the GRCop-84 at 500 °C (932 °F) in vacuum was generally successful. Two samples showed anomalously large strengths and were excluded as outliers. It was felt the outliers were likely caused by small experimental errors that affected the measured loads, which were quite small. Table 9 summarizes the results from the remaining eight tests. Statistical analysis of the longitudinal and long transverse data sets revealed that there were no statistically significant differences in the two populations, so there was no evidence of anisotropy at elevated temperatures. Based on the annealing results, it is likely that the samples underwent partial to full recrystallization during testing due to the 90 percent cold work and the 500 °C test temperature which was known to cause partial annealing in 23 percent cold-worked GRCop-84 sheet.

Figure 38 shows the fracture surface of a specimen tested at 500 °C. There is a definite change in the morphology. There appears to be more shearing occurring. The development of shear stresses is the results of difficulties encountered when attempting to grip and test a foil specimen at elevated temperatures in a vacuum. It would not be surprising if the tests did not have truly uniaxial loading. A shear component will lower the stress to failure and change the morphology of the fracture surfaces. While undesirable to have these deviations, the tensile results are likely representative of the actual foil properties.

The dimple size also appears to change considerably. It is unclear if the smearing of the fracture surface removed the small dimples or if there was an actual change in the dimple size. It appears that the later occurred which would be the most significant change observed in the GRCo-84 fracture surfaces. It also deviated from the other GRCo-84 forms tested at temperatures above 400 °C (752 °F). While not presented, here due to the oxidation of the surfaces during cool down, optical and limited SEM examinations showed fractures at elevated temperatures retained approximately the same dimple size of 1 to 2 μm to 1000 °C (1832 °F).

It was not possible to conclusively determine if this change in dimple size was a result of the processing or if it was a testing artifact. Based upon the history of similarity between all other fracture surfaces and the appearance of the room temperature foil fracture surface, it is felt that it is likely a testing artifact. The problems of getting truly uniaxial loads likely contributed to the observed changes. It is not felt that the vacuum was a contributing factor because observations of fracture surfaces of creep specimens tested in vacuum are similar to tensile specimens in dimples morphology and size (Ref. 15).

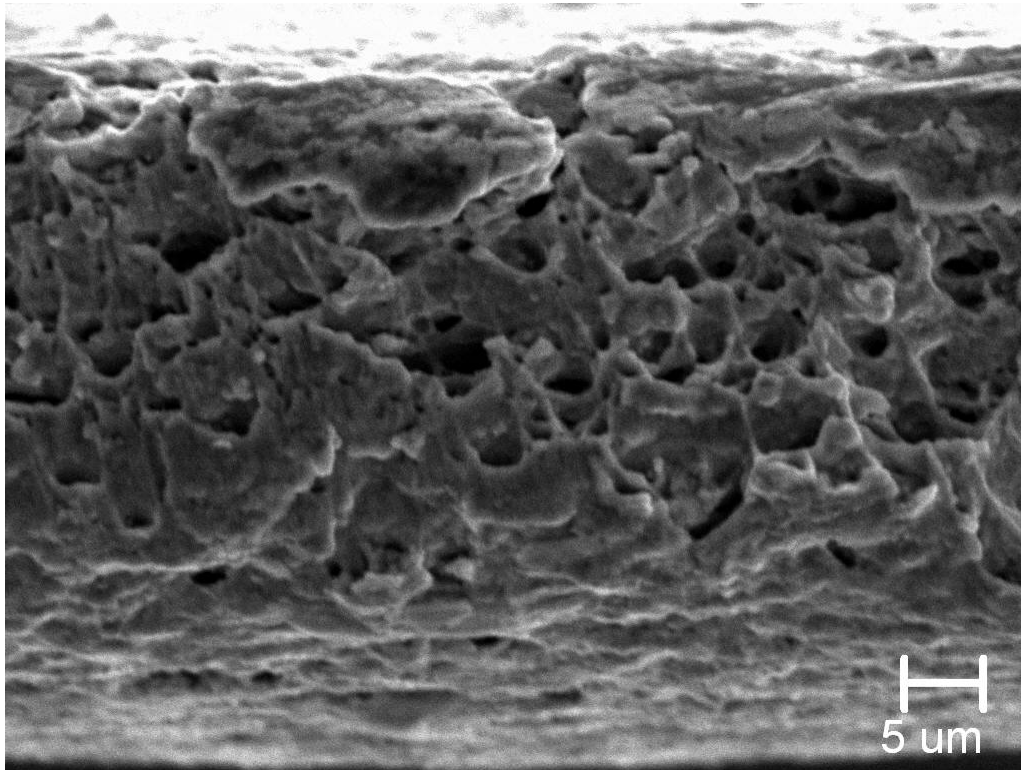


Figure 38.—Typical 500 °C (932 °F) fracture surfaces of 90 percent cold rolled GRCo-84 foil.

TABLE 10.—RESULTS OF GRCoP-84 TUBE TESTING

Sample	Modulus (GPa)	0.2% Offset Yield Strength (MPa)	UTS (MPa)	Strain To Failure (%)
1	115	246	417	21.1
2	116	243	422	25.4
3	113	248	421	21.9
<b>Average</b>	<b>114.7</b>	<b>245.7</b>	<b>420.0</b>	<b>22.8</b>
$\sigma$	1.5	2.5	2.6	2.3

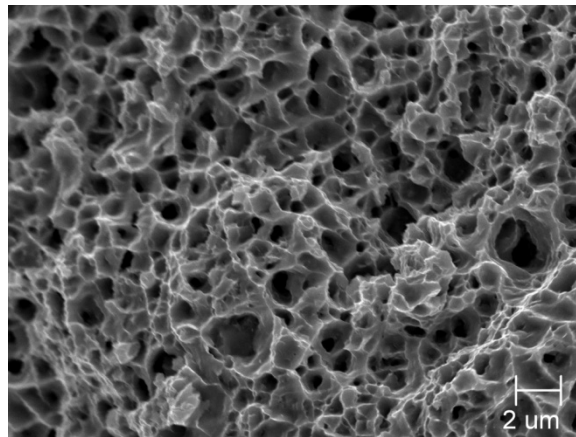


Figure 39.—Fracture surface of a GRCoP-84 production tubing tensile specimen.

### Tubing

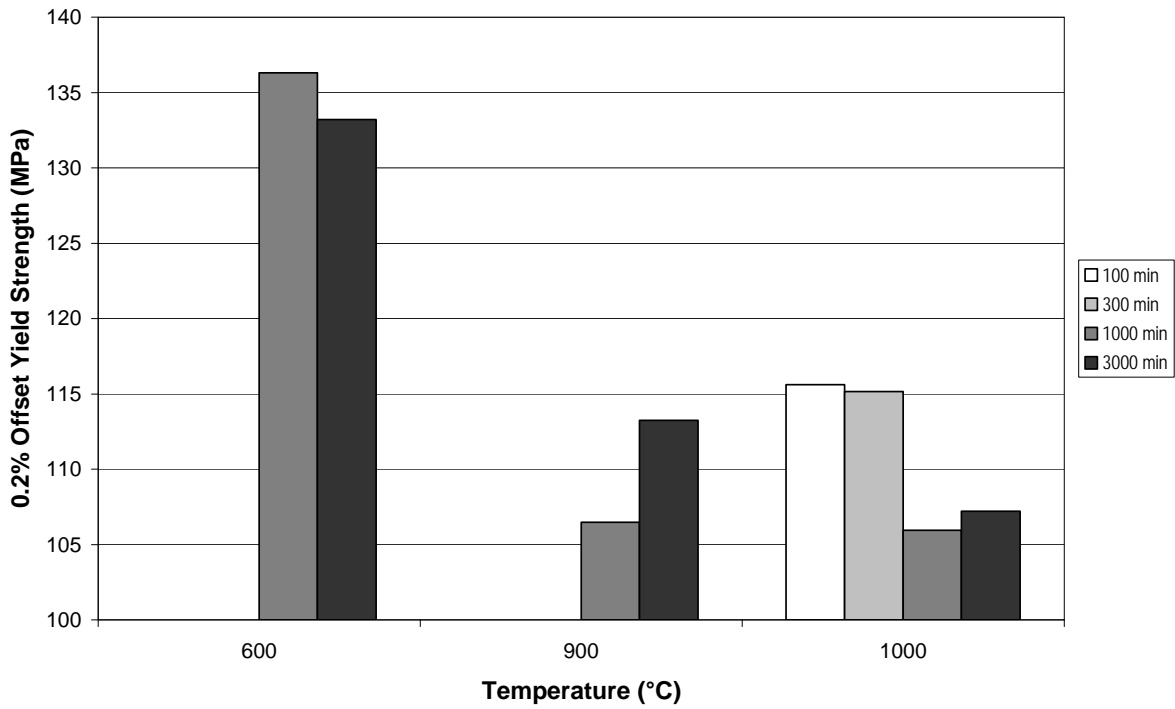
The stress-strain curves for typical tube tests were presented in Figure 9 where the curves were compared to other forms of GRCoP-84. The results for the room temperature tensile tests of GRCoP-84 tubing are presented in Table 10. The results are consistent with annealed GRCoP-84 sheet and the as-extruded GRCoP-84 tensile properties. Modulus is included in these results since a high gain extensometer was used to measure the initial deformation. The repeatability of the tensile properties is very good.

A typical fracture surface is shown in Figure 39. As with the other fracture surfaces the surface is dimpled indicating microvoid coalescence and growth has occurred. Drawing to produce tubing did not result in any discernable changes in the tensile properties of GRCoP-84.

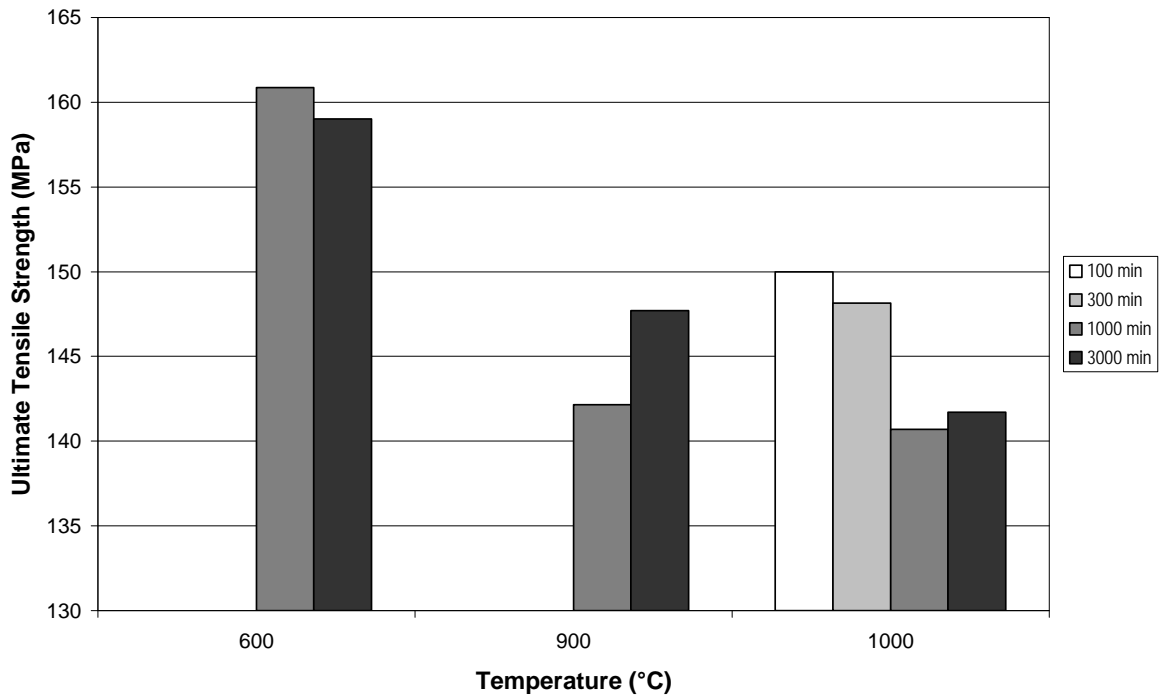
### Effect of High Temperature Thermal Exposures

Specimens from the 6.5 mm plate, 0.43 mm sheet and 0.58 mm sheet were heat-treated in vacuum at 600, 900, and 1000 °C (1112, 1652, and 1832 °F) for 1000 and 3000 min. In addition, specimens were heat treated for 100 and 300 min. at 1000 °C. The 500 °C (932 °F) strength and ductility data for the tests are shown in Figures 40 and 41. For Figure 41, data from both sheet specimens were pooled based upon the observation that all cold work would be fully annealed from the thermal exposures. Each bar in the plots represents the average of at least two tensile tests.

GRCoP-84 demonstrates excellent retention of tensile properties after high temperature thermal exposures, especially for 500 °C tensile tests. Not surprisingly, higher temperature exposures tend to degrade properties. This is likely directly ascribable to the coarsening of the Cr<sub>2</sub>Nb precipitates and grain coarsening during the elevated-temperature exposures. Higher temperatures degrade GRCoP-84 more because the solubility of Cr (Ref. 29) and Nb (Ref. 30), the diffusivity of Cr and Nb (Ref. 31), and the driving forces to grow precipitates (Ref. 32) and grains (Ref. 33) all increase with increasing temperature.

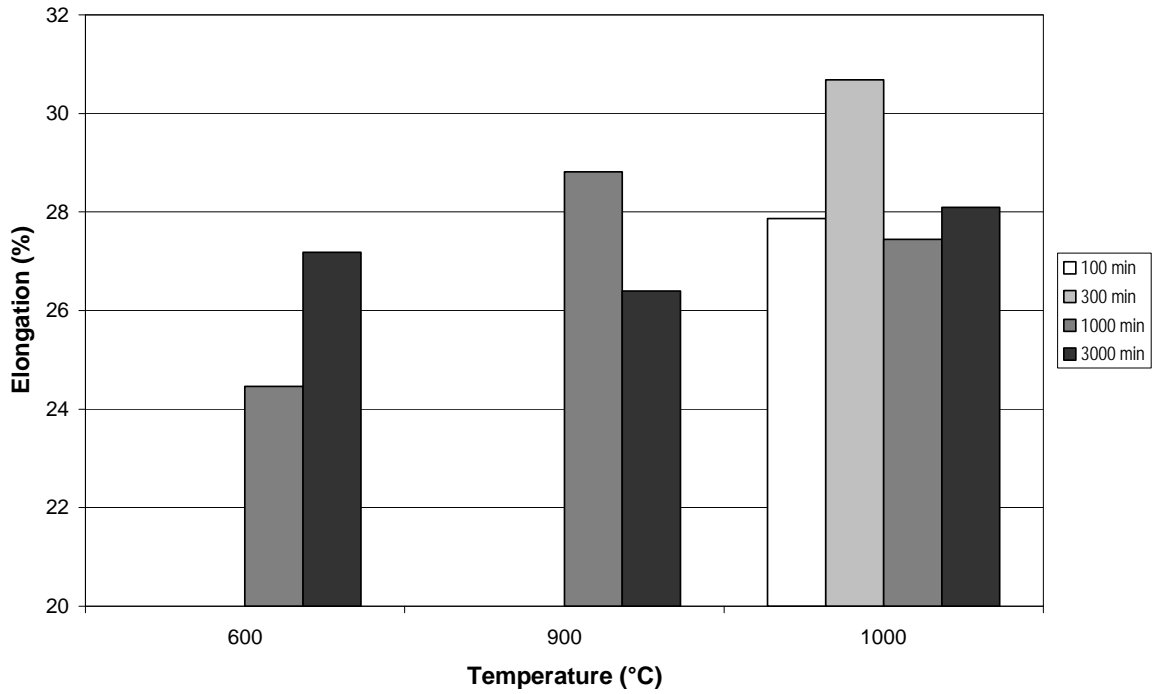


(a) 0.2% Offset Yield Strength

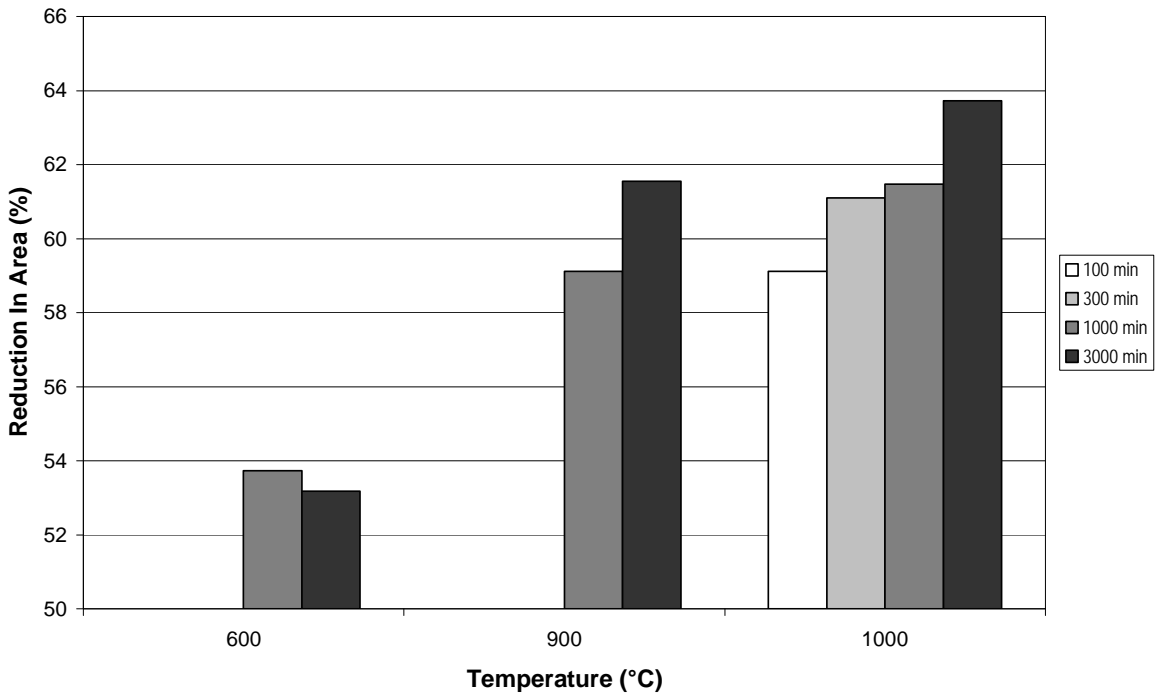


(b) Ultimate Tensile Strength

Figure 40.—500 °C strength and ductility of GRCop-84 6.5 mm plate specimens following long-term, high temperature heat treatments.

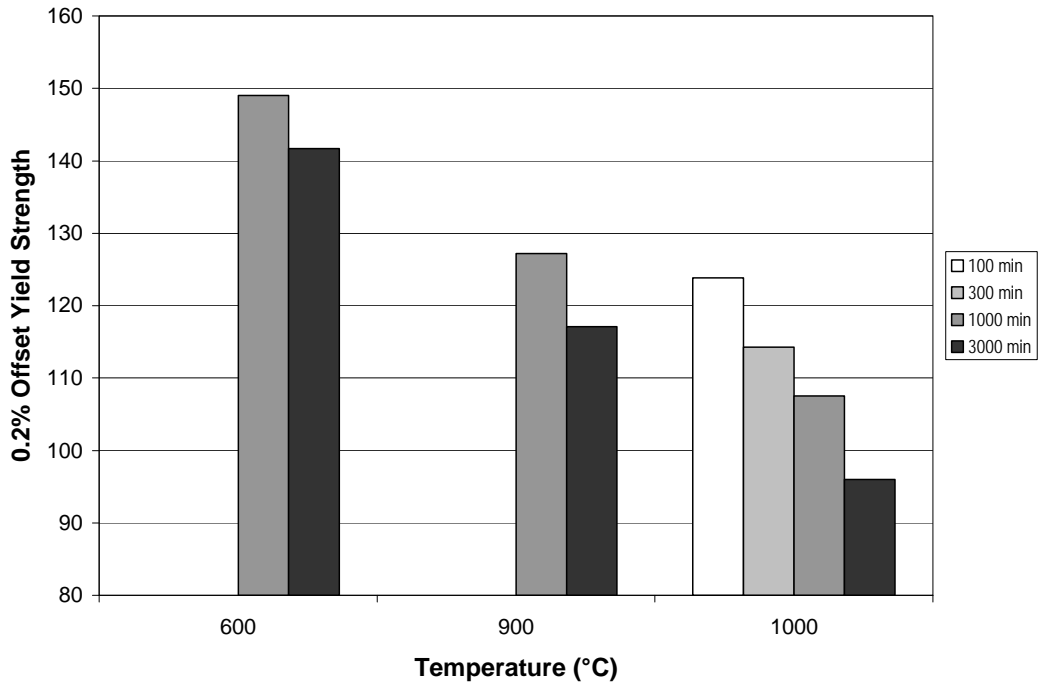


(c) Tensile Elongation

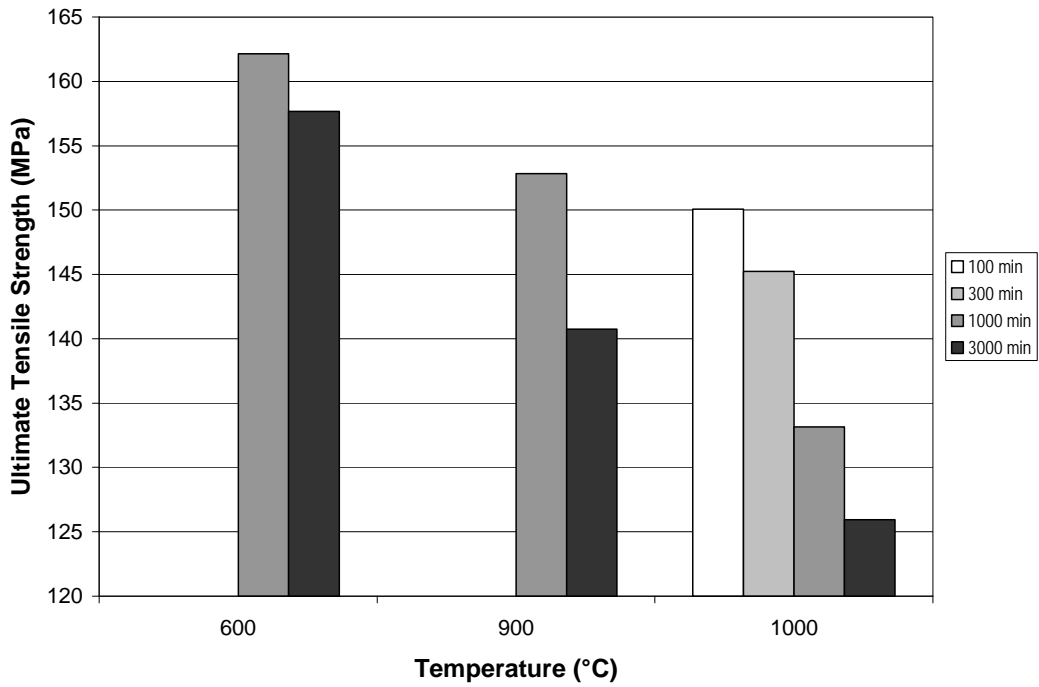


(d) Reduction In Area

Figure 40.—Concluded.

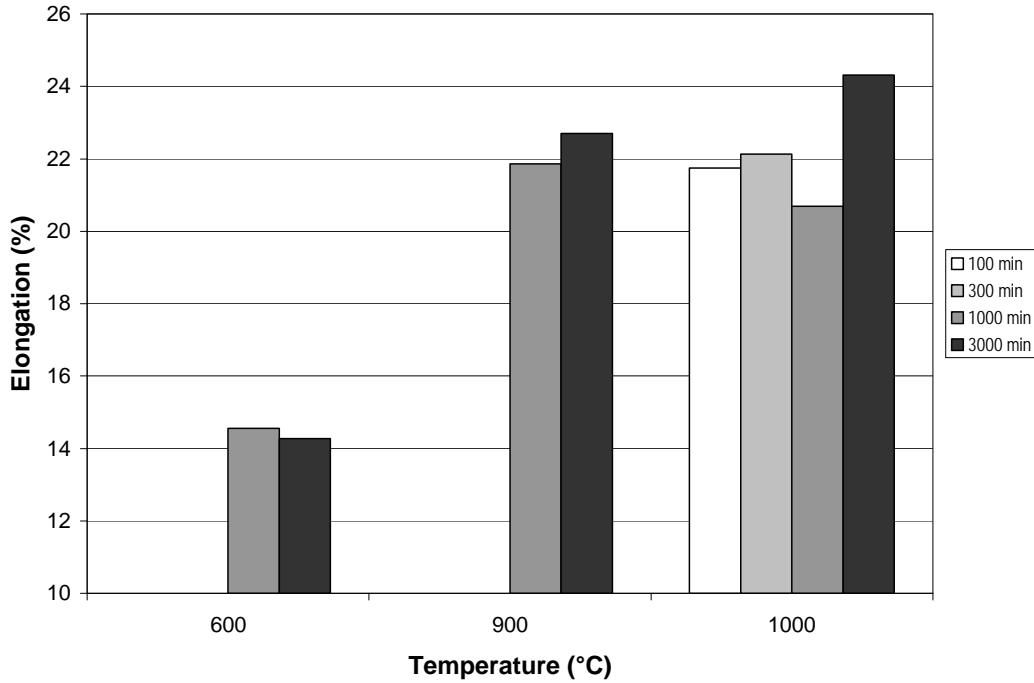


(a) 0.2% Offset yield Strength



(b) Ultimate Tensile Strength

Figure 41.—500 °C strength and ductility of GRCop-84 0.43 and 0.58 mm sheet specimens following long-term, high temperature heat treatments.



(c) Tensile Elongation

Figure 41.—Concluded.

Several differences were noted in the 500 °C tensile properties of sheet and plate samples that had been thermally exposed. The yield strength of sheet was generally superior to the plate specimens. The sheet specimens heat treated at 600 °C in particular showed up to 10 percent greater yield strengths than plate specimens. The average yield strength of sheet samples given a 1000 °C/3000 min. heat-treatment is the only sheet value that falls much below the average plate values. The average ultimate tensile strength values for plate and sheet are also similar except for the 1000 °C/3000 min. condition.

A difference in ductility as measured by tensile elongation was also observed. The sheet specimens consistently had lower elongations than the plate specimens. The specimens heat-treated at 1000 °C were closest in average elongations. Some of the difference in elongation can likely be attributed to specimen geometry differences—flat versus round. Variability in elongation explains most of the remaining differences, so the small differences in the values are not deemed to be particularly significant.

Likewise there was a decrease in elongation values for sheet specimens heat-treated 600 °C/1000 min. and 600 °C/3000 min. After heat-treatment, they fall below the baseline as-extruded GRCop-84 500 °C elongation lower 95 percent confidence interval value of 15 percent at 500 °C. The small difference may again be attributable to the flat (sheet) versus round (extrusion) tensile test specimen geometry. The ductility is still sufficiently high that it should pose no issue for using sheet at 500 °C following similar heat treatments.

## End of Life Retained Tensile Properties

Figure 42 shows the retained properties of the baseline extruded GRCop-84 after exposure for 100 hr at 500 °C (932 °F). The corresponding tensile properties of the as-extruded baseline GRCop-84 are also presented. This exposure was meant to simulate a thermal exposure consistent with the anticipated life and hot-wall temperature of the liners. The strength of the exposed specimens was consistently superior rather than inferior to the one-sided upper 95 percent confidence interval for the as-extruded material up to 600 °C. Above 600 °C the exposed material is generally stronger than the average as-extruded GRCop-84, but the values start to fall below the upper confidence interval. The elongation and reduction in area of the exposed GRCop-84 samples remain above the one-sided lower 95 percent confidence interval for the as-extruded GRCop-84.

Figure 43 shows the fracture surface the aged specimen tested at room temperature. A concern was that the samples would show evidence of the formation of large Cr precipitates such as shown in Figure 29. No such Cr precipitates were observed.

Some Cr and Nb remains in solution after extrusion for the small extrusions that can be precipitated in the 500 °C range (Refs. 22 and 34). These precipitates can provide additional strengthening beyond what is achieved in the baseline extrusions. Based upon these tensile results, the finest precipitates do not coarsen at 500 °C, so their benefit to strength persists over the anticipated life of the liner. The precipitates may result in some loss of ductility as the data tend to fall between the average and lower 95 percent confidence curves in Figure 43. The ductility values are still good and should be sufficient for the liner application.

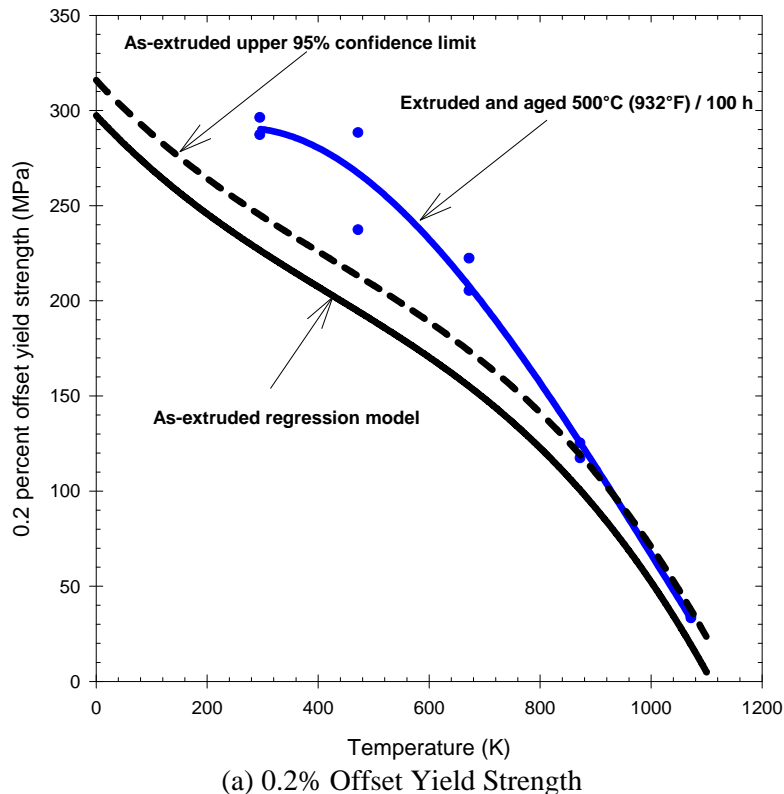
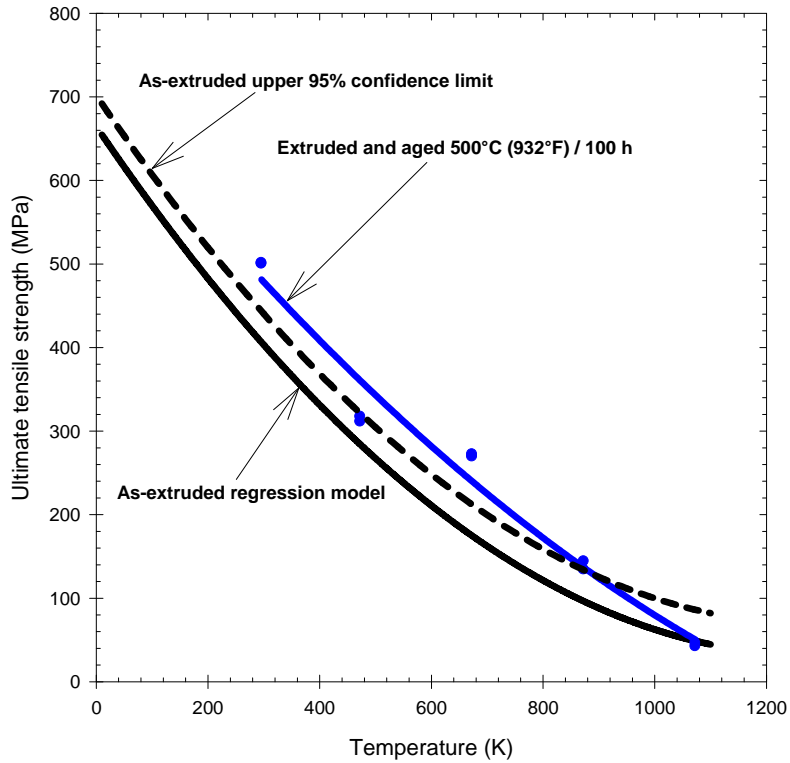
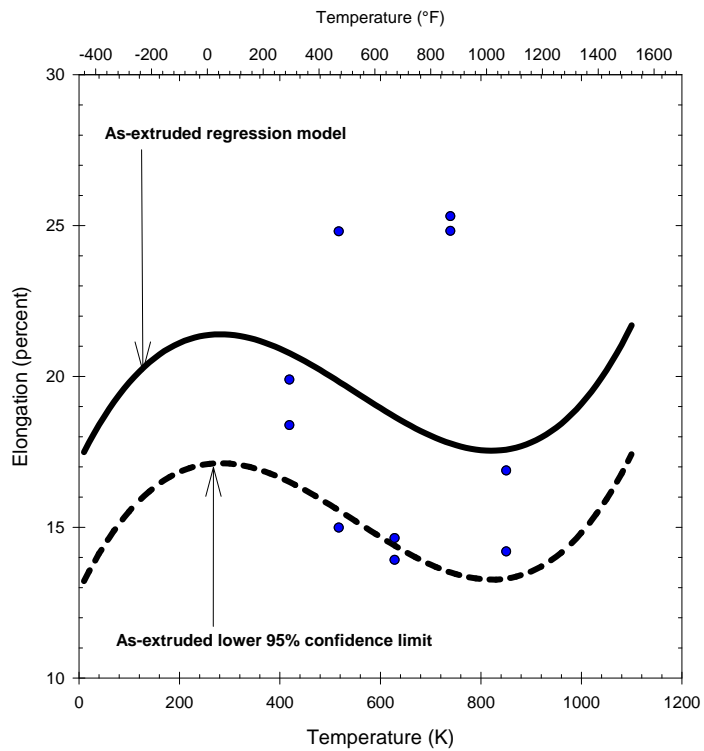


Figure 42.—Retained GRCop-84 tensile properties following 500 °C (932 °F)/100 h thermal exposure.

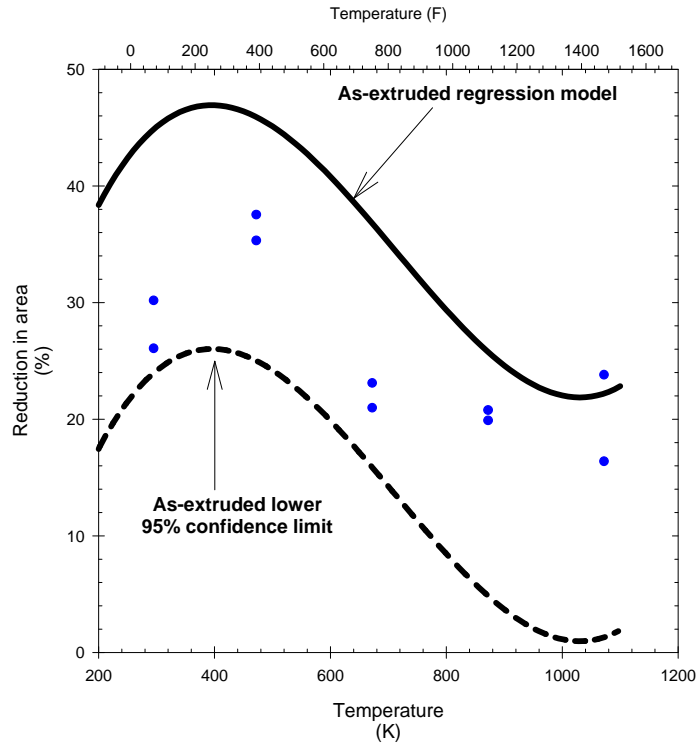


(b) Ultimate Tensile Strength



(c) Elongation

Figure 42.—Continued.



(d) Reduction In Area

Figure 42.—Concluded.

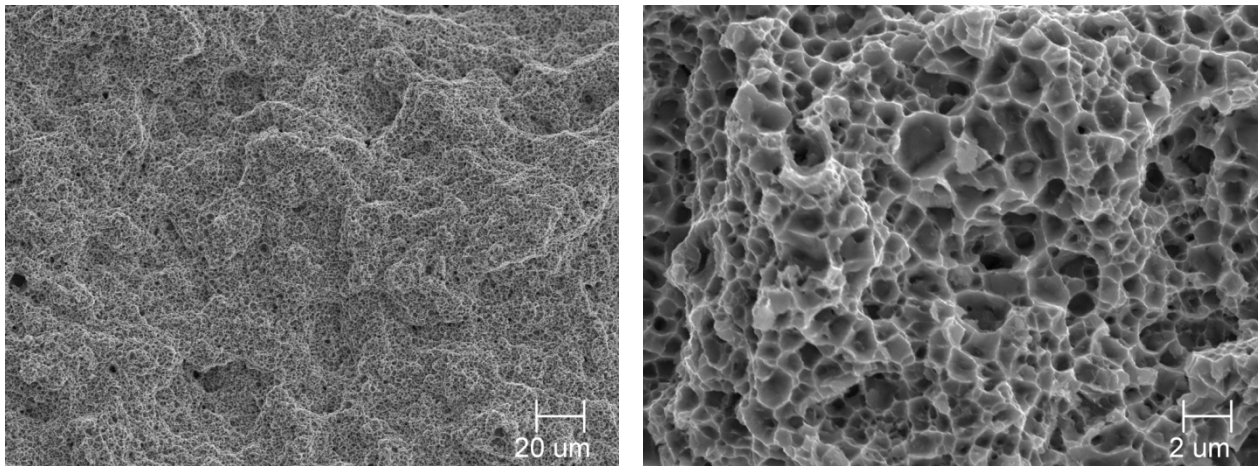


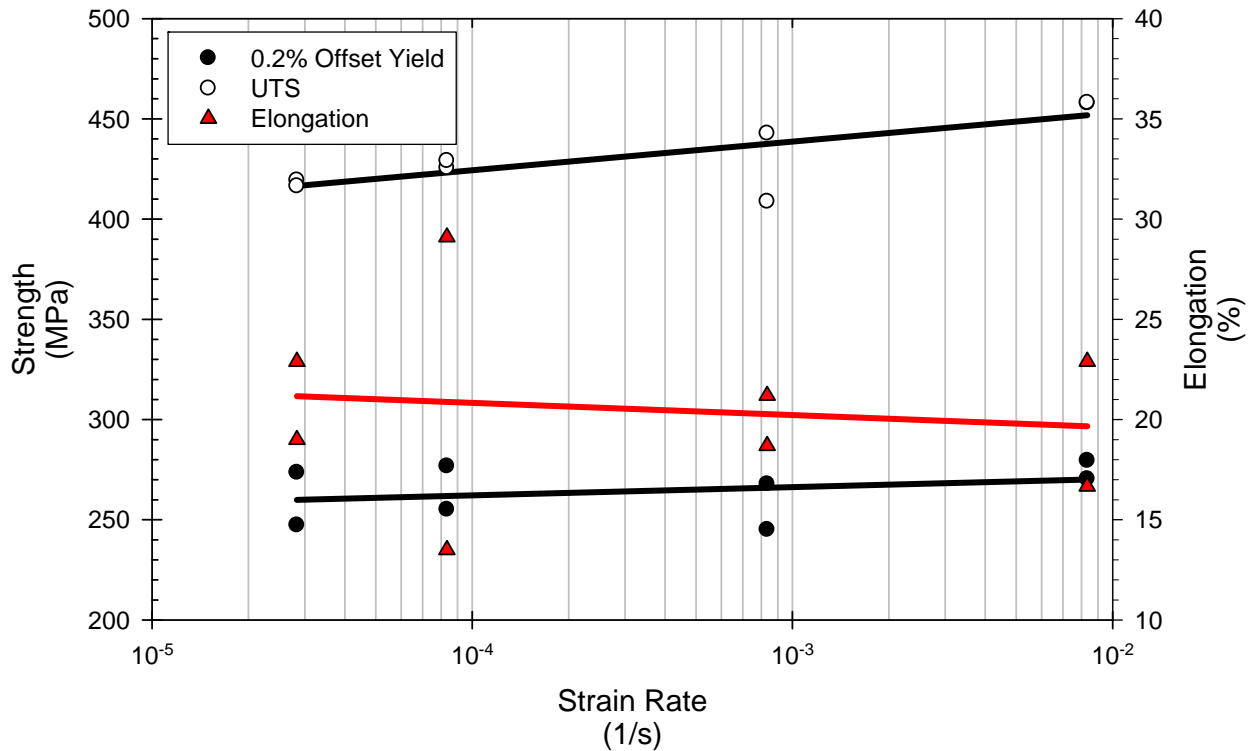
Figure 43.—Fracture surface of 23 °C (73 °F) tensile test specimen exposed at 500 °C (932 °F) for 100 h.

## Strain Rate Sensitivity of GRCo-84 Tensile Properties

The results of the strain rate sensitivity tests are presented in Figure 44. Each data set was fit to an equation in the form of

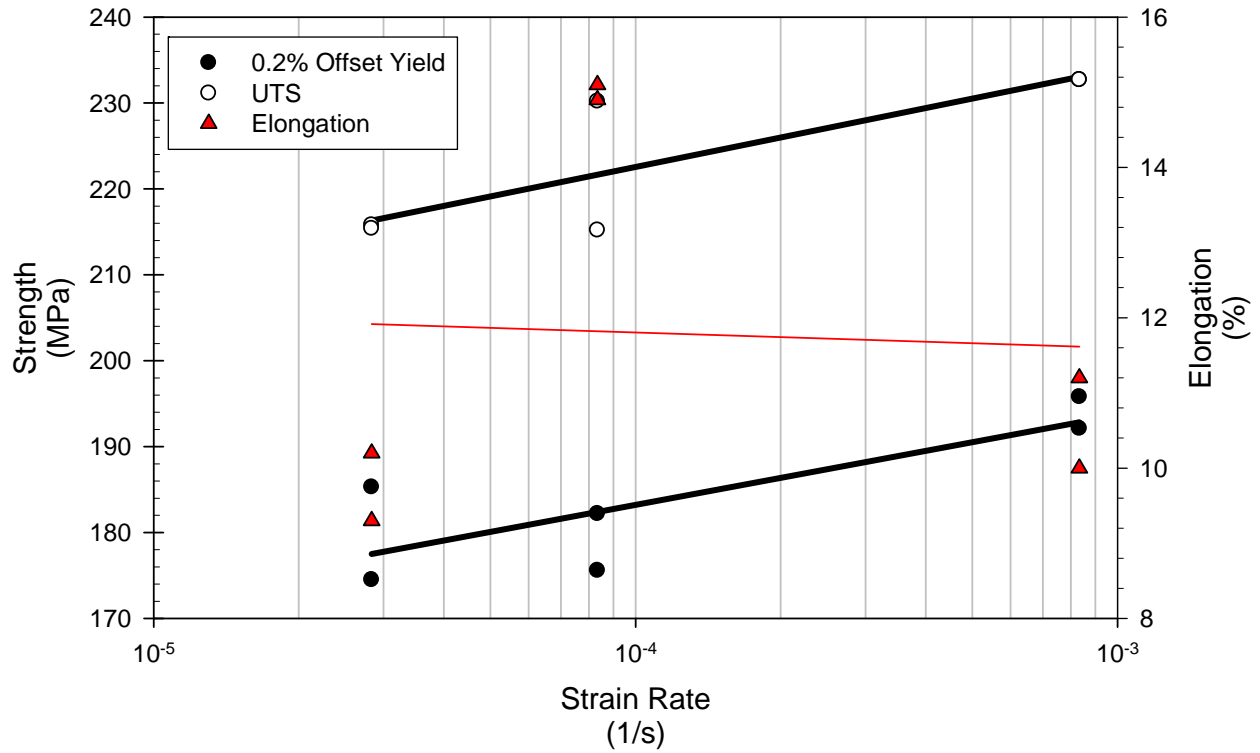
$$\sigma = m \log(\dot{\epsilon}) + b \quad (38)$$

The coefficients are listed in Table 11. There is a considerable range for  $m$  and  $b$  for each property measured, but they tend to cancel each other out, and the strength and ductility do not exhibit much change over the range of strain rates tested. These results are consistent with Cu (Ref. 35) and Cu-based alloys such as GlidCop AL-25 and Cu-Cr-Zr (Ref. 36) which show minimal dependency of tensile properties upon strain rate.

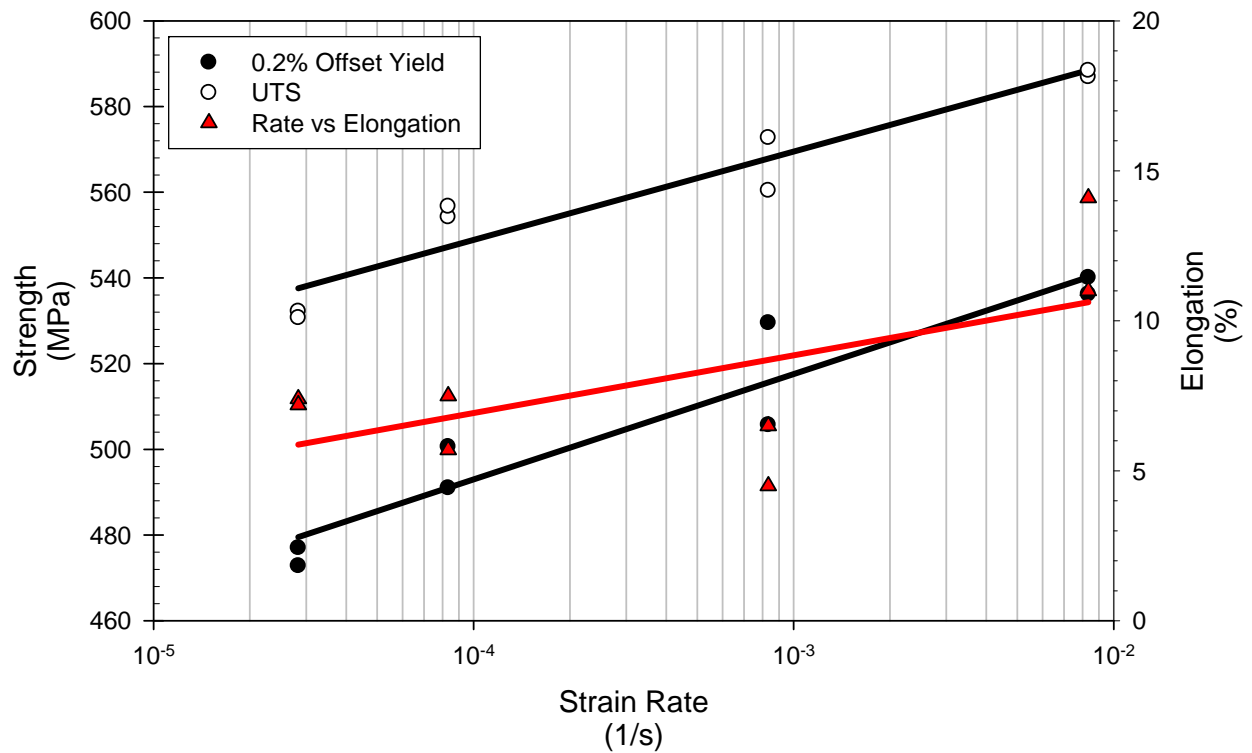


(a) Annealed GRCo-84 Sheet Tested at Room Temperature

Figure 44.—Dependency of tensile properties on strain rate.

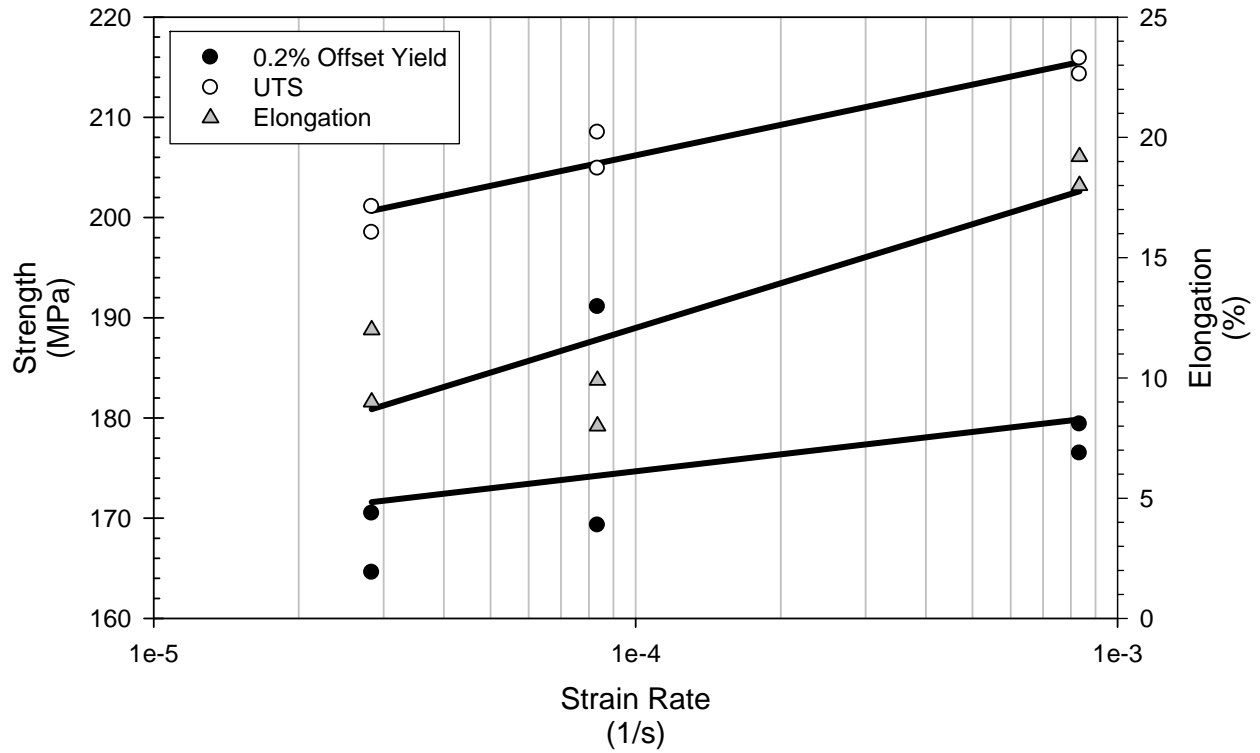


(b) Annealed GRCop-84 Sheet Tested at 400 °C (752 °F)



(c) 47 Percent Cold Rolled GRCop-84 Sheet Tested at Room Temperature

Figure 44.—Continued.



(d) 47 Percent Cold Rolled GRCo-84 Sheet Tested at 400 °C (752 °F)

Figure 44.—Concluded.

TABLE 11.—DEPENDENCY OF GRCo-84 STRENGTH AND ELONGATION ON STRAIN RATE

GRCo-84 Condition	Coefficient	0.2% Offset Yield Strength, MPa	Ultimate Tensile Strength, MPa	Elongation, percent
As-Annealed Room Temperature	b (MPa)	278.67	481.50	18.42
	m (MPa/log(1/sec))	4.11	14.28	-0.60
As-Annealed 400 °C (752 °F)	b (MPa)	224.95	268.09	10.98
	m (MPa/log(1/sec))	10.43	11.39	-0.20
47% Cold Rolled Room Temperature	b (MPa)	591.33	631.28	14.62
	m (MPa/log(1/sec))	24.58	20.60	1.92
47% Cold Rolled 400 °C (752 °F)	b (MPa)	197.13	246.61	36.75
	m (MPa/log(1/sec))	5.61	10.10	6.17

## Discussion

Several observations were made regarding the tensile properties of GRCo-84 and the effects of processing and heat treatment upon them.

### Effect of Processing on GRCo-84 Tensile Properties

While many comparisons and correlations are possible, one of the more informative ones is the effect of processing on the room temperature tensile properties of GRCo-84. Figure 45 shows the effect of production method while Figure 46 shows the effect of thermal exposure.

When comparing the tensile properties in this manner it becomes obvious that the effects of production method, rolling and even high temperature braze cycles are minimal. Long times at the anticipated hot-wall temperature actually had a positive effect on the tensile strength of extruded GRCo-84. The largest difference noted, the reduced strength of HIPed GRCo-84 relative to other consolidation methods, is explained by the exposure of the billet to higher processing temperatures for longer times compared to the other production processes examined. Once a high temperature braze cycle similar to the HIP cycle is applied which is similar in duration and temperature to the HIP cycle, the differences disappear.

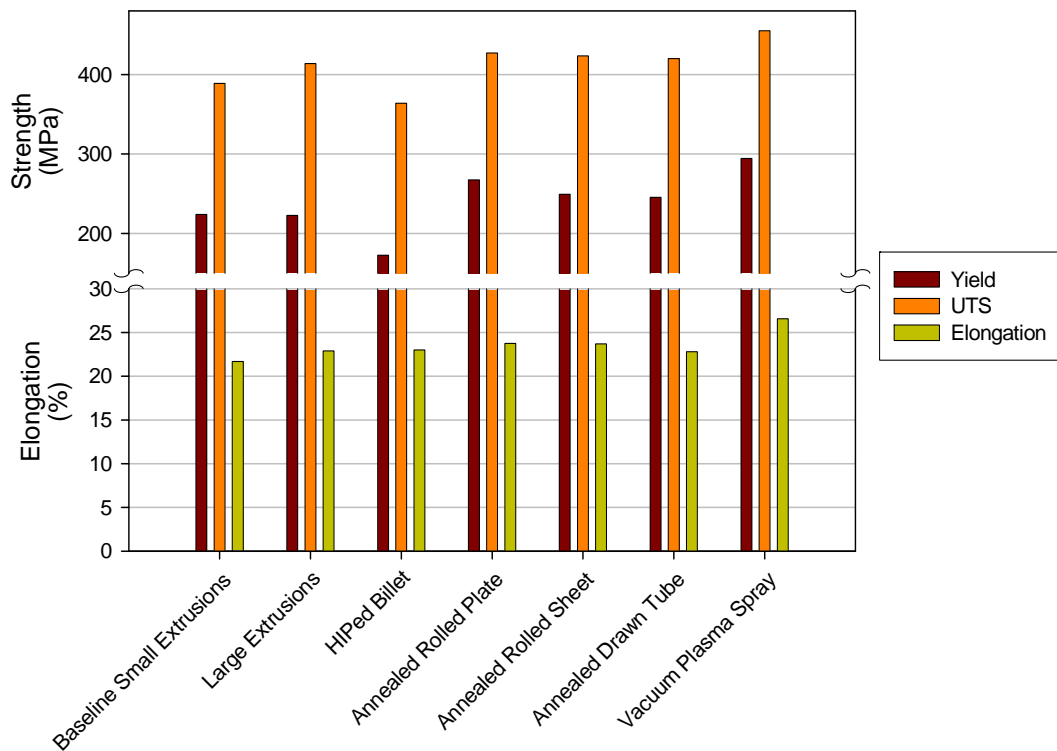


Figure 45.—Effect of consolidation and processing method on GRCo-84 room temperature tensile properties. (VPS data from Refs. 9 and 10).

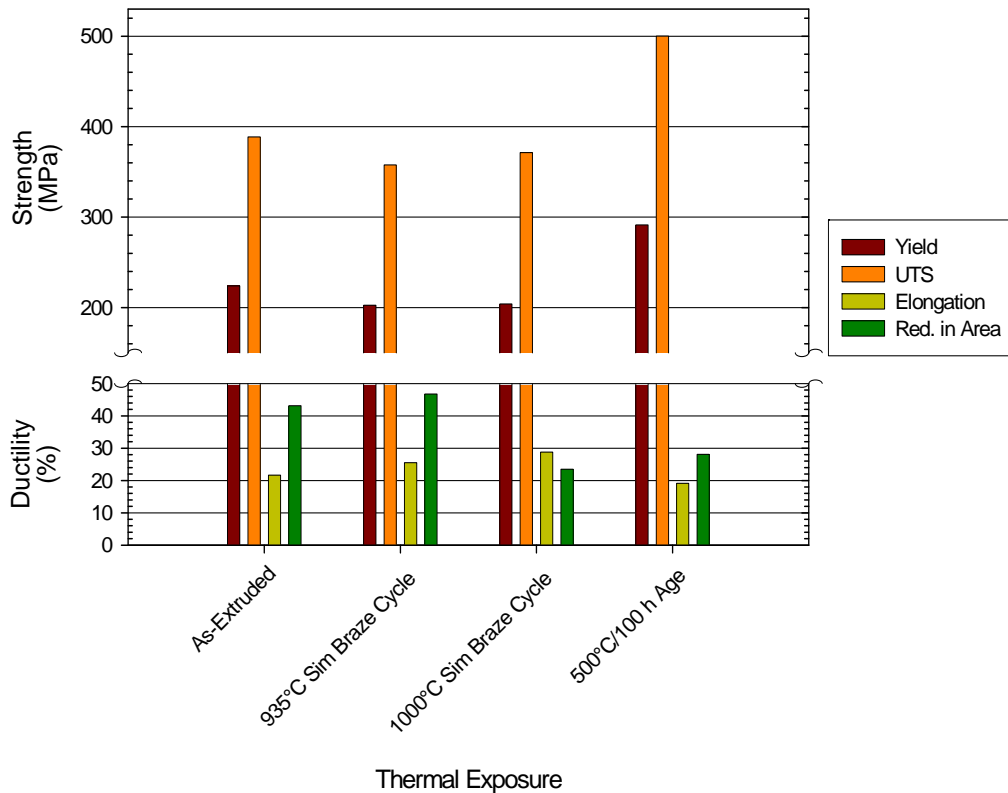


Figure 46.—Effect of various thermal exposures on GRCop-84 room temperature tensile properties.

The stability and insensitivity to processing method of the GRCop-84 has several positive implications. First, the probability of achieving similar properties with new production techniques and forming methods appears to be very high. This greatly reduces the risk associated with implementing a new production technique. It also reduces the risk in using the current properties to assess the feasibility of a design made possible by a new production technique. The amount of testing required to verify the new processing method should also be minimized. As a result development of future rocket engines and other parts using GRCop-84 should be shortened and cost less.

Second, the stability removes some of the potential problems associated with utilizing precipitation-strengthened alloys such as Cu-Cr, Cu-Zr, and Cu-Cr-Zr. As is shown elsewhere in the GRCop-84 task final report (Ref. 37), those alloys lose much of their strength when exposed to high temperatures (generally in the 500 to 600 °C range) that overage or dissolve their precipitates. The liners might be solution heat treated and/or aged again during production to recover some of their strength, but that also may not be possible due to the braze joint metals, jackets and other parts that may not respond favorably to a temperature excursion above 900 °C, the typical solutioning temperature range, or extended thermal exposures between 400 and 550 °C range, the typical precipitation temperature range.

The problem is compounded if the material is in service. During operation, if the liners experience an over-temperature event, the liners would very likely experience large deformations due to the severe decrease in strength. The decrease in strength could well be sufficient to cause the operating stresses to exceed the ultimate tensile strength of the weakened alloy and catastrophically fail the liner. In the case of GRCop-84, the tensile properties would be reduced some during the over-temperature event due to the higher temperature, but the decrease would not be as dramatic as the 90 percent and greater reductions seen in the precipitation-strengthened alloys. Most of the tensile strength would be retained following the return to the normal operating temperature as well. This adds a considerable margin of safety to the liner and reduces the need for frequent inspections.

In the case of Cu-Zr, Cu-Cr and any other alloy that achieves a significant fraction of its strength by retention of cold work, a sufficiently high temperature will also anneal these alloys. Once annealed, all benefit from cold work would be gone and cannot be restored. Since GRCop-84 would normally be used in the annealed condition, it does not have this potential problem. Instead its properties are well-behaved and comparatively insensitive to annealing and other past thermal history.

Third, grain growth can affect properties to varying degrees. The current work on competitive alloys does not address this issue, but, in general, larger grains give lower yield strengths due to less strengthening through the Hall-Petch mechanism. For precipitation-strengthened alloys in particular, considerable grain growth during high temperature brazing and diffusion bonding is a possibility. The high brazing temperatures can dissolve the precipitates that generally act as barriers to grain growth. GRCop-84 and other dispersion strengthened alloys such as GlidCop AL-15 LOX do not suffer from this problem and can retain a fine grain size and the strength advantage associated with it.

Finally, the insensitivity of GRCop-84 to processing and even long-term thermal exposure at the anticipated use-temperature allows for a better design of the liner and confidence that it will not fail due to reduction of tensile properties during usage. While somewhat mundane, this uniformity and consistency of properties is in fact exactly what is desired for a man-rated engine. It eliminates many of the risks associated with the liner and engine.

While additional work examining the effects of specific processing methods and thermal exposures including end-of-life tests for higher operating temperatures and longer times is warranted when an engine is designed, the available information indicates that the properties of GRCop-84 will remain very similar to the properties measured in this task.

### **Effect of Cold Work**

Several alloys such as AMZIRC (Cu-Zr) (Ref. 38) receive a considerable portion of their strengthening from cold work. In the case of Cu-Zr alloys, the  $\text{Cu}_x\text{Zr}$  precipitates increase the recovery and recrystallization temperatures (Ref. 39) and increase the useful maximum operating temperature.

In the case of GRCop-84, cold work can increase the yield strength by up to 50 percent and the ultimate tensile strength by up to 25 percent. The effects of cold work appear to reach a saturation point around 50 percent cold reduction in cold rolled sheet.

Copper shows a considerable range of annealing behavior that is dependent upon the amount of cold work and annealing temperature as shown in Figure 47 (Ref. 26). Chemical analysis of the matrix after extraction of the  $\text{Cr}_2\text{Nb}$  particles showed that the GRCop-84 matrix is nearly pure copper. While the  $\text{Cr}_2\text{Nb}$  particles can pin the grain boundaries (Refs. 32 and 40) their size limits their effectiveness at retarding recovery and recrystallization. Instead they tend to limit grain growth to retain a consistent 1 to 5  $\mu\text{m}$  average grain diameter.

Based upon the current work, GRCop-84 undergoes recovery and recrystallization between 200 °C (392 °F) and 600 °C (1112 °F) depending upon the amount of cold work in the sheet. This result is very similar to those of Yokelson and Balicki (Ref. 26) shown in Figure 47 and reinforces that the GRCop-84 matrix tends to behave similar to pure copper. Unfortunately in this case, that similarity means that cold work may not be a suitable strengthening mechanism for GRCop-84 when it is to be used above 200 °C. This would limit cold-worked GRCop-84 to near room temperature applications. There are other alloys such as Cu-Cr, Cu-Cr-Zr and Cu-Zr that are generally better choices for use in the low temperature range. This conclusion is based upon commercial availability, cost and tensile properties. This is not viewed as a major shortcoming of GRCop-84 because the alloy was purposefully optimized for use in the 300 to 800 °C (572 to 1472 °F) temperature range.

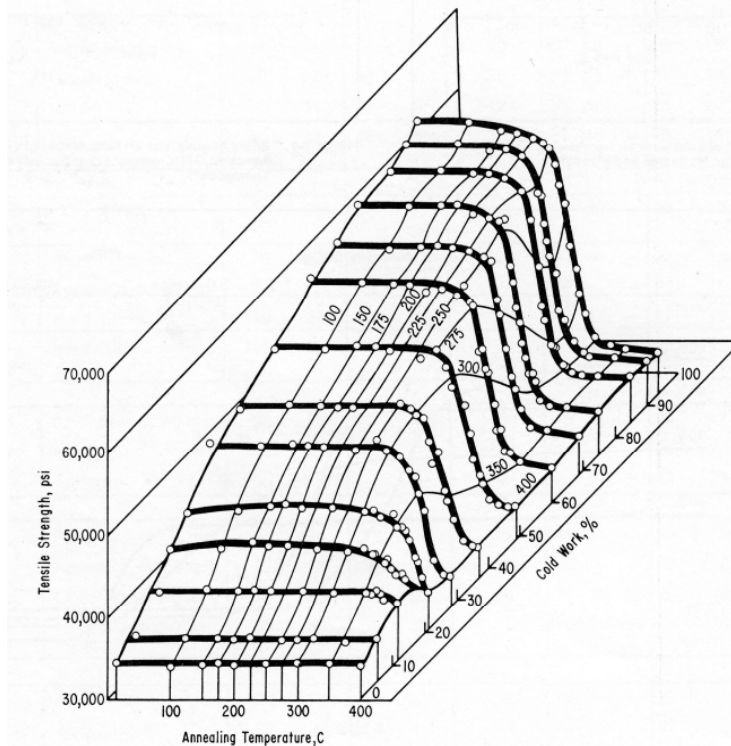


Figure 47.—Relationship between yield strength, cold work and annealing temperature for pure copper (Ref. 26).

Finally, the usefulness of cold working as a strengthening mechanism for a liner application is also suspect. Dispersion strengthening alone maximizes thermal conductivity and avoids the small (for rocket engine combustion chamber liners) but important loss of thermal conductivity caused by cold work (Ref. 41). However this may partially limit the use of GRCop-84 in other applications. Careful analysis using the available tensile and annealing data will be required to make the decision of which is the best alloy to use and if cold-worked GRCop-84 could be a viable choice.

### Effect of Heat Treatments

The heat treatments studied can generally be classified into one of three categories—short duration, low to moderate temperature annealing; medium duration, high temperature brazing; and long-duration exposures at moderate to high temperatures.

#### Annealing

Annealing provides the means to return the cold worked material to the unworked properties and allow more working or forming of the pieces without cracking or other catastrophic failure. The annealing behavior of GRCop-84 is now well documented and understood sufficiently that a commercial annealing cycle has been established (Ref. 14).

The annealing temperature was originally set at 400 °C (752 °F) for 15 min. based upon prior internal work using material produced from Special Metals powder in 1989. The annealing behavior of 35 percent cold worked Special Metals GRCop-84 was evaluated using hardness measurements. Based on those hardness measurements the material was well annealed at 400 °C. The desire to limit potential grain growth and precipitate coarsening led to the adoption of this temperature.

The reduction in cold work to a nominal 23 percent for the cold rolled sheet in the first rolling campaign for the Crucible Research material was sufficient to raise the required annealing temperature to 600 °C for a complete anneal. The increase in required temperature with lower cold work is consistent with the annealing behavior of pure Cu shown in Figure 47. The 300 °C isotherm for example, shows that pure Cu will not be annealed even partially at this temperature until the cold work exceeds 30 and 90 percent cold work is required to achieve complete annealing.

The detailed analysis of the annealing behavior and the elevated-temperature tensile testing indicate that the annealing temperature can be modified to be a function of cold work. It appears that full or nearly full annealing is possible at temperatures as low as 200 °C for 60 percent cold-rolled sheets and 400 °C for 50 percent cold-rolled sheet. There are even some indications that the 90 percent cold-rolled foil recrystallized during rolling at or near room temperature. At all levels of cold work tested, the annealing study and the elevated-temperature tensile testing indicated that the samples were well-annealed at 600 °C. To ensure that all material is fully annealed, it was decided to set the standard annealing temperature to 600 °C. A time of one-half hour was selected for the sheet and plate based to give the material sufficient time to reach temperature at the core. In a production environment where the process is well-characterized and reproducible so that the amount of cold work is consistent, it may be possible to lower the annealing temperature to lower operating costs.

The effects on tensile properties indicate that careful control of the annealing will be needed since it is possible to retain considerable cold work if the annealing temperature is too low or the time too short. As shown in Figure 27, plate samples given a 400 °C anneal retained about 80 percent of their cold work. While this gave the material a higher strength, it also decreases the ductility. This could result in problems for some applications since low cycle-fatigue resistance and toughness generally are proportional to ductility. Improperly annealed GRCop-84 could fail prematurely in these applications. For this reason, it is believed that using the 600 °C anneal to ensure complete annealing is the best option.

### **Simulated Brazing**

No actual brazing was done in this study since the liner jacket material is uncertain. While it likely will be an alloy such as 347 stainless steel, A286 or JBK-75, more advanced options including silicon carbide-reinforced aluminum are possibilities for the future (Ref. 42). The jacket material selected by the designers will determine the braze alloy and temperature used for the brazing. It was therefore deemed not to be a good use of resources to pursue the myriad brazing options. Instead, this work concentrates on representative thermal cycles to simulate the effects of brazing on the liner wall which is far from the braze joint and develop representative GRCop-84 tensile properties. In addition, there is considerable interest in diffusion bonding of GRCop-84 to itself and other alloys especially for the platelet technology liners. These thermal cycles are representative of that process as well and can be used to evaluate the potential effects of the thermal cycle on the base material.

The two braze cycles were selected based upon consultations with Pratt & Whitney, Rocketdyne and Aerojet and are likely representative of the temperature range that will be used for brazing to a steel jacket and diffusion bonding. Typically Ag-, Au-, Cu- and Pd-based braze alloys with liquidus temperatures between 893 °C (1639 °F) (NiCuSil-8) and 1050 °C (1925 °F) (70 Au-30 Ni) would be used to jacket the liner (Ref. 43). Braze alloys with large amounts of an elements that lower the conductivity of copper, e.g., Ti (Ref. 44) in TiCuNi, would likely be avoided to minimize any potential contamination of the GRCop-84 that would result in lowered thermal conductivity of the liner wall. Low temperature brazes are also a possibility for other applications, but the effects of the braze cycle on tensile properties should be minimal below 800 °C, so they were not examined.

High brazing temperatures are desirable since the higher liquidus temperature generally reflect higher strength for the braze metal (Ref. 44) and hence the braze joint. Using a high temperature to jacket the liner also allows for subsequent brazing steps to add manifolds and other parts or thermal processing at lower temperatures without risking melting the braze joint. Higher temperatures are also desirable if a

jacket material requires a solution heat treatment and aging cycle. The solutioning of the alloy can be combined with the braze step into a single processing step.

Diffusion bonding, as its name implies, is based upon diffusion of material across the bond line. Diffusion is exponentially dependent upon the absolute temperature, so the higher the temperature used, the quicker the joining process and the more the bond line can be made to diffuse.

In a large structure such as an RS-83 thrust cell, the heating and cooling rates will be relatively slow due to the large thermal mass even if the brazing is done in an atmosphere rather than a vacuum. While the exact heating and cooling rates would be dependent on the furnace and the thrust cell, the consensus opinion was a rate between 2 and 6 °C (3 and 10 °F) per minute was likely to be representative of the eventual process. It was also deemed likely that, given the high value of the part and closeness to the melting point of GRCop-84, the heating rate would be decreased as the part approached the braze alloy liquidus temperatures. This led to the representative simulated braze cycles shown in Tables 1 and 2.

Brazing occurs in the temperature range where it is likely that Cr<sub>2</sub>Nb will begin to coarsen. The solid solubility of Cr (Ref. 27) and Nb (Ref. 28) as well as the diffusivities of Cr and Nb (Ref. 29) greatly increase above 800 °C (1472 °F). These, in turn, drive the coarsening of the particles based upon the coarsening model developed by Lifshitz, Slyozov and Wagner (generally referred to as the LSW model) (Refs. 45 and 46). The braze cycles have the liner above 800 °C for 150 and 228 min. for the low temperature and high temperature braze cycles, respectively. This combination of temperature and time raised concerns that a braze cycle would cause considerable loss of tensile properties.

The coarsening of the Cr<sub>2</sub>Nb particles leads to lower tensile strengths (Ref. 47). This trend is evident in all forms of GRCop-84 given a simulated braze cycle that were tensile tested. The degradation, though, is minimal. Typically the yield strength decreases by 20 to 35 MPa (3 to 5 ksi). The decrease tends to be uniform for tensile testing conducted from cryogenic temperatures up to approximately 600 °C (1112 °F). Above 600 °C, the effects of brazing are minimized, as data from all conditions tend to collapse to a single value at a given temperature.

Unpublished tensile test results were provided by Pratt & Whitney Rocketdyne for NARloy-Z samples given the low temperature braze cycle followed by an aging step at 482 °C (900 °F). The results, presented in Figure 48, showed that the current SSME liner material does not retain its strength as well as GRCop-84 even with the benefit of the aging step to restore some of the strength. Unlike GRCop-84, NARloy-Z loses almost half of its strength following this thermal cycle. Competitive precipitation strengthening alloys by tested as part of this program show similar, often worse results when subjected to a 935 °C braze cycle. Results for these alloys are also presented in Figure 48 (Ref. 37). Only the dispersion-strengthened alloys GlidCop AL-15 LOX and GRCop-84 retain their high strengths. The GlidCop AL-15 LOX tensile results help validate the selection of dispersion strengthening for liner alloys.

While the retention of mechanical strength is excellent for GRCop-84, it was noted that the reduction in area for plate specimens given the high temperature simulated-braze cycle decreased dramatically as seen in Figure 27(d). This was traced to the development of large (>5 μm) elemental Cr precipitates with weaker interfaces that failed earlier than the Cr<sub>2</sub>Nb-Cu interfaces. This is the only case where a substantial negative effect was noted following a braze cycle. The Cr precipitates occur because the GRCop-84 chemistry is biased towards the Cr-rich side of stoichiometric Cr<sub>2</sub>Nb. The small excess of Cr is the source of the elemental precipitates. Strangely the other samples given the same thermal treatment did not demonstrate an adverse effect for the Cr. It is unclear why this particular set of samples showed a noticeable change in properties. The potential problem merits further investigation if GRCop-84 is to be used with a similar heat treatment in a mission critical application such as an engine liner.

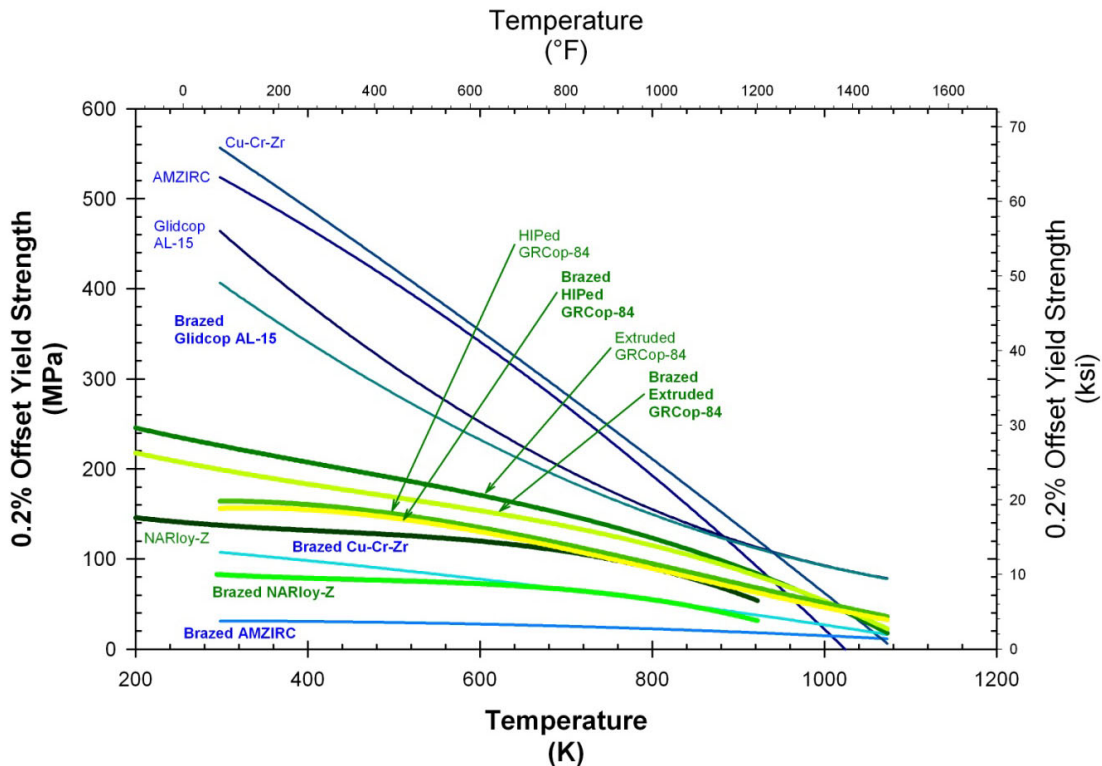


Figure 48.—Comparison of the yield strength of several Cu-based alloys before and after a simulated 935 °C (1715 °F) braze cycle (Ref. 37).

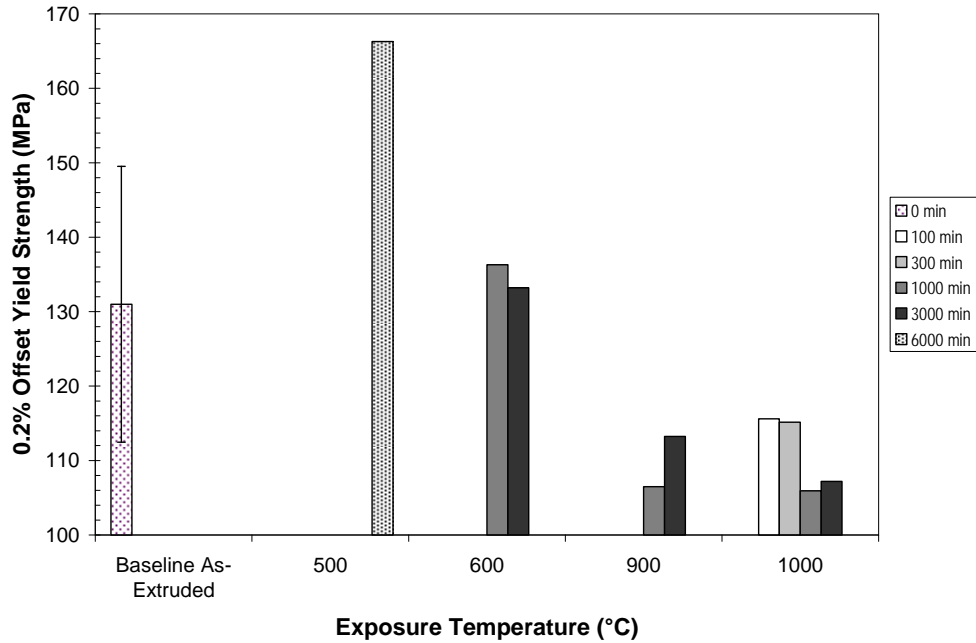
It should be noted that, despite the decrease in the reduction in area for the plate samples, they retain usable ductility. The elongations remain over 10 percent, and the reduction in areas are 6 percent or more with most samples having 10 percent or more reduction in area between 23 and 600 °C (73 and 1112 °F). While less than desired, the properties still should be sufficient for many rocket engine liners. With an understanding of the causes of the decrease in ductility, it should be possible to avoid the problem entirely as demonstrated by the other samples tested.

There is another option available in some cases. The extra Cr is added to the GRCop-84 to minimize potential hydrogen embrittlement that may occur by the formation of niobium hydrides (Ref. 25). This is a major concern for a hydrogen-fueled vehicle using 21 to 35 MPa (3 to 5 ksi) hydrogen for the coolant and hot-wall film cooling, but it may not be a concern for hydrocarbon-fueled vehicles. Hydrocarbons will have a much lower hydrogen activity than pure hydrogen, and it will likely be low enough to prevent hydrogen embrittlement of GRCop-84 even if the amount of Cr is reduced. The elimination of elemental Cr precipitates by reducing the Cr level will presumably allow for processing at 1000 °C and potentially even closer to GRCop-84's melting point of approximately 1080 °C (1976 °F). No low-Cr version of GRCop-84 has been produced, but it may be an area for additional work if hydrocarbon and methane-fueled engines are pursued in the future.

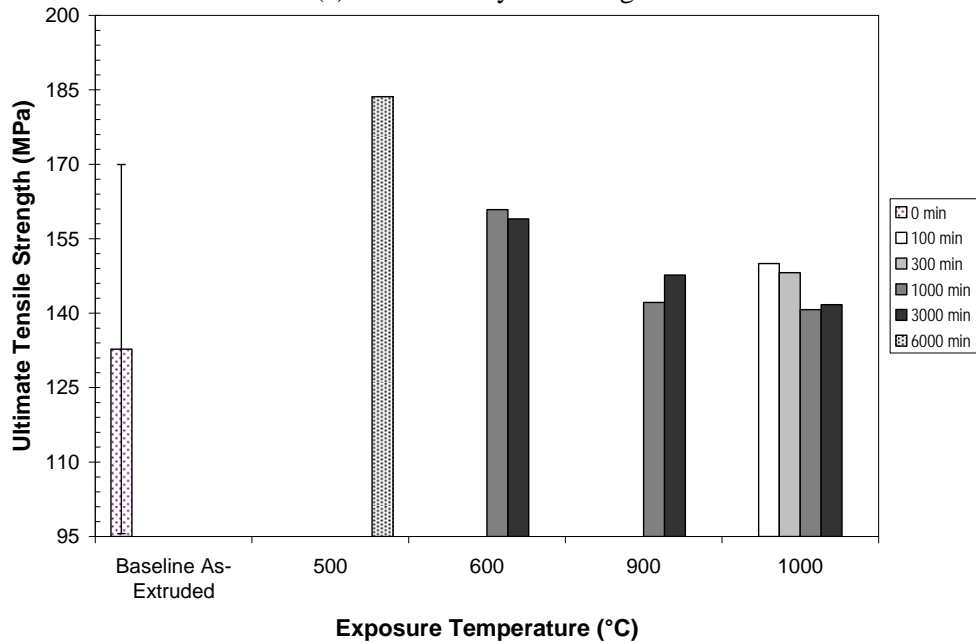
### Long-Term Exposures

Long-term isothermal exposures were conducted to examine the end-of-life properties of GRCop-84 and the potential for improving creep properties through limited grain growth. The temperatures ranged from 500 °C (932 °F) to 1000 °C (1832 °F) or homologous temperatures of 0.57 to 0.94  $T_m$ . It should be noted that few alloys could be subjected to these high fractions of their melting point for extended periods without suffering degradation of properties that are often considerable. GRCop-84 appears to be one of the exceptions.

As shown in Figure 49, there appears to be two responses of GRCop-84 to long-term exposures. Only exposed plate data is presented, but the sheet specimens show similar responses. At 500 °C (932 °F), the yield and ultimate strengths following a 500 °C thermal exposure actually increase and now lie outside the upper 95 percent confidence interval for a one-sided comparison (upper half of error bar for the baseline as-extruded properties). The elongation and reduction in area are not decreased by a statistically significant amount, but the averages are lower.

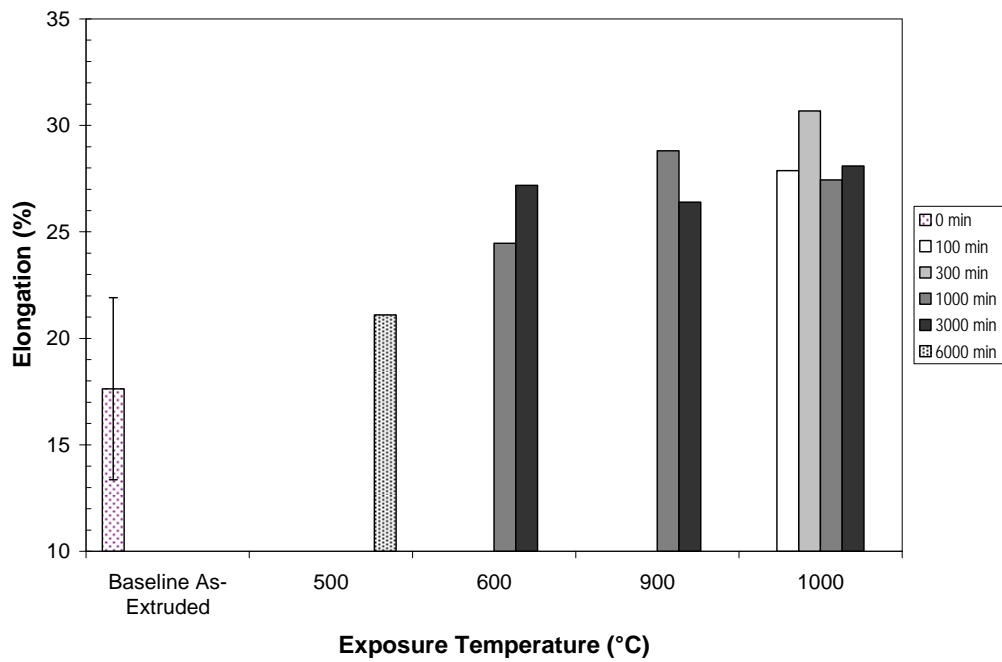


(a) 0.2% offset yield strength

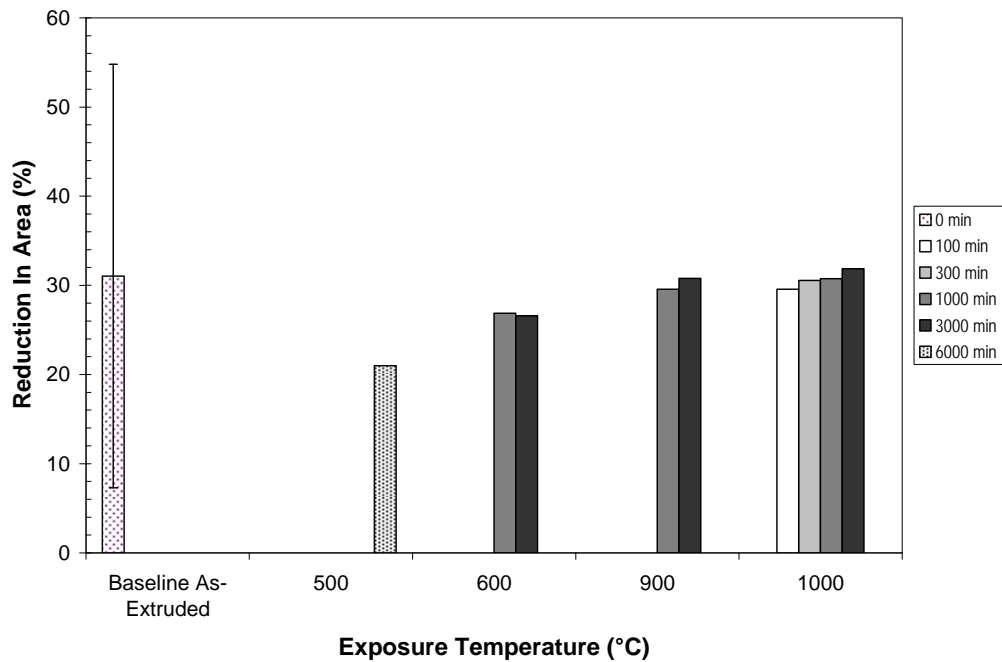


(b) Ultimate tensile strength

Figure 49.—Comparison of 500 °C (932 °F) GRCop-84 tensile properties. (Error bar on baseline as-extruded average represents 90 percent confidence interval. Half of the bar represents one-sided 95 percent confidence interval.)



(c) Tensile elongation



(d) Reduction in area

Figure 49.—Concluded.

Exposures around 600 °C (1112 °F) appear to start a transition to a high-temperature regime where tensile properties can be degraded. The average yield strength decreases slightly but not by a statistically significant amount. The average UTS increases but does not fall outside of the 95 percent confidence interval for a one-sided comparison with the baseline as-extruded average UTS. The average elongations after a 600 °C exposure also increase and lie outside the 95 percent one-sided confidence interval. The average reduction in area remains essentially unchanged compared to the baseline as-extruded properties.

The behavior for the samples exposed to 900 and 1000 °C is similar to that of the 600 °C except that the yield strength decreases to average values slightly below the lower 95 percent one-sided interval for the 1000 and 3000 min. exposures. The average elongations increase and fall outside the 95 percent confidence interval for the baseline as-extruded samples. The average reductions in areas remain essentially unchanged relative to the baseline as-extruded samples.

During prior experimental work (8) it had been noted that GRCop-84 could gain some strength when aged at temperatures between 300 and 500 °C (572 to 932 °F). Based upon the precipitation behavior of Cu-Cr alloys (Ref. 48) and the results of electrical resistivity measurements of GRCop-84 ribbons (Ref. 49), it was believed that this increase is caused by the precipitation of the residual Cr from the Cu matrix. The amount was always thought to be small ( $\ll 1$  vol. %) and not significant since the Cr precipitates would presumably coarsen rapidly and not contribute much to the strength of GRCop-84, especially at elevated temperatures. Based upon the improved strength seen after prolonged aging, it appears that this assumption may not be valid. Instead it now appears that the precipitation of Cr will give a significant increase in properties during aging at temperatures up to at least 500 °C. This new conclusion is also more consistent with microstructural changes observed by Anderson (38) where some fine  $\text{Cr}_2\text{Nb}$  was observed to precipitate following consolidation.

The long-term thermal exposure results reveal a discrepancy in the plate tensile data set. The plate produced in the first rolling campaign clearly has large Cr particles present (Fig. 29) and a reduced reduction in area at all temperatures that is well below the lower 95 percent confidence interval for the baseline as-extruded GRCop-84 (Fig. 27(d)). In contrast, the long-term exposures at 600, 900, and 1000 °C exhibit reductions in area at least as good as the baseline extruded GRCop-84.

The long-term, high temperature exposure specimens were taken from a different plate than the specimens for the 1000 °C braze testing. The braze specimens came from the first set of plates rolled while the long-term exposure samples came from the third and final set of plates. The known differences in the plates are the final thickness of the plates (18.4 mm for the first rolling campaign versus 13.3 mm for the final rolling campaign), the rolling temperature windows (200 to 300 °C for the first rolling campaign versus 200 to 400 °C for the last rolling campaign), and the number of reheats during rolling (two for the first rolling campaign versus none for the last rolling campaign). None of these seems likely to have a large effect on the plates based upon the GRCop-84 rolling parameter study (Ref. 13).

The Cr and Nb content of the plates were within the specified range for GRCop-84 as were the Cr:Nb ratios. Furthermore, Crucible Research practices do not allow mixing of individual powder atomization runs unless all powder runs meet all chemistry requirements. That eliminates the possibility that one batch of powder had too much Cr leading to localized deviations from the average chemistry. It is hypothesized that the third set of plates had a lower amount of excess Cr and that a small additional amount of Cr in the first plate material led to the formation of large elemental Cr precipitates. It is, however, unclear why only the first GRCop-84 plate specimens behaved in this manner, and additional investigation will be required if the problem reoccurs.

It is felt that processing GRCop-84 at or above 1000 °C (1832 °F) must be done with extreme caution. The formation of large elemental Cr precipitates is favored if there is excess Cr above the solid solubility of Cr at the processing temperature. For Cu-Cr-Nb alloys, the Cr solid solubility is driven to much lower values than in Cu-Cr alloys by the presence of Nb (Ref. 50). This decreased solid solubility will drive the creation of a higher volume fraction of Cr precipitates relative to binary Cu-Cr alloys with the same Cr content. This may also help explain why very small differences in Cr content could affect the formation of large precipitates and the reduction in area so much. It is clear from the fractography that the

Cr precipitates act as sites for premature failure at the Cr-Cu interface. Once the interface fails, the precipitates essentially act as substantial voids in the material.

Evidently there is a need for further exploration of the processing of GRCop-84 in the temperature regime between 900 and 1050 °C (1652 and 1922 °F) that includes variations in the excess Cr. It may also be worthwhile to explore a reduction in the Cr:Nb ratio so that no excess Cr is present if there is a need to process GRCop-84 at these high temperatures. The activity of Nb will increase which will make the alloy more prone to hydrogen embrittlement (25). It may be a manageable problem since the activity can still be greatly reduced compared to elemental Nb though proper chemistry control to favor the Cr-rich Cr<sub>2</sub>Nb composition.

### **Effect of Strain Rate**

Examination of Figure 44 and Table 11 show that the strength of GRCop-84 is relatively insensitive to strain rate over the range of strain rates tested. This is not surprising given the relatively small dependency of the yield strength on strain rate for OFHC copper between  $10^{-4}$  and  $3 \times 10^3$  1/sec (Ref. 51). Cold rolling increases the strength of GRCop-84 as expected, but the strain rate dependency remains small and approximately equal to the annealed sheet. This is again consistent with past results for OFHC Cu in uniaxial compression (Ref. 52) and tension (Ref. 53) tests. Since the GRCop-84 matrix is nearly pure Cu, a similar behavior was expected.

The dependency of GRCop-84 elongation on strain rate at room temperature is also relatively small and consistent with expectations. The dependency of the elongation on strain rate at 400 °C (752 °F) is more complex as can be seen in Figures 44(b) and (d). The behavior of GRCop-84 at elevated temperatures appears to be nonlinear for the as-annealed sheet.

The 47 percent cold-rolled sheet showed a marked increase in ductility with increasing strain rate. Normally increasing the strain rate hampers movement of dislocations, promotes dislocation pile-ups and reduces the strain to failure. At this combination of temperature, prior cold work and strain rates the samples may be undergoing dynamic recrystallization during testing. No microstructural work was performed to test this hypothesis. If additional high strain rate testing is conducted in the future, it should include such analysis.

### **Future Work**

The following items were identified for potential future work to more completely understand the tensile behavior of GRCop-84.

1. Additional foil testing at room temperature using an extensometer should be conducted to resolve if the longitudinal and long transverse properties are isotropic or anisotropic. The additional tests will increase the power of the test to detect differences in the average values. If a 3D optical extensometer is used instead of a clip-on extensometer, the difference in properties for the longitudinal and long transverse directions can be directly determined.
2. Additional testing of GRCop-84 produced by the anticipated production method and subjected to simulated-engine thermal cycles is desirable once an engine production plan is selected.
3. Additional microstructural analysis of GRCop-84 following long-term exposure in the 400 to 600 °C (752 to 1112 °F) temperature range may reveal the strengthening mechanism that improves the strength with the exposure. This mechanism could be used to improve GRCop-84 used in liners.
4. The dislocation structure of GRCop-84 tensile specimens tested at various strain rates should be examined to determine if dynamic recrystallization occurs at 400 °C (752 °F). This would aid in understanding the rolling process where very high strain rates are experienced by GRCop-84.

5. Additional testing of cold work sheet should be conducted to better characterize cold-worked material. The data should be used to understand the interactions between tensile properties, cold-work and temperature with a goal of developing better models for cold-worked GRCo-84 tensile properties. Additional analysis using fundamental metallurgical principles may also assist in the analysis and determination of the best selection of data for the models and the form of the models.
6. If more material becomes available, given the high temperature brazing cycles exhibits low reductions in area, additional investigation of the formation of large elemental Cr precipitates and their role in the failure of GRCo-84 will need to be conducted.

## Summary and Conclusions

Testing of GRCo-84 in a wide variety of forms (extrusions, HIPed billets, tubing, plate, sheet and foil) under a extensive array of conditions (temperature, cold work, strain rate, thermal exposure) revealed that GRCo-84 was largely insensitive to processing and thermal exposure save for cold working. Changes in tensile properties, when observed, were generally small. The exception was cold working that could greatly increase strength while decreasing ductility as is normal.

Tensile properties of GRCo-84 are lower than many competitive alloys at temperatures below about 300 °C (572 °F), but they are generally better in the range of 500 to 700 °C (932 to 1292 °F), the range of temperatures expected for the hot wall of a main combustion chamber liner. Useful strength persists up to even 800 °C (1472 °F). This was expected since GRCo-84 was optimized for high temperature use without regard to its low temperature strength.

The real advantage of GRCo-84 is revealed when the various Cu-based alloys that are candidate liner alloys are given a high temperature simulated-braze cycle. Competitive precipitation-strengthened alloys such as NARloy-Z, Cu-Cr, Cu-Zr and Cu-Cr-Zr lose most of their strength and are much inferior to GRCo-84 in the brazed condition. Some of the strength loss may be recovered by aging, but the strength cannot be returned to the fully-precipitation hardened and cold-worked condition. In contrast GRCo-84 has a minimal loss in properties and retains almost all of its as-produced strength, even after being exposed at 1000 °C (1832 °F) or 0.94  $T_m$ . This strength retention is also seen in long-term, high temperature thermal exposures. At an intermediate temperature of 500 °C (932 °F), samples exposed for 6000 min. actually improve their strength. While not tested, it is expected that competitive precipitation-strengthened Cu alloys would overage and lose strength if given a similar thermal exposure.

The combination of elevated temperature tensile properties and thermal stability make GRCo-84 particularly attractive for main combustion chamber liner applications. It also makes the alloy attractive for long-term, high temperature applications beyond main combustion chamber liners.

## References

1. "NASA Relies on Copper for Shuttle Engine," Copper Topics, Ed. 73, (Spring 1992)  
[http://www.copper.org/publications/newsletters/cutopics/Ct73/shuttle\\_engine.html](http://www.copper.org/publications/newsletters/cutopics/Ct73/shuttle_engine.html)
2. B. Feinberg, "Slot Machining for Space Shuttle Engines," Mfg. Eng. Manage. Vol. 73, No. 3, (Sept. 1974), pp. 22–25.
3. W.A. Hayes and D.E. Janke, "Formed Platelet Liner Construction Feasibility, Phase A Final Report," NASA CR-184506, NASA Marshall Space Flight Center, Huntsville, AL (Sept. 1992).
4. G.P. Sutton, *Rocket Propulsion Elements: An Introduction To The Engineering Of Rockets, Fifth Ed.*, John Wiley & Sons, New York, NY, 1986, page 198.
5. J.R. Bullock, M. Popp, J. R. Santiago, RL60 "Demonstrator Engine Design, Manufacture, and Test," AIAA-2003-4489, 39<sup>th</sup> AIAA/ASME/SAE/ASEE Joint Propulsion Conference & Exhibit, July 20–23, 2003, Huntsville, AL.
6. C. Cooley; S. Fentress; T. Jennings, "Hot Firing of a Full Scale Copper Tubular Combustion Chamber," Air Force Report AFRL-PR-ED-TP-2002-078, May 2002.

7. D.L. Ellis, B. Lerch, S. Cummings and G. Ray, "Drawing of GRCop-84 Tubing," NASA/TM—2006-214223, NASA Glenn Research Center, Cleveland, OH, (Dec. 2006).
8. D.L. Ellis and R.L. Dreshfield, "Preliminary Evaluation of a Powder Metal Copper-8 Cr-4 Nb Alloy," *Proc. Advanced Earth-to-Orbit Conference*, NASA MSFC, Huntsville, AL, (May 19-21, 1992).
9. D.L. Ellis, R.L. Dreshfield, M.J. Verrilli, and D.G. Ulmer, "Mechanical Properties of a Cu-8 Cr-4 Nb Alloy," *Proc. Earth-to-Orbit Conference*, Huntsville, AL (May 1994).
10. R. Holmes, S.K. Elam, T. McKechnie, and R. Hickman, "Robust Low Cost Liquid Rocket Combustion Chamber by Advanced Vacuum Plasma Process," *Proc. 39th Space Congress; 29 Apr. - 2 May 2002*, Cocoa Beach, FL.
11. S.K. Elam, R. Holmes, T. McKechnie, R. Hickman and T. Pickens, "VPS GRCOP-84 Chamber Liner Development Efforts," *Proc. 5Second JANNAF Propulsion Meeting/1st Liquid Propulsion Subcommittee Meeting*, Las Vegas, NV (May 2004).
12. D.L. Ellis et al., "A Practical Guide to the Production of Metal Spun NiCrAlY Coated GRCop-84 Liners," NASA/TM—2006-214123, NASA Glenn Research Center, Cleveland, OH (April 2006).
13. W.S. Loewenthal and D.L. Ellis, "GRCop-84 Rolling Parameter Study", NASA/TM—2008-215213, NASA Glenn Research Center, Cleveland, OH, (May 2008).
14. D.L. Ellis and A. Garg, "Annealing of GRCop-84," NASA Glenn Research Center, Cleveland, OH, to be published.
15. D.L. Ellis, W.S. Loewenthal and H. Haller, "Creep Properties of GRCop-84," NASA Glenn Research Center, Cleveland, OH, to be published.
16. ASTM Standard E 8, "Standard Test Methods for Tension Testing of Metallic Materials," ASTM International, West Conshohocken, PA.
17. D.L. Ellis and D.J. Keller, "Thermophysical Properties of GRCop-84," NASA/CR—2000-210055, NASA Glenn Research Center, Cleveland, OH (June 2000).
18. R.P. Heuer. "The Effect of Iron and Oxygen on the Electrical Conductivity of Copper," *J. Amer. Chem. Soc.*, Vol. 49, (1927), p. 2711.
19. H.J. Goldschidt and J. Brand, *J. Less-Common Metals*, Vol. 3, No. 1, (1948), p. 44.
20. D.L. Ellis, B.K. Hastings, "Hydrogen embrittlement resistance of GRCop-84," *Intl. J. of Hydrogen Energy*, Vol. 33, Issue 20, (October 2008), pp. 5661–5671.
21. D.L. Ellis and G.M. Michal, "Precipitation strengthened high strength, high conductivity Cu-Cr-Nb alloys produced by chill block melt spinning," NASA CR-185144, NASA Lewis Research Center, Cleveland, OH (1989).
22. B.A. Lerch, D.L. Ellis and H.M. Yun, "Low Cycle Fatigue of GRCop-84," NASA Glenn Research Center, Cleveland, OH, to be published.
23. K.R. Anderson, J.R. Groza, R.L. Dreshfield, and D.L. Ellis, "High Performance Dispersion Strengthened Cu-8 Cr-4 Nb Alloy," *Met. Trans A*, Vol. 26A, (Sept. 1995), pp. 2197–2206.
24. D.L. Ellis and G.M. Michal, "Mechanical Properties of Two Cu-Cr-Nb Alloys and NARloy-Z," NASA CR-198529, NASA Lewis Research Center, Cleveland, OH, (Oct. 1996).
25. L.G. Vettriano, J.L. Heelan, C.A. Faconti, J.L. Walley, A. Garg, J.R. Groza, J.C. Gibeling, "Influence of processing on the microstructure of Cu-8Cr-4Nb," *J. Mater. Sci.*, <http://www.springerlink.com/content/v17k40h426635387/?p=ab6bf4468e8e4453a0468f9a70472515&pi=3>.
26. H. Suzuki, M. Kanno, and H. Kitano, "High Temperature Embrittleness Of Cu-Cr Alloy," *Nippon Kinzoku Gakkaishi*, Vol. 34, (1970), pp. 497–501. Translated to English in NASA TT-20134, NASA Lewis Research Center, Cleveland, OH (May 1988).
27. D.L. Ellis, A.K. Misra, and R.L. Dreshfield. Effect of hydrogen exposure on a Cu-8 Cr-4 Nb alloy, NASA-TM-106429, NASA Glenn Research Center, Cleveland, OH, Dec. 1993.
28. M.V. Yokelson and M. Balicki, "Progressive Work-Hardening and Reannealing of Five Brands of High-Conductivity Copper, Wire and Wire Products," Oct. 1955, p. 1179.
29. D.J. Chakrabati and D.E. Laughlin, *Bulletin of Alloy Phase Diagrams*, Vol. 5, No. 1, 1984.
30. D.J. Chakrabati and D.E. Laughlin, *Bulletin of Alloy Phase Diagrams*, Vol. 2, No. 4, 1982.

31. D.B. Butrymowicz, J.R. Manning, and M.E. Read, *Diffusion Rate Data and Mass Transport Phenomena for Copper Systems*, Diffusion in Metals Data Center, Institute for Materials Research, National Bureau of Standards, Washington, D.C., (July 1977).
32. C. Wagner, "Theories Associated With Age hardening and Overaging During Ostwald Ripening," *Zeitschrift fur Electrochemic*, Vol. 37, (1931) pp. 581–591.
33. R.E. Reed-Hill, "7.24 The Grain Growth Law," *Physical Metallurgy Principles*, Second Edition, D. Van Nostrand Comp., New York, NY, (1973), pp. 304–310.
34. K.R. Anderson, J.R. Groza, R.L. Dreshfield, and D.L. Ellis, "Microstructural Evaluation of Precipitation-Strengthened Cu-8 Cr-4 Nb Alloy," *Materials Science and Engineering*, A169, (1993), pp. 167–175.
35. Y.M. Wang and E. Ma, "Temperature And Strain Rate Effects On The Strength And Ductility Of Nanostructured Copper," *Appl. Phys. Lett.*, Vol. 83, No. 15, (13 October 2003), pp. 3165–3167.
36. S.J. Zinkle and W.S. Eatherly, "Effect Of Test Temperature And Strain Rate On The Tensile Properties Of High-Strength, High Conductivity Copper Alloys," *Fusion Materials Semiannual Progress Report for Period ending December 31, 1996*, DOE/ER-0313/21, pp. 165–174.
37. H.C. de Groh III, D.L. Ellis, and W.S. Lowenthal, "Comparison of GRCop-84 to Other High Thermal Conductive Cu Alloys," NASA/TM—2007-214633, NASA Glenn Research Center, Cleveland, OH (Feb. 2007).
38. P.W. Taubenblat, W.E. Smith, and A.R. Graviano, "Properties and Applications of High Strength, High Conductivity Coppers and Copper Alloys," *High Conductivity Copper And Aluminum Alloys*, E. Ling and P.W. Taubenblat, Eds., TMS/AIME, Warrendale, PA (1984), pp. 19–29.
39. T. Nagai, Z. Henmi, and S. Koda, "Annealing Behavior In Copper-Chromium, Copper-Zirconium And Copper-Zirconium -Chromium Alloys," *J. Japan Copper and Brass Assn.*, Vol. 14, (1975), p. 16 (CDA Extract 13298).
40. K.R. Anderson, "Effects of Thermal and Mechanical Processing on Microstructures and Desired Properties of Particle-Strengthened Cu-Cr-Nb Alloys," Doctoral dissertation, University of California at Davis, Davis, CA (1999). Also available as NASA/CR—2000-209812. NASA Glenn Research Center, (Feb. 2000).
41. N.S. Benson, J. McKeown and D.N. Mends, "The Creep And Softening Properties Of Copper For Alternator Rotor Windings," *J. Inst., Metals*, Vol. 80, (1951–52), p. 131.
42. S. Elam, J. Lee, R. Holmes and F. Zimmerman, "Lightweight Chambers for Thrust Assemblies," *Proc. 5 Second International Astronautical Congress*; 1–5 Oct. 2001; Toulouse; France, *Alloys By Temperature chart*, Wesgo Metals, Hayward, CA, undated.
43. F. Pawlek and K. Reichel, "The Effect Of Impurities On The Electrical Conductivity Of Copper," *Zeit. Metallkunde*, Vol. 47, 1956, p. 347.
44. M. Lifshitz and V.V. Slyozov, *J. Phys. Chem. Solids*, 19, 35 (1961) p. 35.
45. C. Wagner, *Z. Electrochem.* Vol. 65 (1961) p. 581.
46. C. Zener, *Trans. Am. Inst. Min. Eng.*, Vol. 175, (1948), p. 47.
47. S. Nishikawa, K Nagata and S. Kobayashi, "Reversion Phenomena of Cu-Cr Alloys," *Nippon Kinzoka Gakkaishi*, Vol. 30, No. 8, (1966) pp. 760–765. NASA Technical Translation TM-77780.
48. D.L. Ellis, "Precipitation Strengthened High Strength, High Conductivity Cu-Cr-Nb Alloys Produced by Chill Block Melt Spinning," Doctoral dissertation, Case Western Reserve University, Cleveland, OH (1989). Also available as NASA CR-185144, NASA Lewis Research Center, Cleveland, OH.
49. A.K. Nikolayev and V.M. Rosenberg, *Izert. Akad. Nauk SSR, Metal.*, Vol. 5 (1972), pp. 163–166.
50. A. Adallah, G.M. Michal, D.L. Ellis, and J.J. Lewandowski, "Formability of a High Performance Dispersion Strengthened Cu-Cr-Nb Composite," *Proc. Of 2003 Annual TMS Meeting*, pp. 157–165.
51. D. Ostwaldt and P. Klimanek, "The influence of temperature and strain rate on microstructural evolution of polycrystalline copper," *Matls. Sci. and Eng. A*, Vols. 234–236, (30 Aug. 1997), pp. 810–813.
52. R.P. Carreker Jr., W.R. Hibbard Jr., "Tensile deformation of high-purity copper as a function of temperature, strain rate, and grain size," *Acta Met.*, Vol. 1, Iss. 6, (Nov. 1953), pp. 654–663.

REPORT DOCUMENTATION PAGE			Form Approved OMB No. 0704-0188		
<p>The public reporting burden for this collection of information is estimated to average 1 hour per response, including the time for reviewing instructions, searching existing data sources, gathering and maintaining the data needed, and completing and reviewing the collection of information. Send comments regarding this burden estimate or any other aspect of this collection of information, including suggestions for reducing this burden, to Department of Defense, Washington Headquarters Services, Directorate for Information Operations and Reports (0704-0188), 1215 Jefferson Davis Highway, Suite 1204, Arlington, VA 22202-4302. Respondents should be aware that notwithstanding any other provision of law, no person shall be subject to any penalty for failing to comply with a collection of information if it does not display a currently valid OMB control number.</p> <p>PLEASE DO NOT RETURN YOUR FORM TO THE ABOVE ADDRESS.</p>					
1. REPORT DATE (DD-MM-YYYY) 01-04-2012		2. REPORT TYPE Technical Memorandum		3. DATES COVERED (From - To)	
4. TITLE AND SUBTITLE Tensile Properties of GRCop-84			5a. CONTRACT NUMBER		
			5b. GRANT NUMBER		
			5c. PROGRAM ELEMENT NUMBER		
6. AUTHOR(S) Ellis, David, L.; Loewenthal, William, S.; Yun, Hee Man			5d. PROJECT NUMBER		
			5e. TASK NUMBER		
			5f. WORK UNIT NUMBER WBS 463169.04.03.04.03		
7. PERFORMING ORGANIZATION NAME(S) AND ADDRESS(ES) National Aeronautics and Space Administration John H. Glenn Research Center at Lewis Field Cleveland, Ohio 44135-3191			8. PERFORMING ORGANIZATION REPORT NUMBER E-17784		
9. SPONSORING/MONITORING AGENCY NAME(S) AND ADDRESS(ES) National Aeronautics and Space Administration Washington, DC 20546-0001			10. SPONSORING/MONITOR'S ACRONYM(S) NASA		
			11. SPONSORING/MONITORING REPORT NUMBER NASA/TM-2012-217108		
12. DISTRIBUTION/AVAILABILITY STATEMENT Unclassified-Unlimited Subject Category: 26 Available electronically at <a href="http://www.sti.nasa.gov">http://www.sti.nasa.gov</a> This publication is available from the NASA Center for AeroSpace Information, 443-757-5802					
13. SUPPLEMENTARY NOTES					
14. ABSTRACT This is a chapter in the final report on GRCop-84 for the Reusable Launch Vehicle (RLV) Second Generation/Project Constellation Program. It contains information on the tensile properties of GRCop-84. GRCop-84 (Cu-8 at.% Cr-4 at.% Nb) was produced by extrusion and Hot Isostatic Pressing (HIPing). Some of the extrusions were rolled to plate and sheet while other extrusions were drawn into tubing. The material was further subjected to various heat treatments corresponding to annealing, anticipated typical brazing conditions, an end-of-life condition and various elevated temperature exposures to attempt to improve creep resistance. As anticipated, cold work increased strength while decreasing ductility. Annealing at 600 °C (1112 °F) and higher temperatures was effective. An exposure for 100 h at 500 °C (932 °F) resulted in an increase in strength rather than the anticipated decrease. High temperature simulated-braze cycles and thermal exposures lowered the strength of GRCop-84, but the decreases were small compared to precipitation strengthened copper alloys. It was observed that the excess Cr could form large precipitates that lower the reduction in area though it appears a minimum amount is required. Overall, GRCop-84 exhibits good stability of its tensile properties, which makes it an excellent candidate for rocket engine liners and many other high temperature applications.					
15. SUBJECT TERMS Copper alloys; Tensile test					
16. SECURITY CLASSIFICATION OF:			17. LIMITATION OF ABSTRACT	18. NUMBER OF PAGES	19a. NAME OF RESPONSIBLE PERSON
a. REPORT	b. ABSTRACT	c. THIS PAGE			STI Help Desk (email:help@sti.nasa.gov)
U	U	U	UU	92	19b. TELEPHONE NUMBER (include area code) 443-757-5802

